PACIFIC EARTHQUAKE ENGINEERING
RESEARCH CENTER

Stiffness Analysis of Fiber-Reinforced Elastomeric Isolators

Hsiang-Chuan Tsai
National Taiwan University

and

James M. Kelly
University of California, Berkeley

PEER 2001/05
MAY 2001

STIFFNESS ANALYSIS OF FIBER-REINFORCED ELASTOMERIC ISOLATORS

Hsiang-Chuan Tsai

Professor, Department of Construction Engineering

National Taiwan University of Science and Technology, Taipei, Taiwan

James M. Kelly

Professor, Department of Civil and Environmental Engineering

University of California, Berkeley

PEER Report 2001/05

Pacific Earthquake Engineering Research Center

College of Engineering

University of California, Berkeley

May, 2001

Abstract

The reinforcing elements of multi-layer elastomeric isolation bearings, which are normally steel plates, are replaced by a fiber reinforcement. The fiber-reinforced isolator is significantly lighter and could lead to a much less labor-intensive manufacturing process. In contrast to the steel-reinforced isolator, which is assumed to be rigid both in extension and in flexure, the fiber-reinforced isolator is assumed flexible in extension, but completely without flexural rigidity. This report presents theoretical approaches for analyzing the compressive stiffness and bending stiffness of fiber-reinforced isolators having three types of geometry: infinitely long strip, rectangular and circular. The stiffness formulae of fiber-reinforced isolators are derived. The influence of fiber flexibility on the mechanical properties of fiber-reinforced isolators is studied, and it is shown that it should be possible to produce a fiber-reinforced isolator that equals the advantageous behavior of steel-reinforced isolator.

Acknowledgement

This work was partially supported by the Engineering Research Center for Met-Shape and Die Manufacturing of Pusan National University, Pusan, Korea, which support is gratefully acknowledged. The work of Professor H.-C. Tsai was carried out at the Pacific Earthquake Engineering Research Center during his sabbatical year under a grant from the National Science Council of Taiwan. The publication of this report was supported by the Pacific Earthquake Engineering Research Center through the Earthquake Engineering Research Centers Program of the National Science Foundation under Award number EEC-9701568.

Contents

List of Figures

1 Introduction

1.1 Fiber-Reinforced Elastomeric Isolators

Seismic isolation technology in the United States is applied almost entirely to large, expensive buildings housing sensitive internal equipment, for example, computer centers, chip fabrication factories, emergency operation centers and hospitals. The isolators used in these applications are large, heavy and expensive. An individual isolator can weigh one ton or more. To extend this valuable earthquake-resistant strategy to housing and commercial building, it is necessary to reduce the weight and cost of the isolators.

The primary weight in an isolator is due to the reinforcing steel plates, which are used to provide vertical stiffness to the rubber-steel composite element. A typical rubber isolator has two large end-plates (around 1 inch thick) and 20 thin reinforcing plates (1/8 inch thick). The high cost of producing the isolators results from the labor involved in preparing the steel plates and assembly of the rubber sheets and steel plates for vulcanization bonding in a mold. The steel plates are cut, sand-blasted, acid cleaned and then coated with bonding compound. Next, the compounded rubber sheets with the interleaved steel plates are put into a mold and heated under pressure for several hours to complete the manufacturing process. The research work recently performed by Kelly (1999) suggests that both the weight and the cost of isolators can be significantly reduced by eliminating the steel reinforcing plates and replacing them with a fiber reinforcement.

The reduction in weight is possible because fiber materials are now available with an elastic

stiffness that is of the same order as steel. Thus the reinforcement needed to provide the vertical stiffness may be obtained by using a similar volume of a very much lighter material. Manufacturing costs may also be reduced if the use of fiber allows a simpler, less labor-intensive process. It is also possible that the current approach of vulcanization under pressure in a mold with steam heating can be replaced by microwave heating in an autoclave.

Another benefit of using fiber reinforcement is that it would then be possible to build isolators in long rectangular strips, whereby individual isolators could then be cut to the required size. Currently, all isolators are manufactured as either circular or square in the mistaken belief that if the isolation system for a building is to be isotropic, it needs to be made of symmetrically shaped isolators. Rectangular isolators in the form of long strips would have distinct advantages over square or circular isolators when applied to buildings where the lateral resistance is provided by walls. When isolation is applied to buildings with structural walls, additional wall beams are needed to carry the wall from isolator to isolator. A strip isolator would have a distinct advantage for retrofitting masonry structures and for isolating residential housing constructed from concrete or masonry blocks.

An enormous amount of research funding has been spent over the past ten years on attempting to develop and implement active control techniques for the seismic protection of buildings; several buildings using active control systems have been constructed in Japan. There have also been proposals to develop "smart" isolators and "intelligent" isolation systems. The value of this research endeavor is questionable. While there may be a role for these adaptive systems for expensive buildings in highly seismic areas, such systems will definitely never be of any use in the developing countries. On the other hand, the development of lightweight and cost-effective isolators is crucial if this method of seismic protection is to be applied to a wide range of buildings, such as housing, schools, and medical centers, in earthquake-prone areas of the world.

1.2 Stiffness of Elastomeric Isolators

In modeling the isolator reinforced with steel plates, the plates are assumed to be inextensional and rigid in flexure to constrain the displacement at the top and bottom of the elastomeric layer. The restricted lateral expansion on the bonded surfaces of the elastomer causes a higher compression stiffness than the unbonded elastomeric layer in the direction normal to the layer.

To calculate the compression bending stiffnesses of steel-reinforced bearings, approximate analyses are used. The elastomer is assumed to be strictly incompressible. The normal stress components are approximated by the pressure. Each individual elastomeric layer in the bearing deforms according to two kinematic assumptions: (i) horizontal planes remain planar and (ii) points on a vertical line lie on a parabola after loading. Based on these assumptions, Gent and Lindley (1959) derived the compression stiffness for pads of infinitely long strip shape and circular shape. It was further extended by Gent and Meinecke (1970) to analyze the compression stiffness and bending stiffness for pads of other shapes. The "pressure solution" approach developed by Kelly (1997) is a simplified version of these earlier analyses and is applicable to bearings with shape factors greater than about five. Through the analytical approach (Koh and Kelly, 1989) and the numerical approach (Tsai and Lee, 1998 and 1999), the two kinematic assumptions have been proved to be realistic to describe the deformation of the bonded elastic layers subjected to compression or flexural loading.

The fiber reinforcement is made up of many individual fibers grouped in strands and coiled into a cord of sub-millimeter diameter. The cords are more flexible in tension than the individual fibers; therefore, they may stretch when the bearing is loaded by the weight of a building. On the other hand, they are completely flexible in bending. In contrast to the steel-reinforced isolator where the reinforcement is assumed to be rigid both in extension and flexure, the reinforcement in the fiber-reinforced isolator is assumed to be flexible in extension, but completely without flexural rigidity.

In this report, the extensional flexibility of the fiber reinforcement is incorporated into the "pressure solution" approach which is then applied to analyze the compressive stiffness and bending stiffness of fiber-reinforced isolators with three types of geometry: infinitely long strip, rectangular, and circular. The stiffness formulae of fiber-reinforced isolators are derived. The influence of fiber flexibility on the mechanical properties of fiber-reinforced isolators is also studied.

2 Analysis of Infinitely Long Strip Isolators

2.1 Compression Stiffness of Infinitely Long Strip Isolators

2.1.1 Equilibrium in Elastomeric Layer

A layer of elastomer in an infinitely long, rectangular isolator is shown in Figure 2.1. The elastomeric layer has a width of $2b$ and a thickness of t. The top and bottom surfaces of the layer are perfectly bonded to flexible reinforcements that are modeled as an equivalent sheet with a thickness of t_f. A coordinate system (x, y, z) is established by locating the origin at the center of the layer and the y coordinate direction is attached to the infinitely long side. Under the compression load P in the z direction, the deformation of the elastomer is in a plane strain state, so that the displacement component in the y direction vanishes. The displacement components of the elastomer in the x and z coordinate directions, denoted as u and w, respectively, are assumed to have the form

$$u(x,z) = u_0(x)\left(1 - \frac{4z^2}{t^2}\right) + u_1(x) \tag{2.1}$$

$$w(x,z) = w(z) \tag{2.2}$$

In Eqs. (2.1), the term of u_0 represents the kinematic assumption that vertical lines in the elastomer become parabolic after deformation; the horizontal deformation is supplemented by additional displacement u_1 which is constant through the thickness and is intended to accommodate the stretch of the reinforcement. Eq. (2.2) represents the assumption that horizontal planes in the elastomer remain planar after deformation.

The elastomer is assumed to have linearly elastic behavior with incompressibility. The assumption of incompressibility means that the summation of normal strain components is negligible and produces a constraint on displacements in the form

$$u_{,x} + w_{,z} = 0 \tag{2.3}$$

where the commas imply partial differentiation with respect to the indicated coordinate. Substitution of Eqs. (2.1) and (2.2) into the above equation gives

$$u_{0,x}\left(1 - \frac{4z^2}{t^2}\right) + u_{1,x} + w_{,z} = 0 \tag{2.4}$$

Integration through the thickness of the elastomer from $z = -t/2$ to $z = t/2$ leads to

$$\frac{2}{3}u_{0,x} + u_{1,x} = \epsilon_c \tag{2.5}$$

in which ϵ_c is the nominal compression strain defined as

$$\epsilon_c = -\frac{w(\frac{t}{2}) - w(\frac{-t}{2})}{t} \tag{2.6}$$

The stress state in the elastomer is assumed to be dominated by the internal pressure p, such that the normal stress components σ_{xx} and σ_{zz} are assumed as

$$\sigma_{xx} \approx \sigma_{zz} \approx -p \tag{2.7}$$

Under these stress assumptions, the equilibrium equation of the elastomer in the x direction

$$\sigma_{xx,x} + \sigma_{xz,z} = 0 \tag{2.8}$$

is reduced to

$$-p_{,x} + \sigma_{xz,z} = 0 \tag{2.9}$$

The assumption of linearly elastic behavior for the elastomer means that

$$\sigma_{xz} = G(u_{,z} + w_{,x}) \tag{2.10}$$

with G being the shear modulus of the elastomer. Using the displacement assumptions in Eqs. (2.1) and (2.2), the above equation becomes

$$\sigma_{xz} = -8Gu_0\frac{z}{t^2} \tag{2.11}$$

which gives, from Eq. (2.9),

$$p_{,x} = -\frac{8G}{t^2}u_0 \tag{2.12}$$

Differentiating the above equation with respect to x and then combining the result with Eq. (2.5) to eliminate the term of $u_{0,x}$, we have

$$p_{,xx} = \frac{12G}{t^2}(u_{1,x} - \epsilon_c) \tag{2.13}$$

2.1.2 Equilibrium in Reinforcing Sheet

The deformation of the elastomeric layers bonded to the top and bottom surfaces of the reinforcing sheet generates the bonding shear stresses σ_{xz} on the surfaces of the reinforcing sheet, as shown in Figure 2.2. In an infinitesimal $\mathrm{d}x$ width of the reinforcing sheet, the internal normal force per unit length in the x direction, N_{xx}, is related to these bonding shear stresses through the equilibrium equation

$$\mathrm{d}N_{xx} + \left(\sigma_{xz}|_{z=-\frac{t}{2}} - \sigma_{xz}|_{z=\frac{t}{2}}\right)\mathrm{d}x = 0 \tag{2.14}$$

The shear stresses acting on the top and bottom surfaces of the reinforcing sheet can be derived from Eq. (2.11)

$$\sigma_{xz}|_{z=-\frac{t}{2}} = \frac{4G}{t}u_0 \quad ; \quad \sigma_{xz}|_{z=\frac{t}{2}} = -\frac{4G}{t}u_0 \tag{2.15}$$

Substitution of these into Eq. (2.14) gives

$$N_{xx,x} = -\frac{8G}{t}u_0 \tag{2.16}$$

The displacement in the reinforcement is related to the internal normal forces through the linearly elastic strain-stress relation such that

$$u_{1,x} = \frac{1}{E_f}\left(\frac{N_{xx}}{t_f} - \nu\frac{N_{yy}}{t_f}\right) \tag{2.17}$$

where E_f is the elastic modulus of the reinforcement, ν is Poisson's ratio and N_{yy} is the internal normal force per unit length in the y direction. According to the plane strain condition in the infinitely long strip pad, the normal strain of the reinforcing sheet in the y direction vanishes, so that

$$N_{yy} = \nu N_{xx} \tag{2.18}$$

Substituting this into Eq. (2.17), we have

$$N_{xx} = \frac{E_f t_f}{1-\nu^2} u_{1,x} \tag{2.19}$$

The governing equation of the displacement in the reinforcement is derived by substituting Eq. (2.19) into Eq. (2.16), which leads to

$$u_{1,xx} = -\frac{2}{3}\alpha^2 u_0 \tag{2.20}$$

where α is defined as

$$\alpha = \sqrt{\frac{12G(1-\nu^2)}{E_f t_f t}} \tag{2.21}$$

Differentiating Eq. (2.20) with respect to x and then combining the result with Eq. (2.5) to eliminate the terms of $u_{0,x}$, we have

$$u_{1,xxx} - \alpha^2 u_{1,x} = -\alpha^2 \epsilon_c \tag{2.22}$$

2.1.3 Solution of Pressure

To derive the governing equation of the pressure, arrange Eq. (2.13) to have

$$u_{1,x} = \epsilon_c + \frac{t^2}{12G} p_{,xx} \tag{2.23}$$

and then substitute this into Eq. (2.22), which gives

$$p_{,xxxx} - \alpha^2 p_{,xx} = 0 \tag{2.24}$$

To solve the pressure $p(x)$ from this differential equation, we need the boundary conditions for $p(x)$.

The normal stresses of the elastomer and the reinforcement at the edges of the infinitely long strip pad are free, which means that

$$\sigma_{xx}(\pm b) = 0 \tag{2.25}$$

and

$$N_{xx}(\pm b) = 0 \tag{2.26}$$

Based on the assumption of pressure domination in Eq. (2.7), the condition shown in Eq. (2.25) becomes

$$p(\pm b) = 0 \tag{2.27}$$

From Eq. (2.19), the condition shown in Eq. (2.26) gives $u_{1,x}(\pm b) = 0$, which means, according to Eq. (2.13), that

$$p_{,xx}(\pm b) = -\frac{12G}{t^2}\epsilon_c \tag{2.28}$$

Because the compression loading and the boundary conditions are symmetric with respect to the y axis, the pressure has the following symmetric property

$$p(x) = p(-x) \tag{2.29}$$

which means that

$$p_{,xx}(x) = p_{,xx}(-x) \tag{2.30}$$

From Eq. (2.24), we have the expression of $p_{,xx}$

$$p_{,xx}(x) = c_1 \cosh \alpha x + c_2 \sinh \alpha x \tag{2.31}$$

where c_1 and c_2 are constants to be determined. The condition in Eq. (2.30) gives $c_2 = 0$. Then the condition in Eq. (2.28) gives

$$c_1 = -\epsilon_c \frac{12G}{t^2} \frac{1}{\cosh \alpha b} \tag{2.32}$$

so that

$$p_{,xx}(x) = -\epsilon_c \frac{12G}{t^2} \frac{\cosh \alpha x}{\cosh \alpha b} \tag{2.33}$$

It follows that

$$p(x) = -\epsilon_c \frac{12G}{t^2} \frac{1}{\alpha^2 \cosh \alpha b} (\cosh \alpha x + c_3 x + c_4) \tag{2.34}$$

where c_3 and c_4 are integration constants. The condition in Eq. (2.29) gives $c_3 = 0$. Then the condition in Eq. (2.27) gives $c_4 = -\cosh \alpha b$, so that

$$p(x) = \epsilon_c \frac{12G}{\alpha^2 t^2} \left(1 - \frac{\cosh \alpha x}{\cosh \alpha b}\right) \tag{2.35}$$

2.1.4 Effective Compressive Modulus

The compressive stiffness of the isolator is determined by the effective compressive modulus E_c which is defined as

$$E_c = \frac{\sigma_c}{\epsilon_c} \tag{2.36}$$

where σ_c is the nominal compression stress which is equal to the resultant compression load per unit length P divided by the width of the pad $2b$. According to the assumption in Eq. (2.7), the resultant compression load per unit length P can be expressed as

$$P = -\int_{-b}^{b} \sigma_{zz} \, \mathrm{d}x \approx \int_{-b}^{b} p(x) \, \mathrm{d}x \tag{2.37}$$

Thus, the effective compressive modulus has the form

$$E_c = \frac{1}{2b\epsilon_c} \int_{-b}^{b} p(x) \, \mathrm{d}x \tag{2.38}$$

When the pressure solution in Eq. (2.35) is substituted, the effective compressive modulus becomes

$$E_c = GS^2 \frac{12}{(\alpha b)^2}\left(1 - \frac{\tanh \alpha b}{\alpha b}\right) \tag{2.39}$$

in which S is the shape factor which is defined as the ratio of loaded area to free area and is a dimensionless measure of the aspect ratio of the single layer of the elastomer. For the infinitely long strip layer,

$$S = \frac{b}{t} \tag{2.40}$$

The ratio $E_c/(GS^2)$ is plotted in Figure 2.3 as a function of αb, which shows that the effective compressive modulus decreases with increasing αb. To have high effective compressive modulus, we must keep the value of αb as low as possible. The value of E_c at $\alpha b = 0$ is derived by substituting the following approximation

$$\tanh \alpha b \approx \alpha b - \frac{1}{3}(\alpha b)^3 \tag{2.41}$$

into Eq. (2.39), which gives

$$E_c = 4GS^2 \tag{2.42}$$

This is the effective compressive modulus of an infinitely long strip layer of elastomer bonded to the rigid reinforcement (Kelly, 1997).

For clarification, we define the in-plane stiffness of the reinforcement as

$$k_f = \frac{E_f t_f}{1 - \nu^2} \tag{2.43}$$

From Eq. (2.21), we have

$$\alpha b = S\sqrt{12\frac{Gt}{k_f}} \tag{2.44}$$

The ratio of the in-plane stiffness of the reinforcement to the shear stiffness of the elastomer, $K_f/(Gt)$, versus the shape factor, S, is plotted in Figure 2.4 for several αb values, which shows

that a small αb value is not necessary for high reinforcement stiffness; it depends on the value of the shape factor S. Using the relation in Eq. (2.44), Eq. (2.39) can be rewritten as

$$E_c = \frac{k_f}{t}\left(1 - \frac{\tanh \alpha b}{\alpha b}\right) \tag{2.45}$$

When αb tends to infinity, $\tanh \alpha b = 1$, so that

$$E_c = \frac{k_f}{t} \tag{2.46}$$

Substituting αb in Eq. (2.44) into Eq. (2.39), the normalized effective compressive modulus E_c/G is expressed as a function of the shape factor S and the stiffness ratio of the reinforcement and the elastomer $k_f/(Gt)$. In Figure 2.5, the curves of E_c/G versus $k_f/(Gt)$ for several S values show that the compressive modulus increases with increasing reinforcement stiffness and converges to the value shown in Eq. (2.42). The figure also reveals that the curve of the smaller shape factor reaches the convergence at the smaller reinforcement stiffness. In Figure 2.6, the curves of E_c/G versus $k_f/(Gt)$ for several $k_f/(Gt)$ values show that the compressive modulus increases with increasing the shape factor and converges to the value shown in Eq. (2.46). The figure also reveals that the curve of the smaller reinforcement stiffness reaches the convergence at the smaller shape factor. In other words, when the reinforcement becomes more flexible, the shape factor has less influence on the compressive modulus.

2.1.5 Stresses in Elastomer and Reinforcement

Normalized with respect to the nominal compression stress $\sigma_c = E_c\epsilon_c$, the distribution of pressure in the elastomer given by Eq. (2.35) becomes

$$\frac{p(x)}{E_c\epsilon_c} = \frac{\alpha b(\cosh \alpha b - \cosh \alpha x)}{\alpha b \cosh \alpha b - \sinh \alpha b} \tag{2.47}$$

When α tends to zero, substitution of the following approximation

$$\cosh \alpha x \approx 1 + \frac{1}{2}(\alpha x)^2 \quad ; \quad \sinh \alpha x \approx \alpha x + \frac{1}{6}(\alpha x)^3 \tag{2.48}$$

into Eq. (2.47) gives

$$\frac{p(x)}{E_c\epsilon_c} = \frac{3}{2}\left(1 - \frac{x^2}{b^2}\right) \tag{2.49}$$

which is the pressure distribution in the elastomeric layer bonded to the rigid reinforcement. The distribution of the normalized pressure along the x axis is plotted in Figure 2.7 for $\alpha b = 0$, 1, 2 and 4. The figure shows that the effect of the flexibility of the reinforcement is to make the pressure distribution more uniform and to decrease the maximum value at the center.

Let τ denote the shear stress on the bonding surface between the elastomer and the reinforcement. From Eqs. (2.12) and (2.15), we have

$$\tau(x) = \sigma_{xz}|_{z=-\frac{t}{2}} = -\frac{t}{2}p_{,x} \tag{2.50}$$

Substitution of Eq. (2.47) into the above equation gives the normalized shear stress as

$$\frac{\tau(x)}{E_c\epsilon_c} = \frac{1}{2S}\left[\frac{(\alpha b)^2 \sinh \alpha x}{\alpha b \cosh \alpha b - \sinh \alpha b}\right] \tag{2.51}$$

When α tends to zero, substitution of the approximation in Eq. (2.48) into the above equation leads

$$\frac{\tau(x)}{E_c\epsilon_c} = \frac{3}{2S}\frac{x}{b} \tag{2.52}$$

which is the bonding shear stress for the rigid reinforcement. To show the distribution of the bonding shear stress along the x axis, the curves of $\tau(x)S/(E_c\epsilon_c)$ versus x/b are plotted in Figure 2.8 for $\alpha b = 0$, 1, 2 and 4. The figure demonstrates that the flexibility of the reinforcement makes the distribution of the bonding shear stress more concentrated on the edge and increases the maximum value at the edge. The normalized shear stress at the edge, $\tau(b)/(E_c\epsilon_c)$, is plotted in Figure 2.9 as a function of the stiffness ratio $k_f/(Gt)$ for several S values. The figure shows that $\tau(b)$ decreases with increasing stiffness ratio, and the lower shape factor always has a higher bonding shear stress at the edge.

The in-plane displacement of the reinforcement, $u_1(x)$, can be solved by substituting Eq. (2.35) into Eq. (2.23) and applying the condition $u_1(0) = 0$, which gives

$$u_1(x) = \epsilon_c b \left(\frac{x}{b} - \frac{\sinh \alpha x}{\alpha b \cosh \alpha b} \right) \tag{2.53}$$

This displacement pattern is shown in Figure 2.10 by plotting the curves of $u_1(x)/(b\epsilon_c)$ as a function of x/b for several αb values, which shows that displacement increases with reducing reinforcement stiffness.

The distribution of the internal force $N_{xx}(x)$ in the reinforcement can be solved by substituting Eq. (2.53) into Eq. (2.19). The quantity N_{xx} is unit of force per unit length, which can be normalized by dividing by the nominal compressive stress $\sigma_c = E_c\epsilon_c$ and then becomes dimensionless by dividing by the thickness of the elastomeric layer t

$$\frac{N_{xx}(x)}{E_c\epsilon_c t} = \frac{\alpha b(\cosh \alpha b - \cosh \alpha x)}{\alpha b \cosh \alpha b - \sinh \alpha b} \tag{2.54}$$

which is the same form as the pressure distribution shown in Eq. (2.47), so that the distribution of the internal force plotted in Figure 2.11 is the same as the pressure distribution plotted in Figure 2.7.

2.2 Bending Stiffness of Infinitely Long Strip Isolators

2.2.1 Governing Equation of Pressure

For a layer of elastomer in an infinitely long rectangular isolator, shown in Figure 2.12, the reinforcements bonded to the top and bottom surfaces of the elastomeric layer are subjected to a pure bending moment M. Assuming that the reinforcing sheets remain planar, the top and bottom reinforcements rotate to form an angle ϕ which is symmetric to the x-y plane. Following the same kinematic assumptions used for the compression stiffness, the displacement field of the elastomer

is given by

$$u(x,z) = u_0(x)\left(1 - \frac{4z^2}{t^2}\right) + u_1(x) \tag{2.55}$$

$$w(x,z) = \frac{1}{\rho}xz \tag{2.56}$$

in which ρ is the radius of the bending curvature defined as

$$\rho = \frac{t}{\phi} \tag{2.57}$$

Substituting Eqs. (2.55) and (2.56) into the constraint of elastomer incompressibility in Eq. (2.3) and then integrating the result through the thickness of the elastomer from $z = -t/2$ to $z = t/2$ lead to

$$\frac{2}{3}u_{0,x} + u_{1,x} = -\frac{1}{\rho}x \tag{2.58}$$

Substituting Eqs. (2.55) and (2.56) into the shear stress of elastomer σ_{xz} defined in Eq. (2.10), we have

$$\sigma_{xz} = -Gz\left(\frac{8}{t^2}u_0 - \frac{1}{\rho}\right) \tag{2.59}$$

which gives, according to the equilibrium equation of the elastomer shown in Eq. (2.9),

$$p_{,x} = -G\left(\frac{8}{t^2}u_0 - \frac{1}{\rho}\right) \tag{2.60}$$

Differentiating this equation with respect to x and then combining the result with Eq. (2.58) to eliminate the term of $u_{0,x}$ yield

$$p_{,xx} = \frac{12G}{t^2}\left(u_{1,x} + \frac{1}{\rho}x\right) \tag{2.61}$$

From Eq. (2.59), the bonding shear stresses acting on the top and bottom surfaces of the reinforcing sheet have the forms

$$\sigma_{xz}|_{z=-\frac{t}{2}} = \frac{Gt}{2}\left(\frac{8}{t^2}u_0 - \frac{1}{\rho}\right) \quad ; \quad \sigma_{xz}|_{z=\frac{t}{2}} = -\frac{Gt}{2}\left(\frac{8}{t^2}u_0 - \frac{1}{\rho}\right) \tag{2.62}$$

so that the equilibrium equation of the reinforcement shown in Eq. (2.14) is reduced to

$$N_{xx,x} = -G\left(\frac{8}{t}u_0 - \frac{t}{\rho}\right) \tag{2.63}$$

Substitution of the force-displacement relation of the reinforcement in Eq. (2.19) into this equation gives

$$u_{1,xx} = -\frac{\alpha^2 t^2}{12}\left(\frac{8}{t^2}u_0 - \frac{1}{\rho}\right) \tag{2.64}$$

where α is defined in Eq. (2.21). Differentiating Eq. (2.64) with respect to x and then combining the result with Eq. (2.58) to eliminate the term of $u_{0,x}$, we have

$$u_{1,xxx} = \alpha^2\left(u_{1,x} + \frac{1}{\rho}x\right) \tag{2.65}$$

From Eq. (2.61), we know that

$$u_{1,x} = \frac{t^2}{12G}p_{,xx} - \frac{1}{\rho}x \tag{2.66}$$

Substitution of this into Eq. (2.65) leads to

$$p_{,xxxx} - \alpha^2 p_{,xx} = 0 \tag{2.67}$$

This governing equation of pressure has the same form as Eq. (2.24) used for deriving the compression stiffness.

2.2.2 Solution of Pressure

To solve for pressure $p(x)$, we need the boundary conditions for $p(x)$. The normal stresses of the elastomer and the reinforcement are free at the edges of the infinitely long strip pad, which gives the same boundary conditions shown in Eqs. (2.25) and (2.26). According to the assumption of pressure domination in Eq. (2.7), the stress boundary conditions of the elastomeric layer shown in Eq. (2.25) becomes

$$p(\pm b) = 0 \tag{2.68}$$

Based on the force-displacement relation of the reinforcement in Eq. (2.19), the stress boundary condition of the reinforcing sheet shown in Eq. (2.26) means that $u_{1,x}(\pm b) = 0$, which gives, from Eq. (2.61),

$$p_{,xx}(\pm b) = \pm \frac{12G}{t^2}\frac{b}{\rho} \tag{2.69}$$

Because the deformation of the elastomer induced by the bending moment loading is anti-symmetric with respect to the y axis, the pressure is an odd function of x

$$p(x) = -p(-x) \tag{2.70}$$

which means that

$$p_{,xx}(x) = -p_{,xx}(-x) \tag{2.71}$$

From Eq. (2.67), we have the expression of $p_{,xx}$

$$p_{,xx}(x) = c_1 \cosh \alpha x + c_2 \sinh \alpha x \tag{2.72}$$

where c_1 and c_2 are constants to be determined. The condition in Eq. (2.71) gives $c_1 = 0$. Then, the condition in Eq. (2.69) gives

$$c_2 = \frac{b}{\rho}\frac{12G}{t^2}\frac{1}{\sinh \alpha b} \tag{2.73}$$

so that

$$p_{,xx}(x) = \frac{b}{\rho}\frac{12G}{t^2}\frac{\sinh \alpha x}{\sinh \alpha b} \tag{2.74}$$

It follows that

$$p(x) = \frac{b}{\rho}\frac{12G}{t^2}\frac{1}{\alpha^2 \sinh \alpha b}(\sinh \alpha x + c_3 x + c_4) \tag{2.75}$$

where c_3 and c_4 are integration constants. The condition in Eq. (2.70) gives $c_4 = 0$. Then, the condition in Eq. (2.68) gives $c_3 = -(\sinh \alpha b)/b$, so that

$$p(x) = \frac{b}{\rho}\frac{12G}{\alpha^2 t^2}\left(\frac{\sinh \alpha x}{\sinh \alpha b} - \frac{x}{b}\right) \tag{2.76}$$

2.2.3 Effective Bending Modulus

The bending stiffness $(EI)_{eff}$ of the infinitely long strip pad is defined as

$$(EI)_{eff} = \rho M \tag{2.77}$$

in which M is the resultant bending moment per unit length. Using the assumption in Eq. (2.7), we have

$$M = \int_{-b}^{b} \sigma_{zz} x \, \mathrm{d}x \approx -\int_{-b}^{b} p(x) x \, \mathrm{d}x \tag{2.78}$$

When the pressure solution in Eq. (2.76) is substituted, the bending stiffness becomes

$$(EI)_{eff} = \frac{24GS^2}{\alpha^4 b}\left[1 + \frac{1}{3}(\alpha b)^2 - \frac{\alpha b}{\tanh \alpha b}\right] \tag{2.79}$$

where S is the shape factor defined in Eq. (2.40).

For clarification, we define the effective bending modulus as

$$E_b = \frac{(EI)_{eff}}{I_y} \tag{2.80}$$

in which I_y is the area moment of inertia about the y axis. For a unit length of the strip pad, $I_y = 2b^3/3$. From Eq. (2.79), we have

$$E_b = \frac{36GS^2}{(\alpha b)^4}\left[1 + \frac{1}{3}(\alpha b)^2 - \frac{\alpha b}{\tanh \alpha b}\right] \tag{2.81}$$

The value of E_b at $\alpha b = 0$ is derived by substituting the following approximation

$$\frac{\alpha b}{\tanh \alpha b} \approx 1 + \frac{1}{3}(\alpha b)^2 - \frac{1}{45}(\alpha b)^4 \tag{2.82}$$

into Eq. (2.81), which gives

$$E_b = \frac{4}{5}GS^2 \tag{2.83}$$

This is the effective bending modulus of an infinitely long strip layer of elastomer bonded to the rigid reinforcement. The ratio $E_b/(GS^2)$ is plotted in Figure 2.13 as a function of αb, which shows that the bending modulus decreases with increasing αb.

Using the relation in Eq. (2.44), Eq. (2.81) can be rewritten as

$$E_b = \frac{k_f}{t}\frac{3}{(\alpha b)^2}\left[1 + \frac{1}{3}(\alpha b)^2 - \frac{\alpha b}{\tanh \alpha b}\right] \tag{2.84}$$

where k_f is the reinforcement stiffness defined in Eq. (2.43). When αb tends to infinity,

$$E_b = \frac{k_f}{t} \tag{2.85}$$

The ratio E_b/G can be expressed as a function of the shape factor S and the stiffness ratio $k_f/(Gt)$ by substituting αb in Eq. (2.44) into Eq. (2.81). The variation of E_b/G with $k_f/(Gt)$ is plotted in Figure 2.14 for several S values. The figure shows that the bending modulus increases with increasing reinforcement stiffness and converges to the value shown in Eq. (2.83). The smaller shape factor has faster convergence and reaches the bending modulus in Eq. (2.83) at a smaller stiffness ratio. The variation of E_b/G with shape factor is plotted in Figure 2.15 for several values of stiffness ratio $k_f/(Gt)$. The figure shows that increasing the shape factor will increase the bending modulus until reaching the value shown in Eq. (2.85). The figure also reveals that when the reinforcement stiffness is smaller, the bending modulus converges to the asymptotic value at a smaller shape factor.

2.2.4 Stresses in Elastomer and Reinforcement

The nominal bending stress σ_b is the maximum normal stress created by the moment M. From Eqs. (2.77) and (2.80), we have

$$\sigma_b = \frac{Mb}{I_y} = E_b\frac{b}{\rho} \tag{2.86}$$

Normalization of the pressure distribution in Eq. (2.76) with respect to the nominal bending stress gives

$$\frac{p(x)\rho}{E_b b} = \frac{(\alpha b)^2}{3}\left[\frac{\frac{\sinh \alpha x}{\sinh \alpha b} - \frac{x}{b}}{1 + \frac{1}{3}(\alpha b)^2 - \frac{\alpha b}{\tanh \alpha b}}\right] \tag{2.87}$$

When α tends to zero, substitution of the approximations in Eqs. (2.48) and (2.82) into Eq. (2.87) gives

$$\frac{p(x)\rho}{E_b b} = -\frac{5}{2}\left(\frac{x}{b} - \frac{x^3}{b^3}\right) \tag{2.88}$$

which is the normalized pressure distribution in the elastomeric layer bonded to the rigid reinforcement. The distribution of the normalized pressure along the x axis is plotted in Figure 2.16 for $\alpha b = 0$, 1, 2 and 4, which shows that the effect of the flexibility of the reinforcement is to decrease the maximum pressure and to make the location of the maximum pressure closer to the edge.

Denote $\tau(x)$ as the shear stress on the bonding surface between the elastomer and the reinforcement. From Eq. (2.60) and (2.62)

$$\tau(x) = \sigma_{xz}|_{z=-\frac{t}{2}} = -\frac{t}{2}p_{,x} \tag{2.89}$$

Substitution of Eq. (2.87) into the above equation gives the normalized bonding shear stress as

$$\frac{\tau(x)\rho}{E_b b} = \frac{(\alpha b)^2}{6S}\left[\frac{1 - \alpha b\frac{\cosh \alpha x}{\sinh \alpha b}}{1 + \frac{1}{3}(\alpha b)^2 - \frac{\alpha b}{\tanh \alpha b}}\right] \tag{2.90}$$

Substitution of Eq. (2.88) into Eq. (2.89) gives

$$\frac{\tau(x)\rho}{E_b b} = \frac{5}{4S}\left(1 - 3\frac{x^2}{b^2}\right) \tag{2.91}$$

which is the bonding shear stress for the rigid reinforcement. The distribution of the bonding shear stress along the x axis is plotted in Figure 2.17 for $\alpha b = 0$, 1, 2 and 4. The figure shows that the effect of the flexibility of the reinforcement is to make the shear stress distribution more concentrated on the edge, to decrease the value at the center and to increase the maximum value at the edge. The normalized bonding shear stress at the edge, $\tau(b)\rho/(E_b b)$, is plotted in Figure 2.18 as a function of the stiffness ratio $k_f/(Gt)$ for several S values. The figure shows that, under the same external moment and the same width of the pad, increasing the shape factor or the stiffness ratio of the reinforcement to the elastomer will decrease the bonding shear stress at the edge.

The displacement of the reinforcement $u_1(x)$ can be solved from Eq. (2.66) by applying the condition $u_1(0) = 0$,

$$u_1(x) = \frac{b^2}{\rho}\left(\frac{\cosh \alpha x - 1}{\alpha b \sinh \alpha b} - \frac{1}{2}\frac{x^2}{b^2}\right) \tag{2.92}$$

This displacement pattern is displayed in Figure 2.19 by plotting the curves of $u_1(x)\rho/b^2$ versus b/x for different αb values. The figure shows that the displacement is symmetric to the origin of x, so that the reinforcement has the same direction of deformation on the positive and negative sides of the x axis, which creates tension on the negative x side and compression at the positive x side. This is consistent with the distribution of the internal force in the reinforcement plotted in Figure 2.20. The distribution of the internal force $N_{xx}(x)$ is solved by substituting Eq. (2.92) into Eq. (2.19). After normalized with respect to the nominal bending stress, the dimensionless internal force becomes

$$\frac{N_{xx}(x)\rho}{E_b b t} = \frac{(\alpha b)^2}{3}\left[\frac{\frac{\sinh \alpha x}{\sinh \alpha b} - \frac{x}{b}}{1 + \frac{1}{3}(\alpha b)^2 - \frac{\alpha b}{\tanh \alpha b}}\right] \tag{2.93}$$

This internal force distribution in the reinforcement has the same form of the pressure distribution shown in Eq. (2.87), so that the distribution of the internal force plotted in Figure 2.20 is the same as the pressure distribution plotted in Figure 2.16.

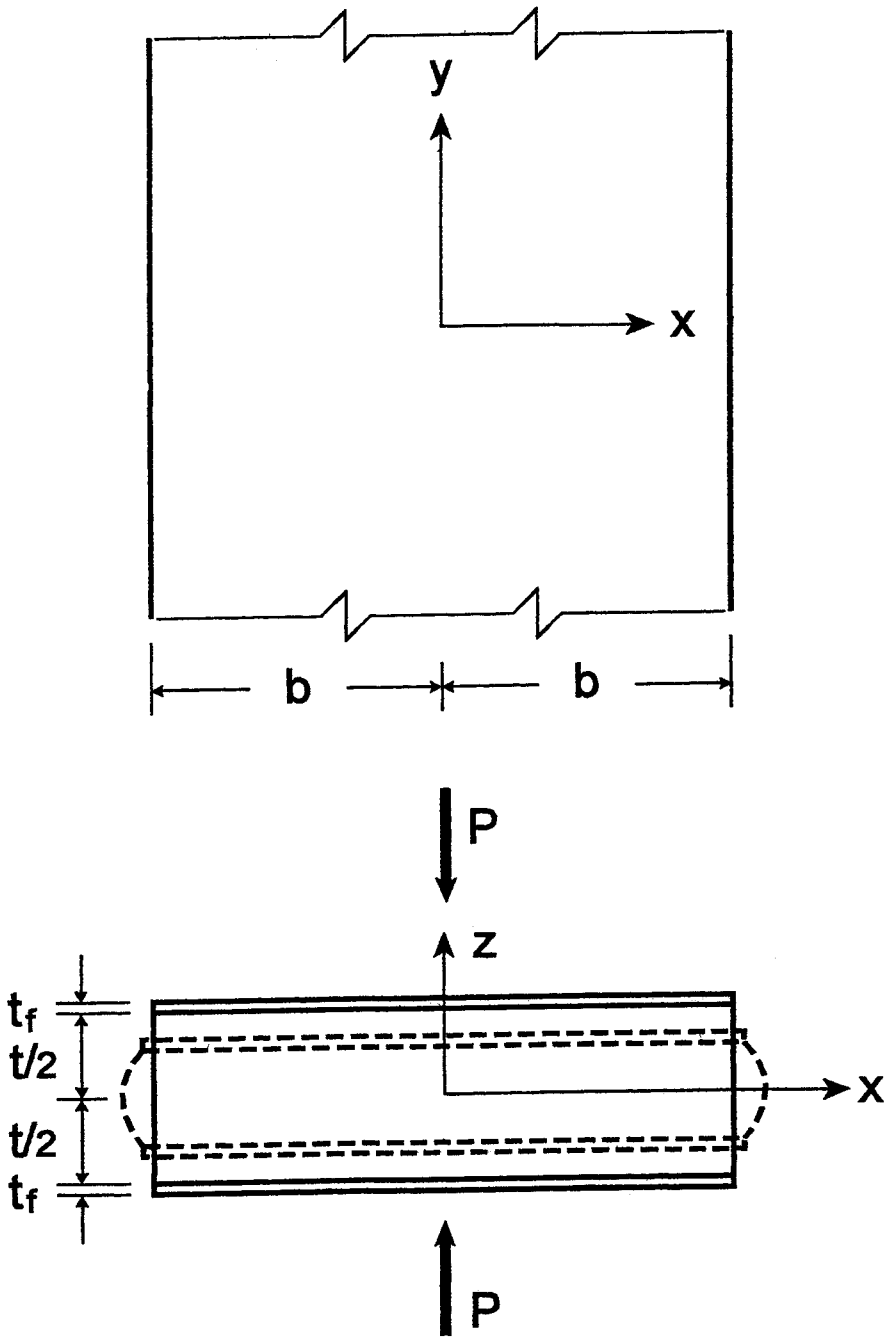

Figure 2.1: Infinitely long strip layer of reinforced elastomer under compression load

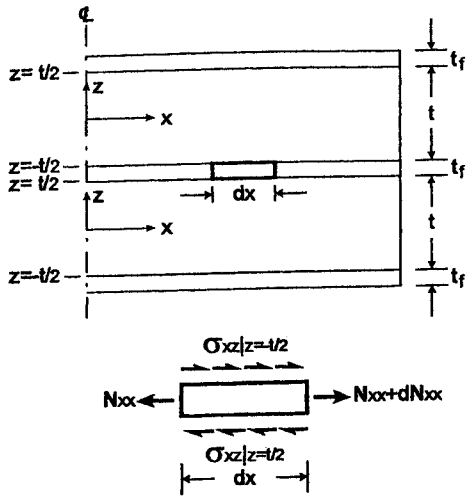

Figure 2.2: Forces in reinforcing sheet bonded to infinitely long strip layers of elastomer

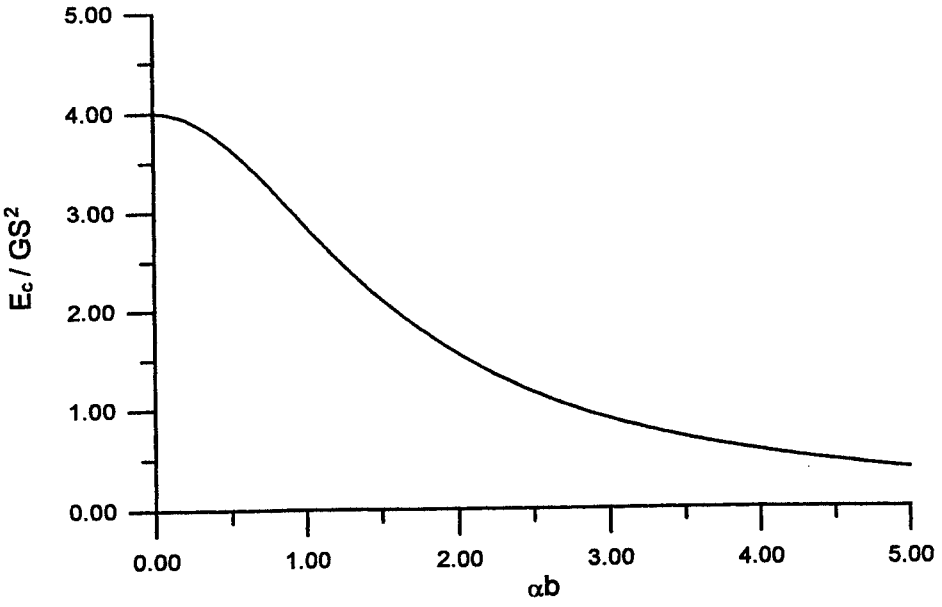

Figure 2.3: Variation of effective compressive modulus with αb in infinitely long strip pad

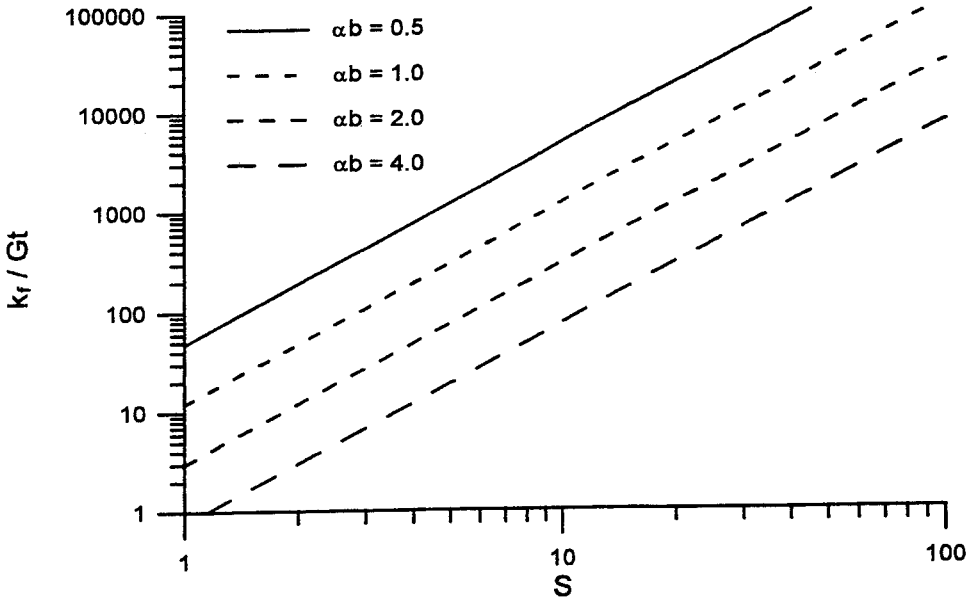

Figure 2.4: Relation between reinforcement stiffness and shape factor for different αb values in infinitely long strip pad

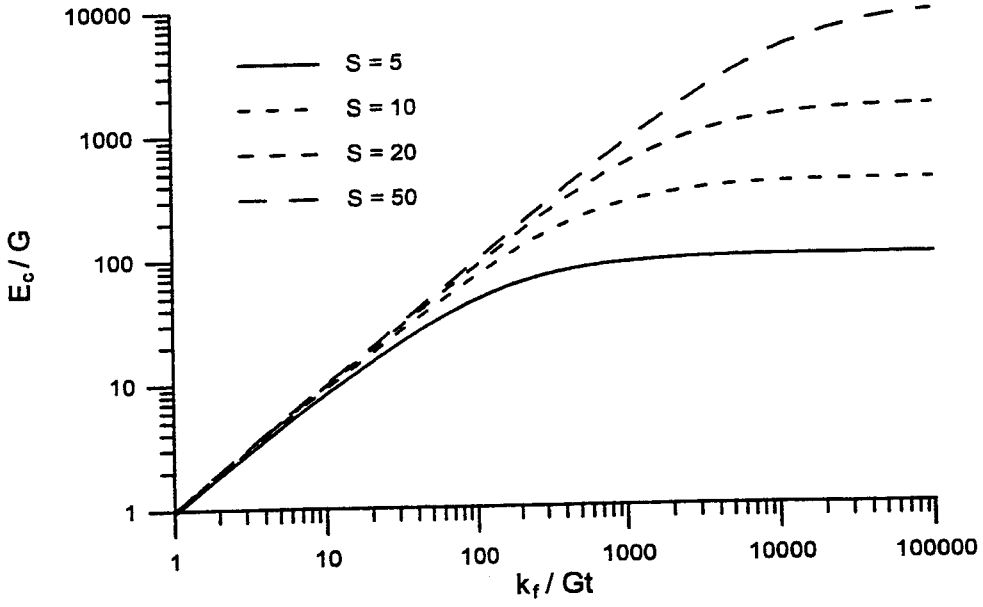

Figure 2.5: Variation of effective compressive modulus with reinforcement stiffness in infinitely long strip pad

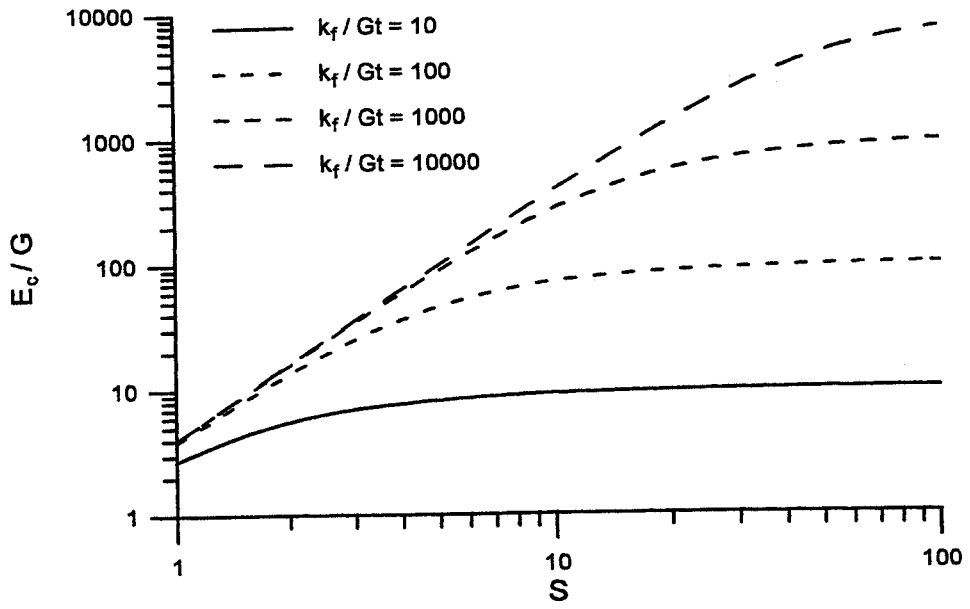

Figure 2.6: Variation of effective compressive modulus with shape factor in infinitely long strip pad

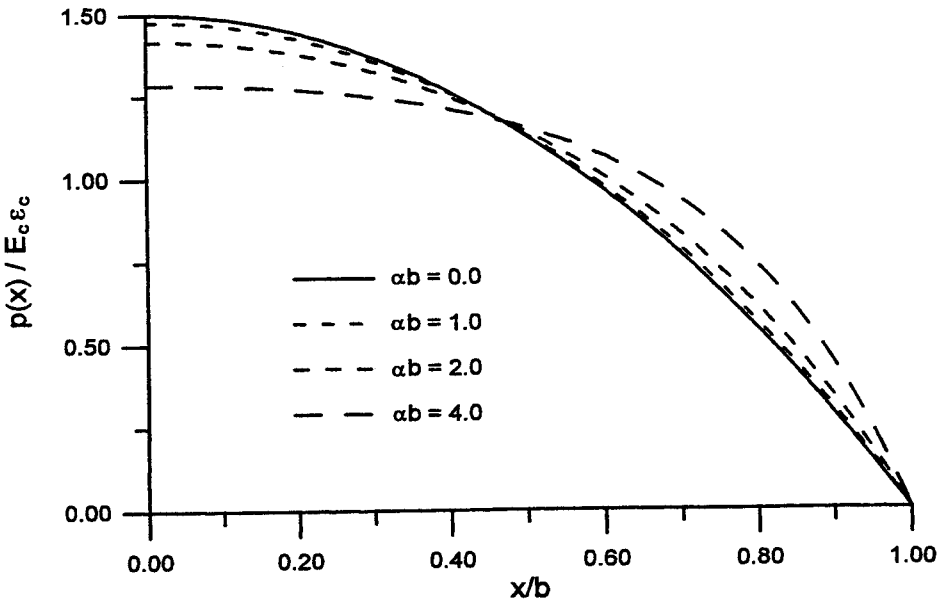

Figure 2.7: Distribution of normalized pressure in infinitely long strip pad under compression load

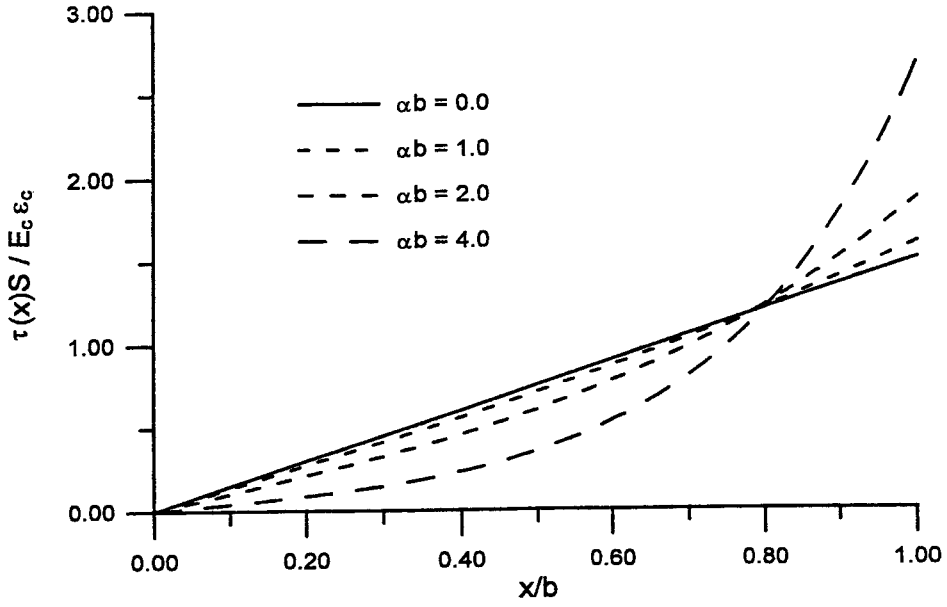

Figure 2.8: Distribution of bonding shear stress in infinitely long strip pad under compression load

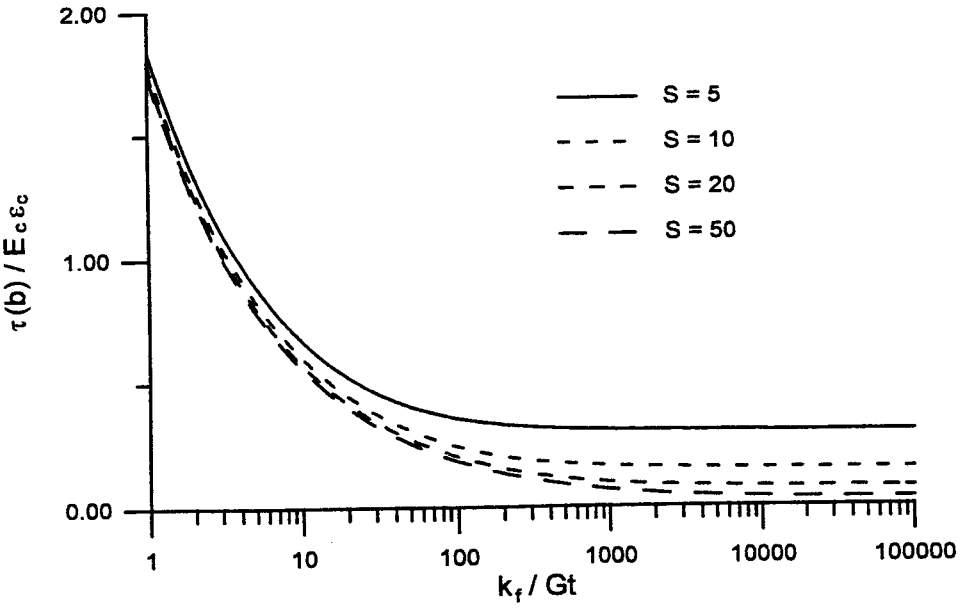

Figure 2.9: Variation of maximum bonding shear stress with reinforcement stiffness in infinitely long strip pad under compression load

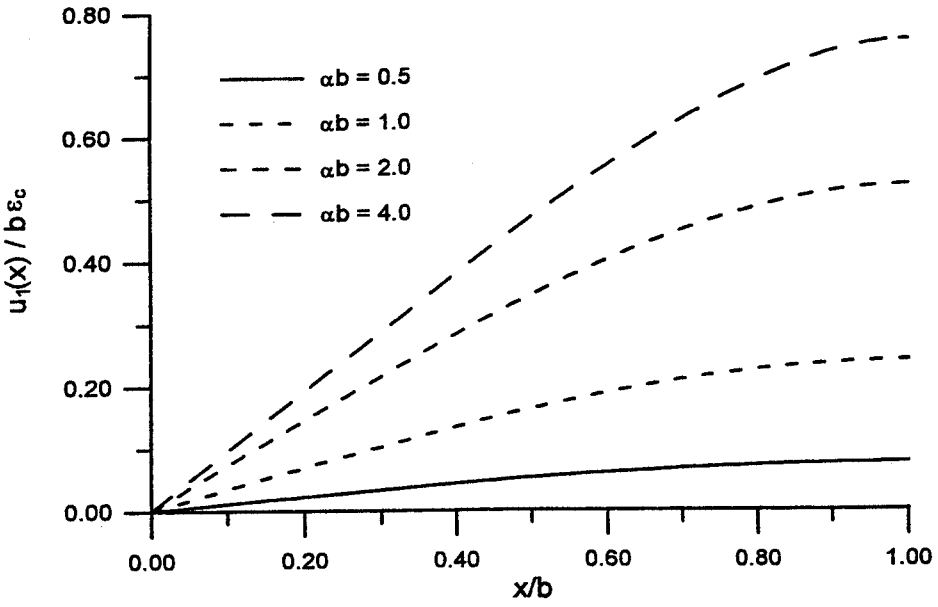

Figure 2.10: Displacement pattern in reinforcement of infinitely long strip pad under compression load

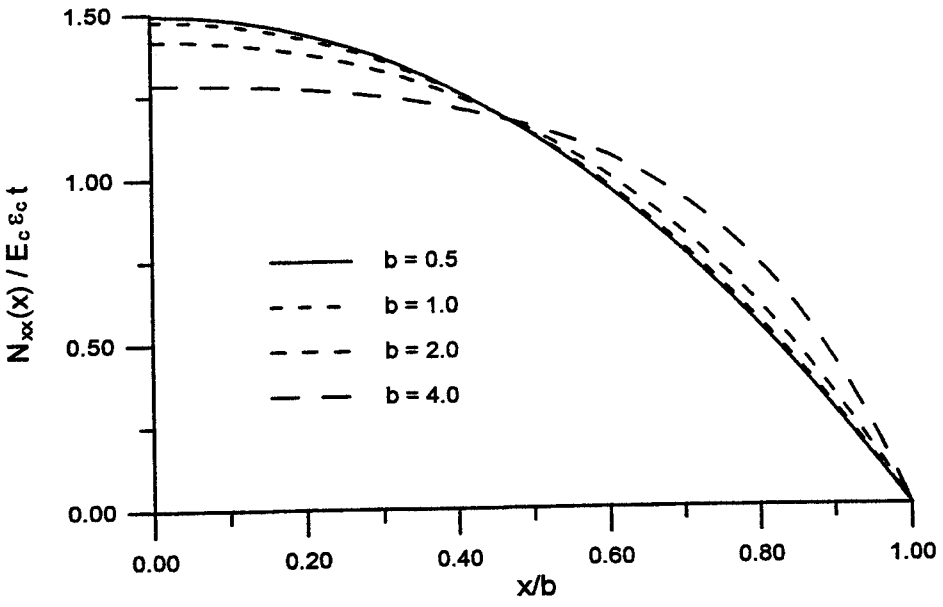

Figure 2.11: Distribution of normal force in reinforcement of infinitely long strip pad under compression load

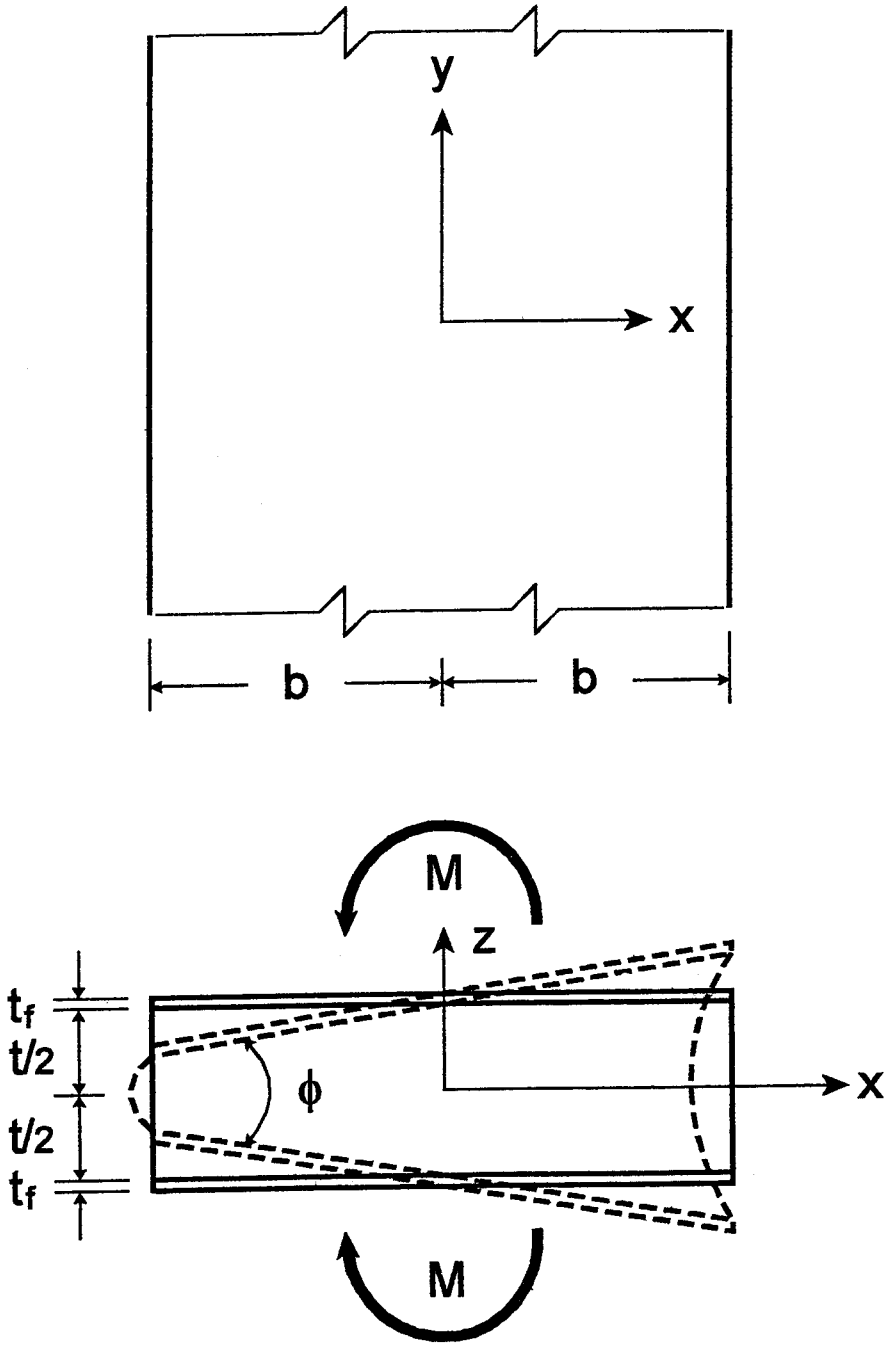

Figure 2.12: Infinitely long strip layer of reinforced elastomer under pure bending load

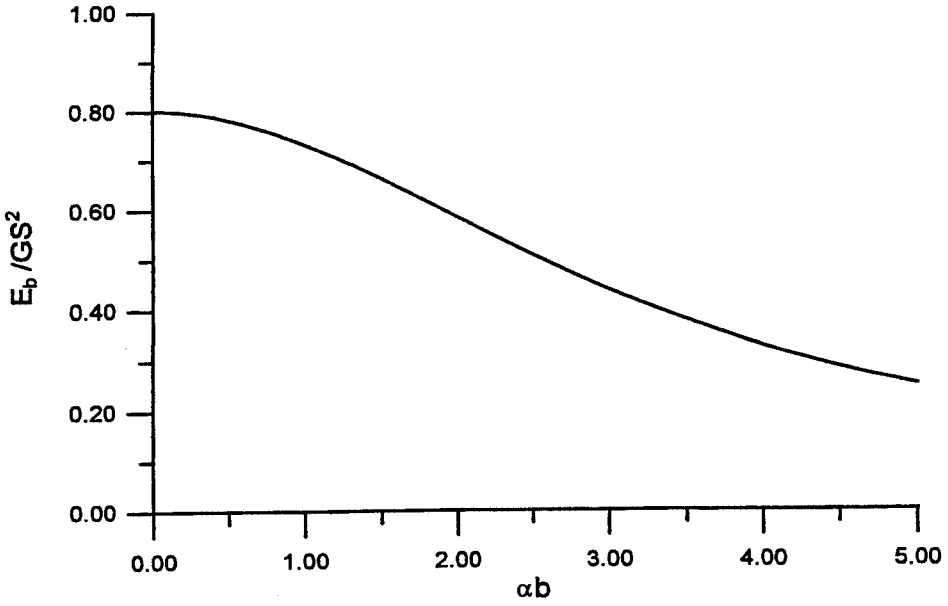

Figure 2.13: Variation of effective bending modulus with αb in infinitely long strip pad

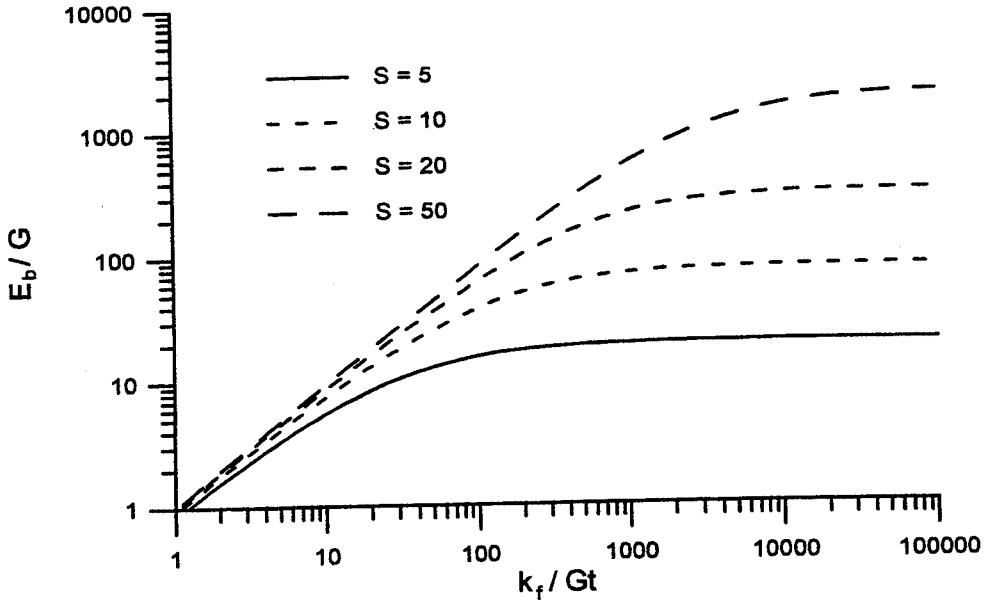

Figure 2.14: Variation of effective bending modulus with reinforcement stiffness in infinitely long strip pad

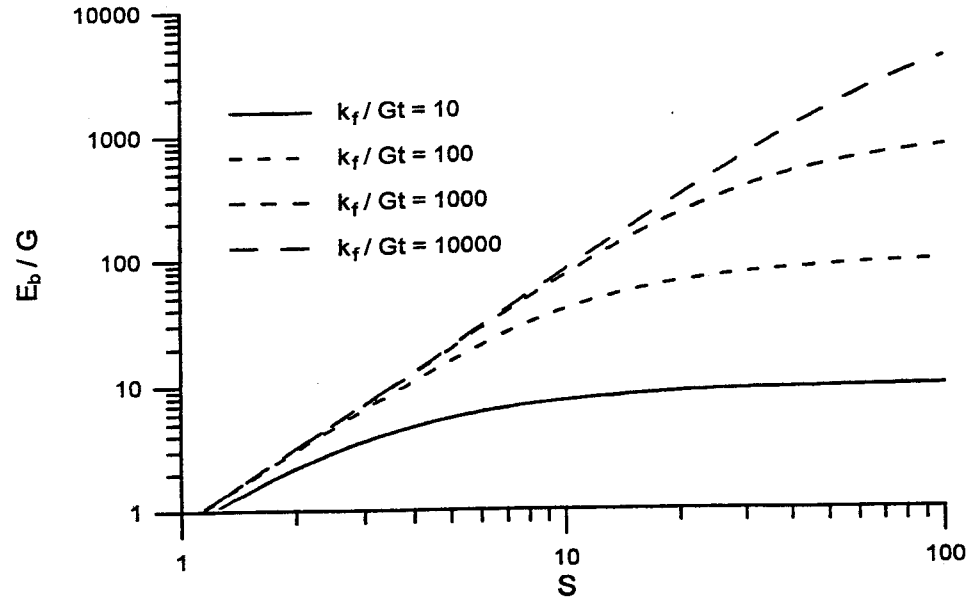

Figure 2.15: Variation of effective bending modulus with shape factor in infinitely long strip pad

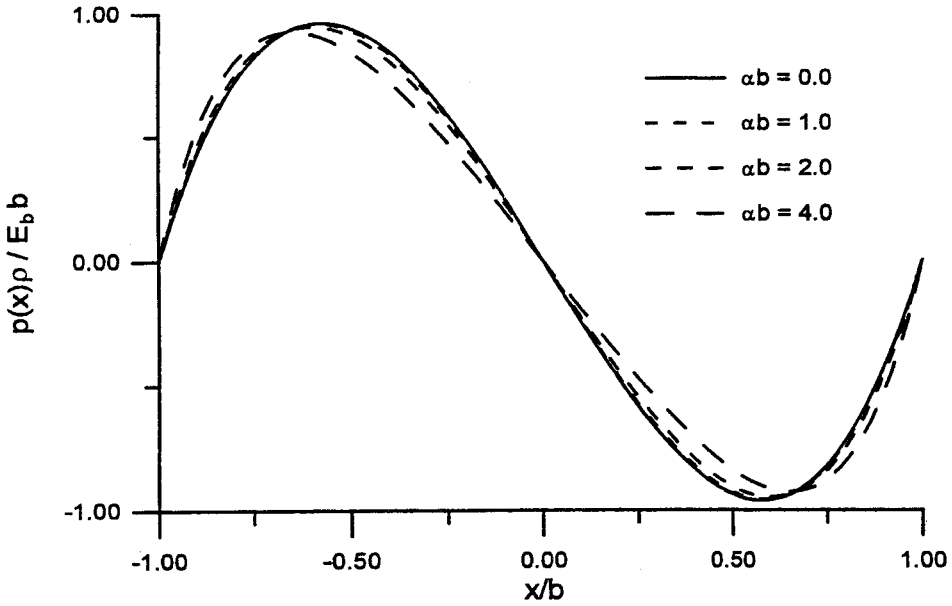

Figure 2.16: Distribution of normalized pressure in infinitely long strip pad under pure bending load

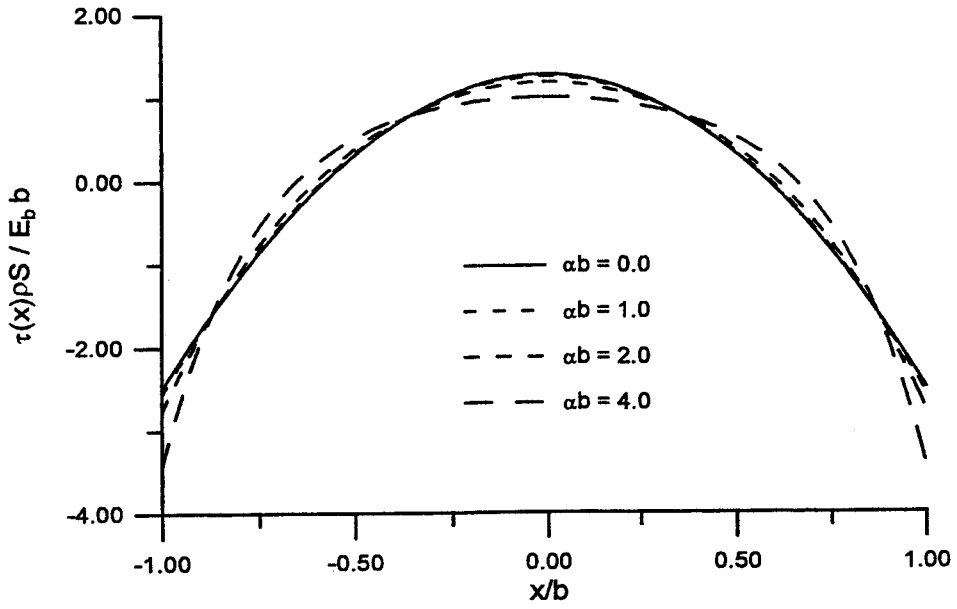

Figure 2.17: Distribution of bonding shear stress in infinitely long strip pad under pure bending load

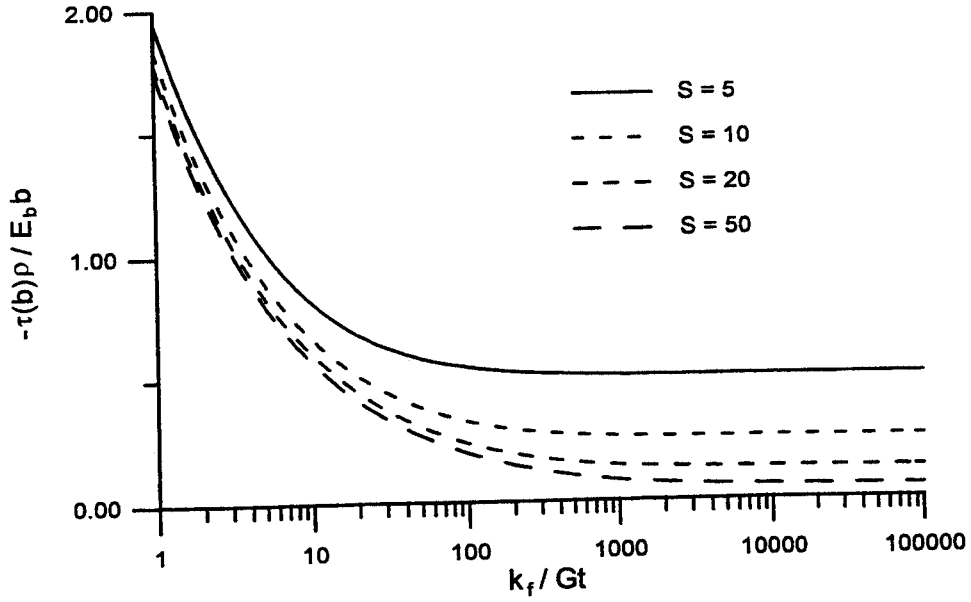

Figure 2.18: Variation of maximum bonding shear stress with reinforcement stiffness in infinitely long strip pad under pure bending load

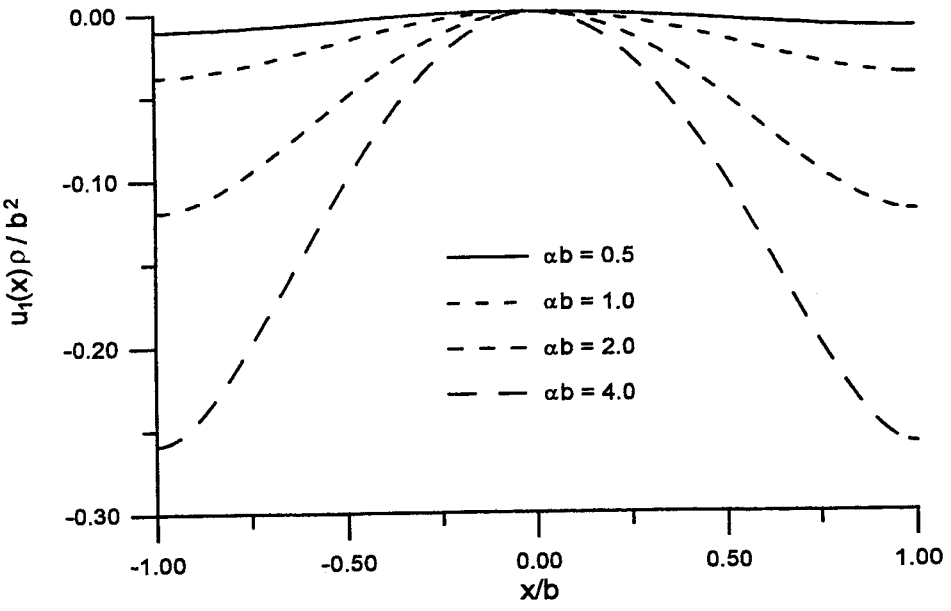

Figure 2.19: Displacement pattern in reinforcement of infinitely long strip pad under pure bending load

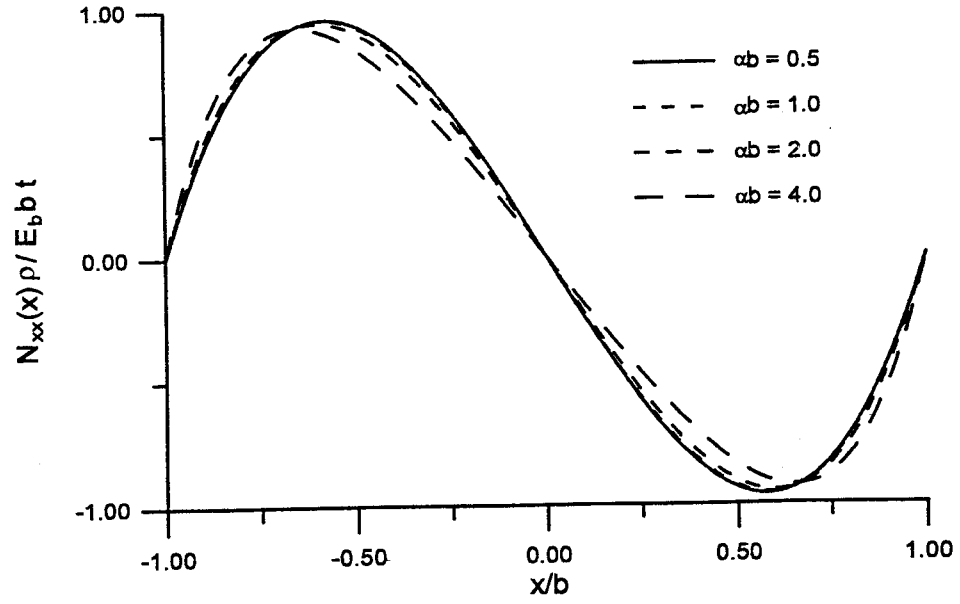

Figure 2.20: Distribution of normal force in reinforcement of infinitely long strip pad under pure bending load

3 Analysis of Rectangular Isolators

3.1 Compression Stiffness of Rectangular Isolators

3.1.1 Equilibrium in Elastomeric Layer

A layer of elastomer in a rectangular isolator is shown in Figure 3.1 where a coordinate system (x, y, z) is established by locating the origin at the center of the elastomeric layer and the x-y plane in the middle plane of the layer. The elastomeric layer has a thickness of t. Its side length parallel to the x axis is $2a$ and the y axis is $2b$. The elastomeric layer's top and bottom surfaces are perfectly bonded to flexible reinforcements which are modeled as an equivalent sheet of thickness t_f. Let u, v and w denote the displacements of the elastomer in the x, y and z coordinate directions, respectively. In addition u_1 and v_1 are denoted as the displacements of the reinforcement in the x and y directions, respectively. Under the compression load P in the z direction, the displacements of the elastomer are assumed to have the form

$$u(x, y, z) = u_0(x, y)\left(1 - \frac{4z^2}{t^2}\right) + u_1(x, y) \tag{3.1}$$

$$v(x, y, z) = v_0(x, y)\left(1 - \frac{4z^2}{t^2}\right) + v_1(x, y) \tag{3.2}$$

$$w(x, y, z) = w(z) \tag{3.3}$$

In Eqs. (3.1) and (3.2), the terms of u_0 and v_0 represent the kinematic assumption of quadratically varied displacements and are supplemented by additional displacements u_1 and v_1, respectively,

which are constant through the thickness and are intended to accommodate the stretch of the reinforcement. Eq. (3.3) represents the assumption that horizontal planes remain planar.

The elastomer is assumed to have linearly elastic behavior with incompressibility. The assumption of incompressibility produces a constraint on displacements in the form

$$u_{,x} + v_{,y} + w_{,z} = 0 \tag{3.4}$$

where the commas imply partial differentiation with respect to the indicated coordinate. Substituting Eqs. (3.1) to (3.3) into the above equation gives

$$(u_{0,x} + v_{0,y})\left(1 - \frac{4z^2}{t^2}\right) + u_{1,x} + v_{1,y} + w_{,z} = 0 \tag{3.5}$$

Integration through the thickness from $z = -t/2$ to $z = t/2$ leads to

$$\frac{2}{3}(u_{0,x} + v_{0,y}) + u_{1,x} + v_{1,y} = \epsilon_c \tag{3.6}$$

in which ϵ_c is the nominal compression strain defined as

$$\epsilon_c = -\frac{w(\frac{t}{2}) - w(-\frac{t}{2})}{t} \tag{3.7}$$

The stress state in the elastomer is assumed to be dominated by the internal pressure p, such that the normal stress components σ_{xx}, σ_{yy} and σ_{zz} differ from $-p$ only by terms of order pt^2/l^2 where l is the smaller value of $2a$ and $2b$. The shear stress components σ_{xz} and σ_{yz}, which are generated by the constraints of the reinforcements at the top and the bottom of the elastomeric layer, are assumed to be of order pt/l; the in-plane shear stress σ_{xy} is assumed to be of order pt^2/l^2. The thickness t of a single elastomeric layer in a rectangular isolator is generally much smaller than the dimension l of the pad. Neglecting the terms of order pt^2/l^2 gives the stress components of the elastomer as

$$\sigma_{xx} \approx \sigma_{yy} \approx \sigma_{zz} \approx -p \quad ; \quad \sigma_{xy} \approx 0 \tag{3.8}$$

Under these stress assumptions, the equilibrium equations in the x and y directions for the stresses of the elastomer

$$\sigma_{xx,x} + \sigma_{xy,y} + \sigma_{xz,z} = 0 \tag{3.9}$$

$$\sigma_{xy,x} + \sigma_{yy,y} + \sigma_{yz,z} = 0 \tag{3.10}$$

are reduced to

$$-p_{,x} + \sigma_{xz,z} = 0 \tag{3.11}$$

$$-p_{,y} + \sigma_{yz,z} = 0 \tag{3.12}$$

The assumption of linearly elastic behavior means that

$$\sigma_{xz} = G(u_{,z} + w_{,x}) \tag{3.13}$$

$$\sigma_{yz} = G(v_{,z} + w_{,y}) \tag{3.14}$$

with G being the shear modulus of the elastomer. Using the displacement assumptions in Eqs. (3.1) to (3.3), the above equations become

$$\sigma_{xz} = -\frac{8G}{t^2}u_0 z \tag{3.15}$$

$$\sigma_{yz} = -\frac{8G}{t^2}v_0 z \tag{3.16}$$

Substitution of these into the equilibrium equations of Eqs. (3.11) and (3.12) leads to

$$p_{,x} = -\frac{8G}{t^2}u_0 \tag{3.17}$$

$$p_{,y} = -\frac{8G}{t^2}v_0 \tag{3.18}$$

Differentiating Eqs. (3.17) and (3.18) with respect to x and y, respectively, and then adding them up yield

$$p_{,xx} + p_{,yy} = -\frac{8G}{t^2}(u_{0,x} + v_{0,y}) \tag{3.19}$$

3.1.2 Equilibrium in Reinforcing Sheet

The internal forces acting in an infinitesimal $\mathrm{d}x$ by $\mathrm{d}y$ area of the reinforcing sheet is shown in Figure 3.2 where N_{xx} and N_{yy} are the normal forces per unit length in the x and y directions, respectively; N_{xy} is the in-plane shear force per unit length. These internal forces are related to the shear stresses, σ_{xz} and σ_{yz}, on the surfaces of the reinforcing sheet bonded to the top and bottom layers of elastomer through two equilibrium equations in the x and y directions

$$\mathrm{d}N_{xx}\mathrm{d}y + \mathrm{d}N_{xy}\mathrm{d}x + \left(\sigma_{xz}|_{z=-\frac{t}{2}} - \sigma_{xz}|_{z=\frac{t}{2}}\right)\mathrm{d}x\mathrm{d}y = 0 \tag{3.20}$$

$$\mathrm{d}N_{yy}\mathrm{d}x + \mathrm{d}N_{xy}\mathrm{d}y + \left(\sigma_{yz}|_{z=-\frac{t}{2}} - \sigma_{yz}|_{z=\frac{t}{2}}\right)\mathrm{d}x\mathrm{d}y = 0 \tag{3.21}$$

From Eqs. (3.15) and (3.16), we have the bonding shear stresses acting on the top surface of the reinforcing sheet

$$\sigma_{xz}|_{z=-\frac{t}{2}} = \frac{4G}{t}u_0 \quad ; \quad \sigma_{yz}|_{z=-\frac{t}{2}} = \frac{4G}{t}v_0 \tag{3.22}$$

and the bonding shear stresses acting on the bottom surface of the reinforcing sheet

$$\sigma_{xz}|_{z=\frac{t}{2}} = -\frac{4G}{t}u_0 \quad ; \quad \sigma_{yz}|_{z=\frac{t}{2}} = -\frac{4G}{t}v_0 \tag{3.23}$$

The equations of equilibrium in the reinforcing sheet in Eqs. (3.20) and (3.21) become

$$N_{xx,x} + N_{xy,y} = -\frac{8G}{t}u_0 \tag{3.24}$$

$$N_{yy,y} + N_{xy,x} = -\frac{8G}{t}v_0 \tag{3.25}$$

Combining these with the equilibrium equations of the elastomeric layer in Eqs. (3.17) and (3.18) to eliminate u_0 and v_0 gives

$$N_{xx,x} + N_{xy,y} = tp_{,x} \tag{3.26}$$

$$N_{yy,y} + N_{xy,x} = tp_{,y} \tag{3.27}$$

The displacements in the reinforcement are related to the internal normal forces through the linearly elastic strain-stress relation such that

$$u_{1,x} = \frac{1}{E_f}\left(\frac{N_{xx}}{t_f} - \nu\frac{N_{yy}}{t_f}\right) \tag{3.28}$$

$$v_{1,y} = \frac{1}{E_f}\left(\frac{N_{yy}}{t_f} - \nu\frac{N_{xx}}{t_f}\right) \tag{3.29}$$

where E_f and ν are the elastic modulus and Poisson's ratio of the reinforcement. By inversion, the normal forces are expressed in terms of the displacement components

$$N_{xx} = \frac{E_f t_f}{1-\nu^2}(u_{1,x} + \nu v_{1,y}) \tag{3.30}$$

$$N_{yy} = \frac{E_f t_f}{1-\nu^2}(v_{1,y} + \nu u_{1,x}) \tag{3.31}$$

The in-plane shear force has the following relation with the displacements

$$N_{xy} = \frac{E_f t_f}{2(1+\nu)}(u_{1,y} + v_{1,x}) \tag{3.32}$$

Substitution of Eqs. (3.30) to (3.32) into Eqs. (3.26) and (3.27) leads to

$$u_{1,xx} + \nu v_{1,yx} + \frac{1-\nu}{2}(u_{1,yy} + v_{1,xy}) = \frac{(1-\nu^2)t}{E_f t_f}p_{,x} \tag{3.33}$$

$$v_{1,yy} + \nu u_{1,xy} + \frac{1-\nu}{2}(u_{1,yx} + v_{1,xx}) = \frac{(1-\nu^2)t}{E_f t_f}p_{,y} \tag{3.34}$$

Differentiating Eqs. (3.33) and (3.34) with respect to x and y, respectively, and then adding them up yield

$$q_{,xx} + q_{,yy} = \frac{(1-\nu^2)t}{E_f t_f}(p_{,xx} + p_{,yy}) \tag{3.35}$$

in which, for clarification, q is denoted as

$$q = u_{1,x} + v_{1,y} \tag{3.36}$$

3.1.3 Governing Equation of Pressure

Combining Eq. (3.6) with Eq. (3.19) to eliminate the terms of u_0 and v_0 and using the definition of q in Eq. (3.36),

$$q = \epsilon_c + \frac{t^2}{12G}(p_{,xx} + p_{,yy}) \tag{3.37}$$

Substitution of this into Eq. (3.35) gives

$$p_{,xxxx} + 2p_{,xxyy} + p_{,yyyy} - \alpha^2(p_{,xx} + p_{,yy}) = 0 \tag{3.38}$$

in which α is defined as

$$\alpha = \sqrt{\frac{12G(1-\nu^2)}{E_f t_f t}} \tag{3.39}$$

To solve the partial differential equation of Eq. (3.38) for the pressure $p(x,y)$, we need the boundary conditions for $p(x,y)$. The normal stresses and shear stresses of the elastomer and the reinforcement are free at the edges, which gives

$$\sigma_{xx}(\pm a, y) = 0 \quad ; \quad \sigma_{xy}(\pm a, y) = 0 \quad ; \quad \sigma_{yy}(x, \pm b) = 0 \quad ; \quad \sigma_{xy}(x, \pm b) = 0 \tag{3.40}$$

and

$$N_{xx}(\pm a, y) = 0 \quad ; \quad N_{xy}(\pm a, y) = 0 \quad ; \quad N_{yy}(x, \pm b) = 0 \quad ; \quad N_{xy}(x, \pm b) = 0 \tag{3.41}$$

According to the assumption of pressure domination in Eq. (3.8), the stress boundary conditions of the elastomeric layer shown in Eq. (3.40) becomes

$$p(\pm a, y) = 0 \quad ; \quad p(x, \pm b) = 0 \tag{3.42}$$

3.1.4 Approximate Boundary Conditions

In Eq. (3.8), the in-plane shear stress of the elastomer, σ_{xy}, is assumed to be of order pt^2/l^2 and becomes negligible,

$$\sigma_{xy}(x,y) = G(u_{,y} + v_{,x}) \approx 0 \tag{3.43}$$

Substituting the displacement assumptions in Eqs. (3.1) and (3.2) into the above equation and taking integration through the thickness of the elastomeric layer lead to

$$\frac{2}{3}(u_{0,y} + v_{0,x}) + (u_{1,y} + v_{1,x}) \approx 0 \tag{3.44}$$

The last term, $u_{1,y} + v_{1,x}$, is equal to the in-plane shear strain of the reinforcement, which means that the in-plane shear strain of the reinforcement is of the order t^2/l^2 and the in-plane shear force of the reinforcement N_{xy} is negligible. Therefore, we can assume

$$N_{xy,x}(a, y) = 0 \quad ; \quad N_{xy,y}(x, b) = 0 \tag{3.45}$$

which give, from Eqs. (3.26) and (3.27),

$$N_{xx,x}(x, b) \approx t p_{,x}(x, b) \tag{3.46}$$

$$N_{yy,y}(a, y) \approx t p_{,y}(a, y) \tag{3.47}$$

We can find another equation relating the pressure of the elastomer with the internal normal forces of the reinforcement by adding Eq. (3.30) to Eq. (3.31), which gives

$$q = \frac{1 - \nu}{E_f t_f}(N_{xx} + N_{yy}) \tag{3.48}$$

and then combining this with Eq. (3.37) to eliminate q,

$$\frac{t^2}{12G}(p_{,xx} + p_{,yy}) = \frac{1 - \nu}{E_f t_f}(N_{xx} + N_{yy}) - \epsilon_c \tag{3.49}$$

From the boundary condition $p(\pm a, y) = 0$ in Eq. (3.42), $p_{,y}(\pm a, y) = 0$ which, when substituted into Eq. (3.47), gives $N_{yy}(\pm a, y)$ being constant. From the boundary conditions in Eq. (3.41), we know $N_{yy}(\pm a, \pm b) = 0$, thus

$$N_{yy}(\pm a, y) = 0 \tag{3.50}$$

Bringing this into Eq. (3.49) and using the boundary condition $N_{xx}(\pm a, y) = 0$ in Eq. (3.41) and $p_{,yy}(\pm a, y) = 0$ from $p(\pm a, y) = 0$ in Eq. (3.42),

$$p_{,xx}(\pm a, y) = -\frac{12G}{t^2}\epsilon_c \tag{3.51}$$

From the boundary condition $p(x, \pm b) = 0$ in Eq. (3.42), $p_{,x}(x, \pm b) = 0$ which, when substituted into Eq. (3.46), gives $N_{xx}(x, \pm b)$ being constant. From the boundary conditions in Eq. (3.41), we know that $N_{xx}(\pm a, \pm b) = 0$, thus

$$N_{xx}(x, \pm b) = 0 \tag{3.52}$$

Bringing this into Eq. (3.49) and using the boundary condition $N_{yy}(x, \pm b) = 0$ in Eq. (3.41) and $p_{,xx}(x, \pm b) = 0$ from $p(x, \pm b) = 0$ in Eq. (3.42),

$$p_{,yy}(x, \pm b) = -\frac{12G}{t^2}\epsilon_c \tag{3.53}$$

It should be noted that N_{xy} is not neglected when we derive the governing equation of the pressure in Eq. (3.38). To solve for pressure in this governing equation, we use the approximate boundary conditions of the pressure in Eqs. (3.51) and (3.53), which are derived by assuming that the derivatives of N_{xy} at the edges are negligible and stem from the assumption that pressure is dominant in the stress field of the elastomer.

3.1.5 Solution of Pressure

To solve for pressure, $p(x, y)$ is decomposed into two pressure components $p_1(x, y)$ and $p_2(x, y)$

$$p(x, y) = p_1(x, y) + p_2(x, y) \tag{3.54}$$

The boundary conditions for pressure in Eqs. (3.42), (3.51) and (3.53) are split into two sets. Each pressure component satisfies a different set of boundary conditions. The first set of boundary conditions is

$$p_1(\pm a, y) = 0 \quad ; \quad p_{1,xx}(\pm a, y) = 0 \tag{3.55}$$

$$p_1(x, \pm b) = 0 \quad ; \quad p_{1,yy}(x, \pm b) = -\frac{12G}{t^2}\epsilon_c \tag{3.56}$$

and the second set of boundary conditions is

$$p_2(\pm a, y) = 0 \quad ; \quad p_{2,xx}(\pm a, y) = -\frac{12G}{t^2}\epsilon_c \tag{3.57}$$

$$p_2(x, \pm b) = 0 \quad ; \quad p_{2,yy}(x, \pm b) = 0 \tag{3.58}$$

Adding the boundary conditions in Eqs. (3.55) to (3.58) yields the same boundary conditions defined in Eqs. (3.42), (3.51) and (3.53). The governing equations for these pressure components are the same as for Eq. (3.38), that is

$$p_{1,xxxx} + 2p_{1,xxyy} + p_{1,yyyy} - \alpha^2(p_{1,xx} + p_{1,yy}) = 0 \tag{3.59}$$

$$p_{2,xxxx} + 2p_{2,xxyy} + p_{2,yyyy} - \alpha^2(p_{2,xx} + p_{2,yy}) = 0 \tag{3.60}$$

Because the compression loading and the boundary conditions are symmetric with respect to the x axis and y axis, the pressure components have the following symmetric properties

$$p_1(x, y) = p_1(-x, y) = p_1(x, -y) \tag{3.61}$$

$$p_2(x, y) = p_2(-x, y) = p_2(x, -y) \tag{3.62}$$

According to the boundary conditions in Eq. (3.55) and the y-axis symmetric property in Eq. (3.61), the first pressure component can be assumed to be a cosine series of x

$$p_1(x, y) = \sum_{n=1}^{\infty} f_n(y) \cos \gamma_n x \tag{3.63}$$

where the amplitudes f_n are the functions of y and

$$\gamma_n = (n - \frac{1}{2})\frac{\pi}{a} \tag{3.64}$$

Substitution of Eq. (3.63) into Eq. (3.59) gives

$$\sum_{n=1}^{\infty} \left(\gamma_n^4 f_n - 2\gamma_n^2 f_{n,yy} + f_{n,yyyy} + \alpha^2\gamma_n^2 f_n - \alpha^2 f_{n,yy}\right) \cos \gamma_n x = 0 \tag{3.65}$$

which indicates

$$f_{n,yyyy} - (2\gamma_n^2 + \alpha^2) f_{n,yy} + \gamma_n^2(\gamma_n^2 + \alpha^2) f_n = 0 \tag{3.66}$$

The solution of this equation has the form

$$f_n(y) = C_1 \cosh \gamma_n y + C_2 \cosh \beta_n y + C_3 \sinh \gamma_n y + C_4 \sinh \beta_n y \tag{3.67}$$

where C_i are constants to be determined and

$$\beta_n = \sqrt{\gamma_n^2 + \alpha^2} \tag{3.68}$$

Using the x-axis symmetric property in Eq. (3.61), $C_3 = C_4 = 0$. The boundary condition $p_1(x, \pm b) = 0$ in Eq. (3.56) gives $f_n(\pm b) = 0$, from which

$$C_2 = -\frac{\cosh \gamma_n b}{\cosh \beta_n b} C_1 \tag{3.69}$$

Thus, $f_n(y)$ has the form

$$f_n(y) = A_n \left(\frac{\cosh \gamma_n y}{\cosh \gamma_n b} - \frac{\cosh \beta_n y}{\cosh \beta_n b} \right) \tag{3.70}$$

with $A_n = C_1 \cosh \gamma_n b$, from which the boundary condition for $p_{1,yy}(x, \pm b)$ in Eq. (3.56) becomes

$$\sum_{n=1}^{\infty} \alpha^2 A_n \cos \gamma_n x = \frac{12G}{t^2} \epsilon_c \tag{3.71}$$

By use of the following orthogonal property

$$\int_{-a}^{a} \cos \gamma_m x \cos \gamma_n x \mathrm{d}x = \begin{cases} a & \text{for} \quad n = m \\ 0 & \text{for} \quad n \neq m \end{cases} \tag{3.72}$$

Eq. (3.71) is reduced to

$$A_n = \epsilon_c \frac{24G}{\pi \alpha^2 t^2} \frac{(-1)^{n-1}}{(n - \frac{1}{2})} \tag{3.73}$$

Combining Eqs. (3.63), (3.70) and (3.73) leads to

$$p_1(x, y) = \epsilon_c \frac{24G}{\pi \alpha^2 t^2} \sum_{n=1}^{\infty} \frac{(-1)^{n-1}}{(n - \frac{1}{2})} \left(\frac{\cosh \gamma_n y}{\cosh \gamma_n b} - \frac{\cosh \beta_n y}{\cosh \beta_n b} \right) \cos \gamma_n x \tag{3.74}$$

According to the boundary conditions in Eq. (3.58) and the x-axis symmetric property in Eq. (3.62), the second pressure component can be assumed to be a cosine series of y

$$p_2(x,y) = \sum_{n=1}^{\infty} \bar{f}_n(x) \cos \bar{\gamma}_n y \tag{3.75}$$

where the amplitudes $\bar{f}_n$ are the functions of x and

$$\bar{\gamma}_n = (n - \frac{1}{2})\frac{\pi}{b} \tag{3.76}$$

Substitution of Eq. (3.75) into Eq. (3.60) gives

$$\sum_{n=1}^{\infty} \left(\bar{\gamma}_n^4 \bar{f}_n - 2\bar{\gamma}_n^2 \bar{f}_{n,xx} + \bar{f}_{n,xxxx} + \alpha^2 \bar{\gamma}_n^2 \bar{f}_n - \alpha^2 \bar{f}_{n,xx} \right) \cos \bar{\gamma}_n y = 0 \tag{3.77}$$

which indicates

$$\bar{f}_{n,xxxx} - (2\bar{\gamma}_n^2 + \alpha^2)\bar{f}_{n,xx} + \bar{\gamma}_n^2(\bar{\gamma}_n^2 + \alpha^2)\bar{f}_n = 0 \tag{3.78}$$

The solution of this equation has the form

$$\bar{f}_n(x) = \bar{C}_1 \cosh \bar{\gamma}_n x + \bar{C}_2 \cosh \bar{\beta}_n x + \bar{C}_3 \sinh \bar{\gamma}_n x + \bar{C}_4 \sinh \bar{\beta}_n x \tag{3.79}$$

where $\bar{C}_i$ are constants to be determined and

$$\bar{\beta}_n = \sqrt{\bar{\gamma}_n^2 + \alpha^2} \tag{3.80}$$

Using the y-axis symmetric property in Eq. (3.62), we have $\bar{C}_3 = \bar{C}_4 = 0$. The boundary condition $p_2(\pm a, y) = 0$ in Eq. (3.57) gives $\bar{f}_n(\pm a) = 0$, from which we have

$$\bar{C}_2 = -\frac{\cosh \bar{\gamma}_n a}{\cosh \bar{\beta}_n a} \bar{C}_1 \tag{3.81}$$

Thus, $\bar{f}_n(x)$ has the form

$$\bar{f}_n(x) = \bar{A}_n \left(\frac{\cosh \bar{\gamma}_n x}{\cosh \bar{\gamma}_n a} - \frac{\cosh \bar{\beta}_n x}{\cosh \bar{\beta}_n a} \right) \tag{3.82}$$

with $\bar{A}_n = \bar{C}_1 \cosh \bar{\gamma}_n a$, from which the boundary condition for $p_{2,xx}(\pm a, y)$ in Eq. (3.57) becomes

$$\sum_{n=1}^{\infty} \alpha^2 \bar{A}_n \cos \bar{\gamma}_n y = \frac{12G}{t^2} \epsilon_c \tag{3.83}$$

By use of the following orthogonal property

$$\int_{-b}^{b} \cos\bar{\gamma}_m y \cos\bar{\gamma}_n y \mathrm{d}y = \begin{cases} b & \text{for} \quad n = m \\ 0 & \text{for} \quad n \neq m \end{cases} \tag{3.84}$$

Eq. (3.83) is reduced to

$$\bar{A}_n = \epsilon_c \frac{24G}{\pi\alpha^2 t^2} \frac{(-1)^{n-1}}{(n-\frac{1}{2})} \tag{3.85}$$

Combining of Eqs. (3.75), (3.82) and (3.85) leads to

$$p_2(x,y) = \epsilon_c \frac{24G}{\pi\alpha^2 t^2} \sum_{n=1}^{\infty} \frac{(-1)^{n-1}}{(n-\frac{1}{2})} \left(\frac{\cosh\bar{\gamma}_n x}{\cosh\bar{\gamma}_n a} - \frac{\cosh\bar{\beta}_n x}{\cosh\bar{\beta}_n a} \right) \cos\bar{\gamma}_n y \tag{3.86}$$

Substitution of $p_1(x,y)$ in Eq. (3.74) and $p_2(x,y)$ in Eq. (3.86) into Eq. (3.54) gives the solution of the pressure $p(x,y)$

$$\begin{aligned} p(x,y) \;=\; & \epsilon_c \frac{24GS^2}{\pi(\alpha a)^2} \left(1+\frac{a}{b}\right)^2 \sum_{n=1}^{\infty} \frac{(-1)^{n-1}}{(n-\frac{1}{2})} \\ & \left[\left(\frac{\cosh\gamma_n y}{\cosh\gamma_n b} - \frac{\cosh\beta_n y}{\cosh\beta_n b} \right) \cos\gamma_n x + \left(\frac{\cosh\bar{\gamma}_n x}{\cosh\bar{\gamma}_n a} - \frac{\cosh\bar{\beta}_n x}{\cosh\bar{\beta}_n a} \right) \cos\bar{\gamma}_n y \right] \end{aligned} \tag{3.87}$$

in which S is the shape factor of the rectangular layer of the elastomer defined as

$$S = \frac{ab}{(a+b)t} \tag{3.88}$$

3.1.6 Effective Compressive Modulus

The compression stiffness of the isolator is determined by the effective compressive modulus E_c defined as

$$E_c = \frac{\sigma_c}{\epsilon_c} \tag{3.89}$$

where σ_c is the nominal compression stress which is equal to the resultant compression load P divided by the area $4ab$. Using the assumption in Eq. (3.8), the resultant compression load P has the form

$$P = -\int_{-b}^{b}\int_{-a}^{a} \sigma_{zz}\, \mathrm{d}x\mathrm{d}y \approx \int_{-b}^{b}\int_{-a}^{a} p(x,y)\, \mathrm{d}x\mathrm{d}y \tag{3.90}$$

which gives

$$E_c = \frac{1}{4ab\epsilon_c} \int_{-b}^{b} \int_{-a}^{a} p(x,y)\, \mathrm{d}x\mathrm{d}y \tag{3.91}$$

Bringing the pressure solution $p(x,y)$ in Eq. (3.87), the effective compressive modulus becomes

$$E_c = \frac{24GS^2}{\pi^2(\alpha a)^2}\left(1+\frac{a}{b}\right)^2 \sum_{n=1}^{\infty} \frac{1}{(n-\frac{1}{2})^2}\left(\frac{\tanh\gamma_n b}{\gamma_n b} - \frac{\tanh\beta_n b}{\beta_n b} + \frac{\tanh\bar{\gamma}_n a}{\bar{\gamma}_n a} - \frac{\tanh\bar{\beta}_n a}{\bar{\beta}_n a}\right) \tag{3.92}$$

If we denote a to be the length of the short side and b to be the length of the long side, the value of the aspect ratio a/b is between 0 and 1. When the aspect ratio a/b tends to zero, $\gamma_n b \to \infty$, $\beta_n b \to \infty$, $\bar{\beta}_n a \to \alpha a$ and $\bar{\gamma}_n a \to 0$ which makes

$$\frac{\tanh\bar{\gamma}_n a}{\bar{\gamma}_n a} = 1 \tag{3.93}$$

Using the following series equation

$$\sum_{n=1}^{\infty} \frac{1}{(n-\frac{1}{2})^2} = \frac{\pi^2}{2} \tag{3.94}$$

Eq. (3.92) is reduced to

$$E_c = \frac{12GS^2}{(\alpha a)^2}\left(1 - \frac{\tanh\alpha a}{\alpha a}\right) \tag{3.95}$$

which is the effective compressive modulus of the infinitely long strip isolator shown in Eq. (2.39).

When the stiffness of the reinforcement becomes rigid, $\alpha \to 0$. β_n defined in Eq. (3.68) can be approximated as a series of α

$$\beta_n \approx \gamma_n\left[1 + \frac{1}{2}\left(\frac{\alpha}{\gamma_n}\right)^2\right] \tag{3.96}$$

and $\tanh\beta_n b$ becomes

$$\tanh\beta_n b \approx \tanh\gamma_n b + \frac{\gamma_n b}{2\cosh^2\gamma_n b}\left(\frac{\alpha}{\gamma_n}\right)^2 \tag{3.97}$$

Similarly, $\bar{\beta}_n$ defined in Eq. (3.80) can be approximated as

$$\bar{\beta}_n \approx \bar{\gamma}_n\left[1 + \frac{1}{2}\left(\frac{\alpha}{\bar{\gamma}_n}\right)^2\right] \tag{3.98}$$

and $\tanh \bar{\beta}_n b$ becomes

$$\tanh \bar{\beta}_n b \approx \tanh \bar{\gamma}_n b + \frac{\bar{\gamma}_n b}{2 \cosh^2 \bar{\gamma}_n b} \left(\frac{\alpha}{\bar{\gamma}_n} \right)^2 \tag{3.99}$$

Substituting these approximations into Eq. (3.92) and neglecting the high-order terms of α, we have

$$E_c = \frac{12GS^2}{\pi^4} \left(1 + \frac{a}{b}\right)^2 \sum_{n=1}^{\infty} \frac{1}{(n - \frac{1}{2})^4} \left[\frac{\tanh \gamma_n b}{\gamma_n b} - \frac{1}{\cosh^2 \gamma_n b} + \frac{b^2}{a^2} \left(\frac{\tanh \bar{\gamma}_n a}{\bar{\gamma}_n a} - \frac{1}{\cosh^2 \bar{\gamma}_n a} \right) \right] \tag{3.100}$$

which is the effective compressive modulus of the rectangular layer of elastomer bonded to the rigid reinforcement.

From Eq. (3.92), it is known that the ratio $E_c/(GS^2)$ is a function of αa and the aspect ratio a/b. The variation of $E_c/(GS^2)$ with αa is plotted in Figure 3.3 for $a/b = 0$, 0.1, 0.2, 0.5 and 1, which shows that the effective compressive modulus decreases with increasing αa. To have a high compressive modulus, the value of αa must be small. The figure also reveals that a larger value of a/b produces a larger value of the effective compressive modulus. To test the convergence of the series solution in Eq. (3.92), the values of $E_c/(GS^2)$ are calculated using the first 1, 2, 5 and 10 terms and then finding the ratios of these values to the value using the first 50 terms. These ratios are plotted in Figure 3.4 as a function of αa for $a/b = 0.5$ and plotted in Figure 3.5 as a function of a/b for $\alpha a = 0.5$. The two figures show that the series solution in Eq. (3.92) converges very fast and that using the first 10 terms is enough to have an accurate solution, except when the aspect ratio a/b is very small.

For clarification, the in-plane stiffness of the reinforcement is defined as

$$k_f = \frac{E_f t_f}{1 - \nu^2} \tag{3.101}$$

From Eq. (3.39),

$$\alpha a = \frac{a}{t} \sqrt{12 \frac{Gt}{k_f}} \tag{3.102}$$

Figure 3.6 plots the ratio of the in-plane stiffness of the reinforcement to the shear stiffness of the elastomer, $K_f/(Gt)$, versus the ratio a/t for several αa values, which indicates that a small αa value is not necessary for high reinforcement stiffness; instead, it depends on the value of a/t. From Eq. (3.88), it is known that the shape factor S is the function of a/t and a/b, of which the range is from $S = 0.5a/t$ for the square layer to $S = a/t$ for the infinitely long layer. Substituting the shape factor S in Eq. (3.88) and αa in Eq. (3.102) into Eq. (3.92), the normalized effective compression modulus E_c/G is expressed as a function of the ratios a/b, a/t and $k_f/(Gt)$. When a/t tends to infinity, $\alpha a \to \infty$, $\beta_n b \to \infty$, $\bar{\beta}_n a \to \infty$, Eq. (3.92) becomes

$$E_c = \frac{2}{\pi^2}\frac{k_f}{t}\sum_{n=1}^{\infty}\frac{1}{(n-\frac{1}{2})^2}\left(\frac{\tanh\gamma_n b}{\gamma_n b}+\frac{\tanh\bar{\gamma}_n a}{\bar{\gamma}_n a}\right) \tag{3.103}$$

The curves of E_c/G versus $k_f/(Gt)$ are plotted in Figure 3.7 for $a/b = 0.5$ and several a/t values, which shows that the effective compressive modulus increases with an increase in the reinforcement stiffness until reaching the asymptotic value in Eq. (3.100). The curve of the smaller shape factor reaches the plateau at the smaller value of $k_f/(Gt)$. The curves of E_c/G versus a/t are plotted in Figure 3.8 for $a/b = 0.5$ and several $k_f/(Gt)$ values, which shows that the effective compressive modulus increases with the increasing shape factor until reaching the asymptotic value in Eq. (3.103). The curve of the smaller value of $k_f/(Gt)$ reaches a plateau at the smaller shape factor.

To study the variation of the effective compressive modulus with the aspect ratio a/b , the ratios of the compressive modulus of the rectangular layers with $a/b > 0$, shown in Eq. (3.92), to the compressive modulus of the infinitely long strip layer ($a/b = 0$), shown in Eq. (3.95), are plotted in Figure 3.9 for $\alpha a = 0$, 1, 2 and 4, which reveals that the effective compressive modulus is almost linearly varied with respect to the aspect ratio a/b. The ratio of E_c at $a/b = 1$ to E_c at $a/b = 0$ is plotted in Figure 3.10 as a function of αa between 0 and 5 which, utilizing the regression analysis,

can be fitted by the four-degree polynomial

$$g(\alpha a) = 0.41 + 0.026\alpha a + 0.074(\alpha a)^2 - 0.022(\alpha a)^3 + 0.0019(\alpha a)^4 \tag{3.104}$$

Assuming that the value of E_c is linearly varied between $a/b = 0$ and $a/b = 1$, an empirical formula for the effective compressive modulus of rectangular reinforced layers can be established from Eqs. (3.95) and (3.104)

$$\begin{aligned} E_c &= \frac{12GS^2}{(\alpha a)^2}\left(1 - \frac{\tanh \alpha a}{\alpha a}\right) \\ &\quad \left\{1 + \frac{a}{b}\left[-0.59 + 0.026\alpha a + 0.074(\alpha a)^2 - 0.022(\alpha a)^3 + 0.0019(\alpha a)^4\right]\right\} \end{aligned} \tag{3.105}$$

The errors of this empirical formula with respect to the exact formula in Eq. (3.92) are plotted in Figure 3.11 as a function of a/b for several values of αa and in Figure 3.12 as a function of αa for several values of a/b, which show that the maximum error is smaller than 4 percent. It should be noted that because the range of the αa values used in the regression analysis is between 0 and 5, the effective compressive modulus in Eq. (3.105) is only applicable to the range of $0 \leq \alpha a \leq 5$.

3.1.7 Stresses in Elastomer

When the pressure distribution in Eq. (3.87) is normalized with respect to the nominal compression stress $\sigma_c = E_c\epsilon_c$, the normalized pressure distribution $p(x,y)/(E_c\epsilon_c)$ can be expressed in terms of αa, a/b, x/a and y/b. A 3-D graph of the normalized pressure distribution for $\alpha a = 0.5$ and $a/b = 0.5$ is plotted in Figure 3.13, which shows that the center of the elastomeric layer has the highest pressure.

When α tends to zero, using Eqs. (3.96) and (3.98) and the following approximations

$$\cosh \beta_n y \approx \cosh \gamma_n y \left[1 + \frac{1}{2}\gamma_n y \tanh \gamma_n y \left(\frac{\alpha}{\gamma_n}\right)^2\right] \tag{3.106}$$

$$\cosh \bar{\beta}_n x \approx \cosh \bar{\gamma}_n x \left[1 + \frac{1}{2}\bar{\gamma}_n x \tanh \bar{\gamma}_n x \left(\frac{\alpha}{\bar{\gamma}_n}\right)^2\right] \tag{3.107}$$

Eq. (3.87) is reduced to

$$p(x,y) = \epsilon_c \frac{12GS^2}{\pi^2}\left(1+\frac{a}{b}\right)^2 \frac{b}{a}\sum_{n=1}^{\infty}\frac{(-1)^{n-1}}{(n-\frac{1}{2})^2}\left[\frac{\cosh\gamma_n y}{\cosh\gamma_n b}\left(\tanh\gamma_n b - \frac{y}{b}\tanh\gamma_n y\right)\cos\gamma_n x + \frac{\cosh\bar{\gamma}_n x}{\cosh\bar{\gamma}_n a}\left(\tanh\bar{\gamma}_n a - \frac{x}{a}\tanh\bar{\gamma}_n x\right)\cos\bar{\gamma}_n y\right] \tag{3.108}$$

which is the pressure distribution in the rectangular layer of elastomer bonded to the rigid reinforcement.

To study the effect of the flexibility of the reinforcement on the pressure distribution, the normalized pressure distributions along the x axis at $y = 0$ and along the y axis at $x = 0$ are plotted in Figures 3.14 and 3.15, respectively, for the aspect ratio $a/b = 0.5$ and $\alpha a = 0$, 1, 2 and 4, which show that decreasing the stiffness of the reinforcement makes the pressure distribution more uniform and reduces the maximum value at the center. For the elastomeric layers of different aspect ratios a/b, the distribution of the normalized pressure along the x axis at $y = 0$ is plotted in Figure 3.16 with $\alpha a = 0.5$, which reveals that the maximum value of the pressure becomes smaller as the layer has smaller value of a/b.

If τ_x and τ_y denote the shear stresses in the x and y directions, respectively, on the bonding surface between the elastomer and the reinforcement, from Eqs. (3.17), (3.18) and (3.22)

$$\tau_x(x,y) = \sigma_{xz}|_{z=-\frac{t}{2}} = -\frac{t}{2}p_{,x} \tag{3.109}$$

$$\tau_y(x,y) = \sigma_{yz}|_{z=-\frac{t}{2}} = -\frac{t}{2}p_{,y} \tag{3.110}$$

Substituting Eq. (3.87) into Eqs. (3.109) and (3.110), we have the bonding shear stresses as

$$\tau_x(x,y) = \epsilon_c \frac{12GS}{(\alpha a)^2}\left(1+\frac{a}{b}\right)\sum_{n=1}^{\infty}(-1)^n\left[-\left(\frac{\cosh\gamma_n y}{\cosh\gamma_n b} - \frac{\cosh\beta_n y}{\cosh\beta_n b}\right)\sin\gamma_n x + \frac{a}{b}\left(\frac{\sinh\bar{\gamma}_n x}{\cosh\bar{\gamma}_n a} - \frac{\bar{\beta}_n\sinh\bar{\beta}_n x}{\bar{\gamma}_n\cosh\bar{\beta}_n a}\right)\cos\bar{\gamma}_n y\right] \tag{3.111}$$

$$\tau_y(x,y) = \epsilon_c \frac{12GS}{(\alpha a)^2}\left(1+\frac{a}{b}\right)\sum_{n=1}^{\infty}(-1)^n\left[\left(\frac{\sinh\gamma_n y}{\cosh\gamma_n b} - \frac{\beta_n\sinh\beta_n y}{\gamma_n\cosh\beta_n b}\right)\cos\gamma_n x\right.$$

$$-\frac{a}{b}\left(\frac{\cosh\bar{\gamma}_n x}{\cosh\bar{\gamma}_n a}-\frac{\cosh\bar{\beta}_n x}{\cosh\bar{\beta}_n a}\right)\sin\bar{\gamma}_n y\Bigg] \tag{3.112}$$

When α tends to zero, using Eqs. (3.96), (3.98), (3.106) and (3.107) and the following approximations

$$\sinh\beta_n y \approx \sinh\gamma_n y\left[1+\frac{\gamma_n y}{2\tanh\gamma_n y}\left(\frac{\alpha}{\gamma_n}\right)^2\right] \tag{3.113}$$

$$\sinh\bar{\beta}_n x \approx \sinh\bar{\gamma}_n x\left[1+\frac{\bar{\gamma}_n x}{2\tanh\bar{\gamma}_n x}\left(\frac{\alpha}{\bar{\gamma}_n}\right)^2\right] \tag{3.114}$$

Eqs. (3.111) and (3.112) are reduced to

$$\begin{aligned}\tau_x(x,y) &= \epsilon_c\frac{6GS}{\pi}\left(1+\frac{a}{b}\right)\sum_{n=1}^{\infty}\frac{(-1)^n}{(n-\frac{1}{2})}\left\{-\frac{b}{a}\left(\tanh\gamma_n b-\frac{y}{b}\tanh\gamma_n y\right)\frac{\cosh\gamma_n y}{\cosh\gamma_n b}\sin\gamma_n x\right.\\ &\left.+\left[\left(\tanh\bar{\gamma}_n a-\frac{1}{\bar{\gamma}_n a}\right)\frac{\sinh\bar{\gamma}_n x}{\cosh\bar{\gamma}_n a}-\left(\frac{x}{a}\right)\frac{\cosh\bar{\gamma}_n x}{\cosh\bar{\gamma}_n a}\right]\cos\bar{\gamma}_n y\right\}\end{aligned} \tag{3.115}$$

$$\begin{aligned}\tau_y(x,y) &= \epsilon_c\frac{6GS}{\pi}\left(1+\frac{a}{b}\right)\sum_{n=1}^{\infty}\frac{(-1)^n}{(n-\frac{1}{2})}\left\{-\left(\tanh\bar{\gamma}_n a-\frac{x}{a}\tanh\bar{\gamma}_n x\right)\frac{\cosh\bar{\gamma}_n x}{\cosh\bar{\gamma}_n a}\sin\bar{\gamma}_n y\right.\\ &\left.+\frac{b}{a}\left[\left(\tanh\gamma_n b-\frac{1}{\gamma_n b}\right)\frac{\sinh\gamma_n y}{\cosh\gamma_n b}-\left(\frac{y}{b}\right)\frac{\cosh\gamma_n y}{\cosh\gamma_n b}\right]\cos\gamma_n x\right\}\end{aligned} \tag{3.116}$$

which are the bonding shear stresses for the rigid reinforcement.

When the bonding shear stresses are normalized with respect to the nominal compression stress, the quantities $\tau_x S/(E_c\epsilon_c)$ and $\tau_y S/(E_c\epsilon_c)$ can be expressed in terms of αa, a/b, x/a and y/b. The distributions of these two quantities are plotted as 3-D graphs in Figures 3.17 and 3.18, respectively, for $\alpha a = 0.5$ and $a/b = 0.5$. These figures indicate that the compression load makes the reinforcement in the stretch condition. The distributions of $\tau_x S/(E_c\epsilon_c)$ along the x axis at $y = 0$ and $\tau_y S/(E_c\epsilon_c)$ along the y axis at $x = 0$ are plotted in Figures 3.19 and 3.20, respectively, for the aspect ratio $a/b = 0.5$ and $\alpha a = 0$, 1, 2 and 4, which shows that the flexibility of the reinforcement makes the distribution of the bonding shear stresses more concentrated on the edges and increases the maximum values at the edges.

The shear resultant $\tau(x,y)$ is defined as

$$\tau(x,y) = \sqrt{\tau_x^2(x,y)+\tau_y^2(x,y)} \tag{3.117}$$

The distribution of $\tau(x,y)S/(E_c\epsilon_c)$ is plotted as a 3-D graph in Figure 3.21 for $\alpha a = 0.5$ and $a/b = 0.5$, which shows that the maximum shear resultant locates at $x = \pm a$ and $y = 0$. The normalized maximum shear resultant, $\tau(a,0)/(E_c\epsilon_c)$, is plotted as a function of the stiffness ratio $k_f/(Gt)$ in Figure 3.22 for $a/b = 0.5$ and several a/t values, and in Figure 3.23 for $a/t = 10$ and several a/b values, which show that the maximum shear resultant decreases with increasing the stiffness ratio; the lower shape factor always has a higher shear resultant.

3.1.8 Solution for Rigid Reinforcement

Although the effective compressive modulus of the rigid-reinforced elastomer is derived from the asymptotic solution of the flexible-reinforced elastomer by setting $\alpha \to 0$ in the previous sections, the effective compressive modulus of the rigid-reinforced elastomer can be directly solved and is described in this section.

For a layer of elastomer in a rectangular isolator under compression loading as shown in Figure 3.1, if the top and bottom surfaces of the elastomeric layer are bonded to rigid reinforcements, the displacements of the elastomer can be assumed as

$$u(x,y,z) = u_0(x,y)\left(1 - \frac{4z^2}{t^2}\right) \tag{3.118}$$

$$v(x,y,z) = v_0(x,y)\left(1 - \frac{4z^2}{t^2}\right) \tag{3.119}$$

$$w(x,y,z) = w(z) \tag{3.120}$$

Substituting these into the displacement constraint in Eq. (3.4), attributed to the assumption of incompressibility of the elastomer, and then taking the integration through the thickness lead to

$$\frac{2}{3}(u_{0,x} + v_{0,y}) = \epsilon_c \tag{3.121}$$

where ϵ_c is the nominal compression strain defined in Eq. (3.7).

Attributed to the assumption that the stress state in the elastomer is dominated by the internal pressure p, the equilibrium equations in the x and y directions defined in Eqs. (3.9) and (3.10) are reduced to

$$-p_{,x} + \sigma_{xz,z} = 0 \tag{3.122}$$

$$-p_{,y} + \sigma_{yz,z} = 0 \tag{3.123}$$

in which σ_{xz} and σ_{yz} are the shear stress components of the elastomer defined in Eqs. (3.13) and (3.14). Using the displacement assumptions in Eqs. (3.118) to (3.120), the shear stress components become

$$\sigma_{xz} = -\frac{8G}{t^2}u_0 z \tag{3.124}$$

$$\sigma_{yz} = -\frac{8G}{t^2}v_0 z \tag{3.125}$$

Substitution of these into Eqs. (3.122) and (3.123) gives

$$p_{,x} = -\frac{8G}{t^2}u_0 \tag{3.126}$$

$$p_{,y} = -\frac{8G}{t^2}v_0 \tag{3.127}$$

Differentiating Eqs. (3.126) and (3.127) with respect to x and y, respectively, then adding them up and applying the relation in Eq. (3.121) yield

$$p_{,xx} + p_{,yy} = -\frac{12G}{t^2}\epsilon_c \tag{3.128}$$

According to the boundary condition $p(\pm a, y) = 0$ and the symmetric property $p(x, y) = p(-x, y)$, the pressure p can be assumed to be a cosine series of x

$$p(x, y) = \sum_{n=1}^{\infty} f_n(y) \cos \gamma_n x \tag{3.129}$$

where the amplitude f_n is a function of y, and γ_n is defined in Eq. (3.64). Substitution of Eq. (3.129) into Eq. (3.128) gives

$$\sum_{n=1}^{\infty} \left(f_{n,yy} - \gamma_n^2 f_n\right) \cos \gamma_n x = -\frac{12G}{t^2}\epsilon_c \tag{3.130}$$

which, by use of the orthogonal property in Eq. (3.72), can be reduced to

$$f_{n,yy} - \gamma_n^2 f_n = -\frac{24G}{t^2}\epsilon_c \frac{(-1)^{n-1}}{(n-\frac{1}{2})\pi} \tag{3.131}$$

The boundary condition $p(x, \pm b) = 0$ and the symmetric property $p(x, y) = p(x, -y)$ give $f_n(\pm b) = 0$ and $f_n(y) = f_n(-y)$, from which $f_n(y)$ can be solved and the pressure p has the form

$$p(x, y) = \epsilon_c \frac{24GS^2}{\pi^3}\left(1 + \frac{a}{b}\right)^2 \sum_{n=1}^{\infty} \frac{(-1)^{n-1}}{(n-\frac{1}{2})^3}\left(1 - \frac{\cosh \gamma_n y}{\cosh \gamma_n b}\right)\cos \gamma_n x \tag{3.132}$$

where S is the shape factor defined in Eq. (3.88). This series expression for the pressure distribution is different from the expression depicted in Eq. (3.108), but the numerical results of the two equations are the same. The series expression in Eq. (3.108) exhibits second-order convergence, whereas Eq. (3.132) has third-order convergence.

Substituting Eq. (3.132) into the formula of the effective compressive modulus in Eq. (3.91), we have

$$E_c = \frac{24GS^2}{\pi^4}\left(1 + \frac{a}{b}\right)^2 \sum_{n=1}^{\infty} \frac{1}{(n-\frac{1}{2})^4}\left(1 - \frac{\tanh \gamma_n b}{\gamma_n b}\right) \tag{3.133}$$

Although the above series expression is different from the expression depicted in Eq. (3.100), the numerical results of the two equations are the same. To compare the convergence of the series solutions, the ratios of the values using the first 1 and 2 terms to the value of the first 50 terms are calculated from Eqs. (3.100) and (3.133) and are plotted in Figure 3.24 as a function of the aspect ratio a/b. The figure reveals that when a/b is small, the convergence rate of Eq. (3.133) is much faster than that of Eq. (3.100); when a/b is close to unity, the convergence rate of Eq. (3.100) becomes better than Eq. (3.133).

When the aspect ratio a/b tends to zero, $\gamma_n b \to \infty$. Using the following series equation

$$\sum_{n=1}^{\infty} \frac{1}{(n-\frac{1}{2})^4} = \frac{\pi^4}{6} \tag{3.134}$$

Eq. (3.133) is reduced to

$$E_c = 4GS^2 \tag{3.135}$$

which is the effective compressive modulus of the infinitely long strip of elastomer bonded to rigid reinforcements shown in Eq. (2.42).

From Eqs. (3.124) to (3.127), we have the shear stresses on the bonding surface between the elastomer and the reinforcement

$$\tau_x(x,y) = \sigma_{xz}|_{z=-\frac{t}{2}} = -\frac{t}{2}p_{,x} \tag{3.136}$$

$$\tau_y(x,y) = \sigma_{yz}|_{z=-\frac{t}{2}} = -\frac{t}{2}p_{,y} \tag{3.137}$$

Substitution of Eq. (3.132) into these leads to

$$\tau_x(x,y) = \epsilon_c \frac{12GS}{\pi^2}\left(1+\frac{a}{b}\right)\sum_{n=1}^{\infty}\frac{(-1)^{n-1}}{(n-\frac{1}{2})^2}\left(1-\frac{\cosh\gamma_n y}{\cosh\gamma_n b}\right)\sin\gamma_n x \tag{3.138}$$

$$\tau_y(x,y) = \epsilon_c \frac{12GS}{\pi^2}\left(1+\frac{a}{b}\right)\sum_{n=1}^{\infty}\frac{(-1)^{n-1}}{(n-\frac{1}{2})^2}\left(\frac{\sinh\gamma_n y}{\cosh\gamma_n b}\right)\cos\gamma_n x \tag{3.139}$$

Although the series expressions of the above two equations are different from the expressions depicted in Eqs. (3.115) and (3.116), the numerical results of the two sets of equations are the same.

3.2 Bending Stiffness of Rectangular Isolators

3.2.1 Governing Equation of Pressure

For a layer of elastomer in a rectangular isolator as shown in Figure 3.25, the reinforcements bonded to the top and bottom surfaces of the elastomeric layer are subjected to a pure bending moment M and rotate about the y axes. Assume the reinforcements remain planar, so that the rotation forms an angle ϕ between the reinforcing sheets and is symmetric to the x-y plane. Following the same kinematic assumptions used in the previous sections for the compression stiffness, the displacement field of the elastomer is given by

$$u(x,y,z) = u_0(x,y)\left(1-\frac{4z^2}{t^2}\right) + u_1(x,y) \tag{3.140}$$

$$v(x,y,z) = v_0(x,y)\left(1 - \frac{4z^2}{t^2}\right) + v_1(x,y) \tag{3.141}$$

$$w(x,y,z) = \frac{1}{\rho}xz \tag{3.142}$$

in which ρ is the radius of the bending curvature defined as

$$\rho = \frac{t}{\phi} \tag{3.143}$$

Substituting Eqs. (3.140) to (3.142) into the constraint of incompressibility of the elastomer in Eq. (3.4) and then integrating it through the thickness of the elastomeric layer from $z = -t/2$ to $z = t/2$ lead to

$$\frac{2}{3}(u_{0,x} + v_{0,y}) + u_{1,x} + v_{1,y} = -\frac{1}{\rho}x \tag{3.144}$$

Substitution of Eqs. (3.140) to (3.142) into the shear stress components of elastomer σ_{xz} and σ_{yz} defined in Eqs. (3.13) and (3.14) gives

$$\sigma_{xz} = \left(-\frac{8G}{t^2}u_0 + \frac{G}{\rho}\right)z \tag{3.145}$$

$$\sigma_{yz} = -\frac{8G}{t^2}v_0 z \tag{3.146}$$

Bringing these into the equilibrium equations of elastomer in Eqs. (3.11) and (3.12), which have been simplified by assuming that the pressure is dominated in the stress field of elastomer, leads to

$$p_{,x} = -\frac{8G}{t^2}u_0 + \frac{G}{\rho} \tag{3.147}$$

$$p_{,y} = -\frac{8G}{t^2}v_0 \tag{3.148}$$

Differentiating Eqs. (3.147) and (3.148) with respect to x and y, respectively, and then adding them up yield

$$p_{,xx} + p_{,yy} = -\frac{8G}{t^2}(u_{0,x} + v_{0,y}) \tag{3.149}$$

which is the same as Eq. (3.19) used for the compression stiffness. Combination of Eqs. (3.144) and (3.149) to eliminate the terms of u_0 and v_0 gives

$$q = -\frac{1}{\rho}x + \frac{t^2}{12G}(p_{,xx} + p_{,yy}) \tag{3.150}$$

where q has been defined in Eq. (3.36).

Substituting the shear stresses σ_{xz} and σ_{yz} in Eqs. (3.145) and (3.146) into the equilibrium equations of the reinforcement in Eqs. (3.20) and (3.21), we have

$$N_{xx,x} + N_{xy,y} = -\frac{8G}{t}u_0 + \frac{Gt}{\rho} \tag{3.151}$$

$$N_{yy,y} + N_{xy,x} = -\frac{8G}{t}v_0 \tag{3.152}$$

Combination of these with the equilibrium equations of the elastomer in Eqs. (3.147) and (3.148), respectively, leads to

$$N_{xx,x} + N_{xy,y} = tp_{,x} \tag{3.153}$$

$$N_{yy,y} + N_{xy,x} = tp_{,y} \tag{3.154}$$

The above two equations are the same as Eqs. (3.26) and (3.27) used for the compression stiffness. Therefore, when bringing the force-displacement relations of the reinforcement in Eqs. (3.30) to (3.32) into the above two equations, we obtain the same equation as Eq. (3.35)

$$q_{,xx} + q_{,yy} = \frac{(1-\nu^2)t}{E_f t_f}(p_{,xx} + p_{,yy}) \tag{3.155}$$

Substituting Eq. (3.150) into the above equation, we have

$$p_{,xxxx} + 2p_{,xxyy} + p_{,yyyy} - \alpha^2(p_{,xx} + p_{,yy}) = 0 \tag{3.156}$$

which is the same form of the pressure governing equation for the compression stiffness in Eq. (3.38).

3.2.2 Boundary Conditions of Pressure

A relation between the pressure of the elastomer and the normal forces of the reinforcement is established by substituting Eq. (3.150) into the displacement-force relation of the reinforcement in Eq. (3.48), which gives

$$\frac{t^2}{12G}(p_{,xx} + p_{,yy}) = \frac{1-\nu}{E_f t_f}(N_{xx} + N_{yy}) + \frac{1}{\rho}x \tag{3.157}$$

The normal stresses and shear stresses of the elastomer and the reinforcement are free at the edges, which gives the same boundary conditions as shown in Eqs. (3.40) and (3.41). To find the boundary conditions for the pressure, as discussed in Section 3.1.4, the in-plane shear force N_{xy} at the edges of the reinforcement is assumed to satisfy the conditions in Eq. (3.45), from which we find out that $N_{yy}(x,y)$ satisfies the condition in Eq. (3.50) and that $N_{xx}(x,y)$ satisfies the condition in Eq. (3.52).

From the boundary conditions in Eq. (3.40), the pressure domination of the elastomer gives

$$p(\pm a, y) = 0 \quad ; \quad p(x, \pm b) = 0 \tag{3.158}$$

Substituting $p(\pm a, y) = 0$, $N_{xx}(\pm a, y) = 0$ in Eq. (3.41) and $N_{yy}(\pm a, y) = 0$ in Eq. (3.50) into Eq. (3.157), we have

$$p_{,xx}(\pm a, y) = \pm \frac{12G}{t^2}\frac{a}{\rho} \tag{3.159}$$

Substituting $p(x, \pm b) = 0$, $N_{xx}(x, \pm b) = 0$ in Eq. (3.52) and $N_{yy}(x, \pm b) = 0$ in Eq. (3.41) into Eq. (3.157), we have

$$p_{,yy}(x, \pm b) = \frac{12G}{t^2}\frac{1}{\rho}x \tag{3.160}$$

The pressure $p(x,y)$ is solved by superposing the two pressure components $p_1(x,y)$ and $p_2(x,y)$

$$p(x,y) = p_1(x,y) + p_2(x,y) \tag{3.161}$$

The boundary conditions for the pressure in Eqs. (3.158), (3.159) and (3.160) are split into two

sets. Corresponding to the pressure component p_1, the first set of boundary conditions is

$$p_1(\pm a, y) = 0 \quad ; \quad p_{1,xx}(\pm a, y) = 0 \tag{3.162}$$

$$p_1(x, \pm b) = 0 \quad ; \quad p_{1,yy}(x, \pm b) = \frac{12G}{t^2}\frac{1}{\rho}x \tag{3.163}$$

Corresponding to the pressure component p_2, the second set of boundary conditions is

$$p_2(\pm a, y) = 0 \quad ; \quad p_{2,xx}(\pm a, y) = \pm\frac{12G}{t^2}\frac{a}{\rho} \tag{3.164}$$

$$p_2(x, \pm b) = 0 \quad ; \quad p_{2,yy}(x, \pm b) = 0 \tag{3.165}$$

The governing equations for the pressure components p_1 and p_2 are the same as Eq. (3.156), that is

$$p_{1,xxxx} + 2p_{1,xxyy} + p_{1,yyyy} - \alpha^2(p_{1,xx} + p_{1,yy}) = 0 \tag{3.166}$$

$$p_{2,xxxx} + 2p_{2,xxyy} + p_{2,yyyy} - \alpha^2(p_{2,xx} + p_{2,yy}) = 0 \tag{3.167}$$

3.2.3 Solution of Pressure

Because the loading and the boundary conditions are symmetric with respect to the x axis and anti-symmetric with respect to the y axis, the pressure components have the following properties

$$p_1(x, y) = -p_1(-x, y) = p_1(x, -y) \tag{3.168}$$

$$p_2(x, y) = -p_2(-x, y) = p_2(x, -y) \tag{3.169}$$

According to the boundary conditions in Eq. (3.162) and the y-axis anti-symmetric property in Eq. (3.168), the first pressure component can be assumed to be a sine series of x

$$p_1(x, y) = \sum_{n=1}^{\infty} f_n(y) \sin \tilde{\gamma}_n x \tag{3.170}$$

where the amplitudes f_n are the functions of y and

$$\tilde{\gamma}_n = n\frac{\pi}{a} \tag{3.171}$$

Substitution of Eq. (3.170) into Eq. (3.166) gives

$$\sum_{n=1}^{\infty}\left(\tilde{\gamma}_n^4 f_n - 2\tilde{\gamma}_n^2 f_{n,yy} + f_{n,yyyy} + \alpha^2\tilde{\gamma}_n^2 f_n - \alpha^2 f_{n,yy}\right)\sin\tilde{\gamma}_n x = 0 \tag{3.172}$$

which indicates

$$f_{n,yyyy} - (2\tilde{\gamma}_n^2 + \alpha^2)f_{n,yy} + \tilde{\gamma}_n^2(\tilde{\gamma}_n^2 + \alpha^2)f_n = 0 \tag{3.173}$$

The solution of this equation has the form

$$f_n(y) = C_1\cosh\tilde{\gamma}_n y + C_2\cosh\tilde{\beta}_n y + C_3\sinh\tilde{\gamma}_n y + C_4\sinh\tilde{\beta}_n y \tag{3.174}$$

where C_i are constants to be determined and

$$\tilde{\beta}_n = \sqrt{\tilde{\gamma}_n^2 + \alpha^2} \tag{3.175}$$

Using the x-axis symmetric property in Eq. (3.168), $C_3 = C_4 = 0$. The boundary condition $p_1(x, \pm b) = 0$ in Eq. (3.163) gives $f_n(\pm b) = 0$, from which we have

$$C_2 = -\frac{\cosh\tilde{\gamma}_n b}{\cosh\tilde{\beta}_n b}C_1 \tag{3.176}$$

Thus, $f_n(y)$ has the form

$$f_n(y) = A_n\left(\frac{\cosh\tilde{\gamma}_n y}{\cosh\tilde{\gamma}_n b} - \frac{\cosh\tilde{\beta}_n y}{\cosh\tilde{\beta}_n b}\right) \tag{3.177}$$

with $A_n = C_1\cosh\tilde{\gamma}_n b$, from which the boundary condition for $p_{1,yy}(x, \pm b)$ in Eq. (3.163) becomes

$$\sum_{n=1}^{\infty}\alpha^2 A_n\sin\tilde{\gamma}_n x = -\frac{12G}{t^2}\frac{1}{\rho}x \tag{3.178}$$

By use of the following orthogonal property

$$\int_{-a}^{a}\sin\tilde{\gamma}_m x\sin\tilde{\gamma}_n x\mathrm{d}x = \begin{cases} a & \text{for} \quad n = m \\ 0 & \text{for} \quad n \neq m \end{cases} \tag{3.179}$$

Eq. (3.178) is reduced to

$$A_n = \frac{a}{\rho}\frac{24G}{\pi\alpha^2 t^2}\frac{(-1)^n}{n} \tag{3.180}$$

Combination of Eqs. (3.170), (3.177) and (3.180) leads to

$$p_1(x,y) = \frac{a}{\rho}\frac{24G}{\pi\alpha^2 t^2}\sum_{n=1}^{\infty}\frac{(-1)^n}{n}\left(\frac{\cosh\tilde{\gamma}_n y}{\cosh\tilde{\gamma}_n b} - \frac{\cosh\tilde{\beta}_n y}{\cosh\tilde{\beta}_n b}\right)\sin\tilde{\gamma}_n x \tag{3.181}$$

According to the boundary conditions in Eq. (3.165) and the x-axis symmetric property in Eq. (3.169), the second pressure component can be assumed to be a cosine series of y

$$p_2(x,y) = \sum_{n=1}^{\infty}\bar{f}_n(x)\cos\bar{\gamma}_n y \tag{3.182}$$

where the amplitudes $\bar{f}_n$ are the functions of x and $\bar{\gamma}_n$ has been defined in Eq. (3.76). Substitution of Eq. (3.182) into Eq. (3.167) gives

$$\sum_{n=1}^{\infty}\left(\bar{\gamma}_n^4\bar{f}_n - 2\bar{\gamma}_n^2\bar{f}_{n,xx} + \bar{f}_{n,xxxx} + \alpha^2\bar{\gamma}_n^2\bar{f}_n - \alpha^2\bar{f}_{n,xx}\right)\cos\bar{\gamma}_n y = 0 \tag{3.183}$$

which indicates

$$\bar{f}_{n,xxxx} - (2\bar{\gamma}_n^2 + \alpha^2)\bar{f}_{n,xx} + \bar{\gamma}_n^2(\bar{\gamma}_n^2 + \alpha^2)\bar{f}_n = 0 \tag{3.184}$$

The solution of this equation has the form

$$\bar{f}_n(x) = \bar{C}_1\cosh\bar{\gamma}_n x + \bar{C}_2\cosh\bar{\beta}_n x + \bar{C}_3\sinh\bar{\gamma}_n x + \bar{C}_4\sinh\bar{\beta}_n x \tag{3.185}$$

where $\bar{C}_i$ are constants to be determined and $\bar{\beta}_n$ has been defined in Eq. (3.80). Using the y-axis anti-symmetric property in Eq. (3.169), $\bar{C}_1 = \bar{C}_2 = 0$. The boundary condition $p_2(\pm a, y) = 0$ in Eq. (3.164) gives $\bar{f}_n(\pm a) = 0$, from which

$$\bar{C}_4 = -\frac{\sinh\bar{\gamma}_n a}{\sinh\bar{\beta}_n a}\bar{C}_3 \tag{3.186}$$

Thus, $\bar{f}_n(x)$ has the form

$$\bar{f}_n(x) = \bar{A}_n\left(\frac{\sinh\bar{\gamma}_n x}{\sinh\bar{\gamma}_n a} - \frac{\sinh\bar{\beta}_n x}{\sinh\bar{\beta}_n a}\right) \tag{3.187}$$

with $\bar{A}_n = \bar{C}_3\sinh\bar{\gamma}_n a$, from which the boundary condition for $p_{2,xx}(\pm a, y)$ in Eq. (3.164) becomes

$$\sum_{n=1}^{\infty}\alpha^2\bar{A}_n\cos\bar{\gamma}_n y = -\frac{12G}{t^2}\frac{a}{\rho} \tag{3.188}$$

By use of the orthogonal property in Eq. (3.84), this can be reduced to

$$\bar{A}_n = \frac{a}{\rho}\frac{24G}{\pi\alpha^2 t^2}\frac{(-1)^n}{(n-\frac{1}{2})} \tag{3.189}$$

Combination of Eqs. (3.182), (3.187) and (3.189) leads to

$$p_2(x,y) = \frac{a}{\rho}\frac{24G}{\pi\alpha^2 t^2}\sum_{n=1}^{\infty}\frac{(-1)^n}{(n-\frac{1}{2})}\left(\frac{\sinh\bar{\gamma}_n x}{\sinh\bar{\gamma}_n a} - \frac{\sinh\bar{\beta}_n x}{\sinh\bar{\beta}_n a}\right)\cos\bar{\gamma}_n y \tag{3.190}$$

Substitution of $p_1(x,y)$ in Eq. (3.181) and $p_2(x,y)$ in Eq. (3.190) into Eq. (3.161) gives the solution of the pressure $p(x,y)$

$$\begin{aligned} p(x,y) \;=\; & \frac{a}{\rho}\frac{24GS^2}{\pi(\alpha a)^2}\left(1+\frac{a}{b}\right)^2\sum_{n=1}^{\infty}(-1)^n \\ & \left[\left(\frac{\cosh\tilde{\gamma}_n y}{\cosh\tilde{\gamma}_n b} - \frac{\cosh\tilde{\beta}_n y}{\cosh\tilde{\beta}_n b}\right)\frac{\sin\tilde{\gamma}_n x}{n} + \left(\frac{\sinh\bar{\gamma}_n x}{\sinh\bar{\gamma}_n a} - \frac{\sinh\bar{\beta}_n x}{\sinh\bar{\beta}_n a}\right)\frac{\cos\bar{\gamma}_n y}{\left(n-\frac{1}{2}\right)}\right] \end{aligned} \tag{3.191}$$

in which S is the shape factor of the rectangular layer of the elastomer defined in Eq. (3.88).

3.2.4 Effective Bending Modulus

The effective bending stiffness $(EI)_{eff}$ of the isolator is defined as

$$(EI)_{eff} = \rho M \tag{3.192}$$

Using the assumption of pressure domination in Eq. (3.8), the bending moment M is expressed as

$$M = \int_{-b}^{b}\int_{-a}^{a}\sigma_{zz}x\mathrm{d}x\mathrm{d}y \approx -\int_{-b}^{b}\int_{-a}^{a}p(x,y)x\mathrm{d}x\mathrm{d}y \tag{3.193}$$

For clarification, we define the effective bending modulus as

$$E_b = \frac{(EI)_{eff}}{I_y} \tag{3.194}$$

where I_y is the moment of inertia of the rectangular area about the y axis, defined as

$$I_y = \frac{4}{3}a^3 b \tag{3.195}$$

By substituting the expression of $p(x,y)$ in Eq. (3.191) into Eq. (3.193), the effective bending modulus becomes

$$E_b = \frac{72GS^2}{\pi^2(\alpha a)^2}\left(1+\frac{a}{b}\right)^2 \sum_{n=1}^{\infty}\left\{\frac{1}{n^2}\left(\frac{\tanh\tilde{\gamma}_n b}{\tilde{\gamma}_n b}-\frac{\tanh\tilde{\beta}_n b}{\tilde{\beta}_n b}\right)\right.$$
$$\left.+\frac{1}{(n-\frac{1}{2})^2}\left[\frac{1}{\bar{\gamma}_n a\tanh\bar{\gamma}_n a}-\frac{1}{(\bar{\gamma}_n a)^2}-\frac{1}{\bar{\beta}_n a\tanh\bar{\beta}_n a}+\frac{1}{(\bar{\beta}_n a)^2}\right]\right\} \tag{3.196}$$

When the aspect ratio a/b tends to zero, $\tilde{\gamma}_n b \to \infty$, $\tilde{\beta}_n b \to \infty$, $\bar{\beta}_n a \to \alpha a$ and $\bar{\gamma}_n a \to 0$ which makes

$$\frac{1}{\bar{\gamma}_n a\tanh\bar{\gamma}_n a}-\frac{1}{(\bar{\gamma}_n a)^2}=\frac{1}{3} \tag{3.197}$$

Using the series equation in Eq. (3.94), Eq. (3.196) is reduced to

$$E_b = \frac{36GS^2}{(\alpha a)^4}\left(1+\frac{1}{3}(\alpha a)^2-\frac{\alpha a}{\tanh\alpha a}\right) \tag{3.198}$$

which is the effective bending modulus of the infinitely long strip isolator shown in Eq. (2.81).

When the stiffness of the reinforcement becomes rigid, $\alpha \to 0$. Similar to the approximations of $\bar{\beta}_n$ in Eqs. (3.98) and (3.99), $\tilde{\beta}_n$ defined in Eq. (3.175) can be approximated as

$$\tilde{\beta}_n \approx \tilde{\gamma}_n\left[1+\frac{1}{2}\left(\frac{\alpha}{\tilde{\gamma}_n}\right)^2\right] \tag{3.199}$$

and $\tanh\tilde{\beta}_n b$ becomes

$$\tanh\tilde{\beta}_n b \approx \tanh\tilde{\gamma}_n b+\frac{\tilde{\gamma}_n b}{2\cosh^2\tilde{\gamma}_n b}\left(\frac{\alpha}{\tilde{\gamma}_n}\right)^2 \tag{3.200}$$

Substituting these approximations into Eq. (3.196) and neglecting the high-order terms of α,

$$E_b = \frac{36GS^2}{\pi^4}\left(1+\frac{a}{b}\right)^2 \sum_{n=1}^{\infty}\left\{\frac{1}{n^4}\left(\frac{\tanh\tilde{\gamma}_n b}{\tilde{\gamma}_n b}-\frac{1}{\cosh^2\tilde{\gamma}_n b}\right)\right.$$
$$\left.+\frac{1}{(n-\frac{1}{2})^4}\left(\frac{b}{a}\right)^2\left[\frac{1}{\bar{\gamma}_n a\tanh\bar{\gamma}_n a}+\frac{1}{\sinh^2\bar{\gamma}_n a}-\frac{2}{(\bar{\gamma}_n a)^2}\right]\right\} \tag{3.201}$$

which is the effective bending modulus of the rectangular layer of elastomer bonded to the rigid reinforcement.

The ratio $E_b/(GS^2)$ is plotted in Figure 3.26 as a function of αa for the aspect ratio $a/b = 0$, 0.1, 0.2, 0.5 and 1, which shows that the effective bending modulus decreases with increasing αa. The figure also reveals that the smaller the value of the aspect ratio a/b, the smaller the value of the effective bending modulus. To test the convergence of the series solution in Eq. (3.196), we calculate the values of $E_b/(GS^2)$ using the first 1, 2, 5 and 10 terms and then find the ratios of these values to the value using the first 50 terms. These ratios are plotted in Figure 3.27 as a function of αa for $a/b = 0.5$ and plotted in Figure 3.28 as a function of a/b for $\alpha a = 0.5$. The two figures show that the series solution in Eq. (3.196) converges very fast and using the first 10 terms is enough to have an accurate solution except when the aspect ratio a/b is very small.

Substituting the shape factor S in Eq. (3.88) and αa in Eq. (3.102) into Eq. (3.196), we have the normalized effective bending modulus E_b/G expressed as a function of the ratios a/b, a/t and $k_f/(Gt)$. When a/t tends to infinity, $\alpha a \to \infty$, $\tilde{\beta}_n b \to \infty$, $\bar{\beta}_n a \to \infty$ and Eq. (3.196) becomes

$$E_b = \frac{6}{\pi^2}\frac{k_f}{t}\sum_{n=1}^{\infty}\left\{\frac{1}{n^2}\frac{\tanh\tilde{\gamma}_n b}{\tilde{\gamma}_n b} + \frac{1}{(n-\frac{1}{2})^2}\left[\frac{1}{\bar{\gamma}_n a \tanh\bar{\gamma}_n a} - \frac{1}{(\bar{\gamma}_n a)^2}\right]\right\} \tag{3.202}$$

The curves of E_b/G versus $k_f/(Gt)$ are plotted in Figure 3.29 for $a/b = 0.5$ and several a/t values, which shows that the effective bending modulus increases with increasing the reinforcement stiffness until reaching the asymptotic value in Eq. (3.201). The curve of the smaller shape factor reaches the plateau at the smaller value of $k_f/(Gt)$. The curves of E_b/G versus a/t are plotted in Figure 3.30 for $a/b = 0.5$ and several $k_f/(Gt)$ values, which shows that the effective bending modulus increases with increasing the shape factor until reaching the asymptotic value in Eq. (3.202). The curve of the smaller value of $k_f/(Gt)$ reaches the plateau at the smaller shape factor.

To study the variation of the effective bending modulus with the aspect ratio a/b, the ratios of the bending modulus of the rectangular layers with $a/b > 0$ shown in Eq. (3.196) to the bending modulus of the infinitely long strip layer $a/b = 0$ shown in Eq. (3.198) are plotted in Figure 3.31 for $\alpha a = 0$, 1, 2 and 4, which reveals that the effective bending modulus is almost linearly varied

with the aspect ratio a/b. The ratio of E_b at $a/b = 1$ to E_b at $a/b = 0$ is plotted in Figure 3.32 as a function of αa between 0 and 5 which, utilizing the regression analysis, can be fitted by the four-degree polynomial

$$g(\alpha a) = 0.70 - 0.0024\alpha a + 0.021(\alpha a)^2 - 0.0045(\alpha a)^3 + 0.00030(\alpha a)^4 \tag{3.203}$$

Assuming the value of E_b is linearly varied between $a/b = 0$ and $a/b = 1$, an empirical formula for the effective bending modulus of rectangular reinforced layers can be established from Eqs. (3.198) and (3.203)

$$\begin{aligned} E_b &= \frac{36GS^2}{(\alpha a)^4}\left[1 + \frac{1}{3}(\alpha a)^2 - \frac{\alpha a}{\tanh \alpha a}\right] \\ &\quad \left\{1 + \frac{a}{b}\left[-0.30 - 0.0024\alpha a + 0.021(\alpha a)^2 - 0.0045(\alpha a)^3 + 0.00030(\alpha a)^4\right]\right\} \end{aligned} \tag{3.204}$$

The errors of this empirical formula with respect to the exact formula in Eq. (3.196) are plotted in Figure 3.33 as a function of a/b for several values of αa and in Figure 3.34 as a function of αa for several values of a/b, which show that the maximum error is smaller than 0.6 percent. It should be noted that because the range of the αa values used in the regression analysis is between 0 and 5, the effective bending modulus in Eq. (3.204) is only applicable to the range of $0 \leq \alpha a \leq 5$.

3.2.5 Stresses in Elastomer

The nominal bending stress σ_b is the maximum normal stress created by the moment M. From Eqs. (3.192) and (3.194)

$$\sigma_b = \frac{Ma}{I_y} = E_b \frac{a}{\rho} \tag{3.205}$$

When the pressure distribution in Eq. (3.191) is normalized with respect to the nominal bending stress σ_b, the normalized pressure distribution $p(x, y)\rho/(E_b a)$ can be expressed in terms of αa, a/b, x/a and y/b. A 3-D graph of the normalized pressure distribution for $\alpha a = 0.5$ and $a/b = 0.5$ is

plotted in Figure 3.35, which shows that the bending moment creates the positive pressure at the side of the negative x axis and the negative pressure at the side of the positive x axis.

When α tends to zero, using the approximations of $\bar{\beta}_n$ in Eqs. (3.98), (3.107) and (3.114) and the approximations of $\tilde{\beta}_n$ in Eq. (3.199) and the following

$$\cosh \tilde{\beta}_n x \approx \cosh \tilde{\gamma}_n x \left[1 + \frac{1}{2}\tilde{\gamma}_n x \tanh \tilde{\gamma}_n x \left(\frac{\alpha}{\tilde{\gamma}_n}\right)^2\right] \tag{3.206}$$

$$\sinh \tilde{\beta}_n x \approx \sinh \tilde{\gamma}_n x \left[1 + \frac{\tilde{\gamma}_n x}{2 \tanh \tilde{\gamma}_n x} \left(\frac{\alpha}{\tilde{\gamma}_n}\right)^2\right] \tag{3.207}$$

Eq. (3.191) is reduced to

$$\begin{aligned} p(x,y) = \frac{a}{\rho}\frac{12GS^2}{\pi^2}\left(1+\frac{a}{b}\right)^2 \frac{b}{a}\sum_{n=1}^{\infty}(-1)^n \Bigg\{ &\left(\tanh \bar{\gamma}_n b - \frac{y}{b}\tanh \bar{\gamma}_n y\right)\left(\frac{\cosh \bar{\gamma}_n y}{\cosh \bar{\gamma}_n b}\right)\frac{\sin \tilde{\gamma}_n x}{n^2} \\ &+ \left[\left(\frac{1}{\tanh \bar{\gamma}_n a}\right)\frac{\sinh \bar{\gamma}_n x}{\sinh \bar{\gamma}_n a} - \left(\frac{x}{a}\right)\frac{\cosh \bar{\gamma}_n x}{\sinh \bar{\gamma}_n a}\right]\frac{\cos \bar{\gamma}_n y}{(n-\frac{1}{2})^2}\Bigg\} \end{aligned} \tag{3.208}$$

which is the pressure distribution of the rectangular layer of elastomer bonded to the rigid reinforcement.

To study the effect of the flexibility of the reinforcement on the pressure distribution, the normalized pressure distribution along the x axis at $y = 0$ is plotted in Figures 3.36 for the aspect ratio $a/b = 0.5$ and $\alpha a = 0$, 1, 2 and 4, which shows that decreasing the stiffness of the reinforcement reduces the maximum pressure. For the elastomeric layers of different aspect ratios a/b, the distribution of the normalized pressure along the x axis at $y = 0$ is plotted in Figure 3.37 with $\alpha a = 0.5$, which reveals that the maximum value of the pressure becomes smaller as the layer has smaller value of a/b.

If τ_x and τ_y denote the shear stresses in the x and y directions, respectively, on the bonding surface between the elastomer and the reinforcement, from Eqs. (3.145) and (3.147)

$$\tau_x(x,y) = \sigma_{xz}|_{z=-\frac{t}{2}} = -\frac{t}{2}p_{,x} \tag{3.209}$$

and, from Eqs. (3.146) and (3.148),

$$\tau_y(x,y) = \sigma_{yz}|_{z=-\frac{t}{2}} = -\frac{t}{2}p_{,y} \tag{3.210}$$

Substituting Eq. (3.191) into Eqs. (3.209) and (3.210), we have the bonding shear stresses as

$$\begin{aligned}\tau_x(x,y) &= \frac{a}{\rho}\frac{12GS}{(\alpha a)^2}\left(1+\frac{a}{b}\right)\sum_{n=1}^{\infty}(-1)^{n-1}\left[\left(\frac{\cosh\tilde{\gamma}_n y}{\cosh\tilde{\gamma}_n b}-\frac{\cosh\tilde{\beta}_n y}{\cosh\tilde{\beta}_n b}\right)\cos\tilde{\gamma}_n x\right.\\ &\left.+\frac{a}{b}\left(\frac{\cosh\bar{\gamma}_n x}{\sinh\bar{\gamma}_n a}-\frac{\bar{\beta}_n\cosh\bar{\beta}_n x}{\bar{\gamma}_n\sinh\bar{\beta}_n a}\right)\cos\bar{\gamma}_n y\right]\end{aligned} \tag{3.211}$$

$$\begin{aligned}\tau_y(x,y) &= \frac{a}{\rho}\frac{12GS}{(\alpha a)^2}\left(1+\frac{a}{b}\right)\sum_{n=1}^{\infty}(-1)^{n-1}\left[\left(\frac{\sinh\tilde{\gamma}_n y}{\cosh\tilde{\gamma}_n b}-\frac{\tilde{\beta}_n\sinh\tilde{\beta}_n y}{\tilde{\gamma}_n\cosh\tilde{\beta}_n b}\right)\sin\tilde{\gamma}_n x\right.\\ &\left.-\frac{a}{b}\left(\frac{\sinh\bar{\gamma}_n x}{\sinh\bar{\gamma}_n a}-\frac{\sinh\bar{\beta}_n x}{\sinh\bar{\beta}_n a}\right)\sin\bar{\gamma}_n y\right]\end{aligned} \tag{3.212}$$

When α tends to zero, using the approximations of $\bar{\beta}_n$ in Eqs. (3.98), (3.107) and (3.114) and the approximations of $\tilde{\beta}_n$ in Eq. (3.199), (3.206) and (3.207), the above two equations are reduced to

$$\begin{aligned}\tau_x(x,y) &= \frac{a}{\rho}\frac{6GS}{\pi}\left(1+\frac{a}{b}\right)\sum_{n=1}^{\infty}(-1)^{n-1}\left[\frac{b}{a}\left(\tanh\tilde{\gamma}_n b-\frac{y}{b}\tanh\tilde{\gamma}_n y\right)\left(\frac{\cosh\tilde{\gamma}_n y}{\cosh\tilde{\gamma}_n b}\right)\frac{\cos\tilde{\gamma}_n x}{n}\right.\\ &\left.+\left(\frac{1}{\tanh\bar{\gamma}_n a}-\frac{1}{\bar{\gamma}_n a}-\frac{x}{a}\tanh\bar{\gamma}_n x\right)\left(\frac{\cosh\bar{\gamma}_n x}{\sinh\bar{\gamma}_n a}\right)\frac{\cos\bar{\gamma}_n y}{(n-\frac{1}{2})}\right]\end{aligned} \tag{3.213}$$

$$\begin{aligned}\tau_y(x,y) &= \frac{a}{\rho}\frac{6GS}{\pi}\left(1+\frac{a}{b}\right)\sum_{n=1}^{\infty}(-1)^{n-1}\left\{-\left[\left(\frac{1}{\tanh\bar{\gamma}_n a}\right)\frac{\sinh\bar{\gamma}_n x}{\sinh\bar{\gamma}_n a}-\left(\frac{x}{a}\right)\frac{\cosh\bar{\gamma}_n x}{\sinh\bar{\gamma}_n a}\right]\frac{\sin\bar{\gamma}_n y}{(n-\frac{1}{2})}\right.\\ &\left.+\frac{b}{a}\left[\left(\tanh\tilde{\gamma}_n b-\frac{1}{\tilde{\gamma}_n b}\right)\frac{\sinh\tilde{\gamma}_n y}{\cosh\tilde{\gamma}_n b}-\left(\frac{y}{b}\right)\frac{\cosh\tilde{\gamma}_n y}{\cosh\tilde{\gamma}_n b}\right]\frac{\sin\tilde{\gamma}_n x}{n}\right\}\end{aligned} \tag{3.214}$$

which are the bonding shear stresses for the rigid reinforcement.

When these bonding shear stresses are normalized with respect to the nominal bending stress, the quantities $\tau_x\rho S/(E_b a)$ and $\tau_y\rho S/(E_b a)$ can be expressed in terms of αa, a/b, x/a and y/b. The distributions of these two quantities are plotted as 3-D graphs in Figures 3.38 and 3.39, respectively, for $\alpha a = 0.5$ and $a/b = 0.5$. These figures indicate that the loading of the bending moment makes

the negative x portion of the reinforcement in the stretch state and the positive x portion in the contraction state. The distributions of $\tau_x \rho S/(E_b a)$ along the x axis at $y = 0$ and along the y axis at $x = 0$ are plotted in Figures 3.40 and 3.41, respectively, for the aspect ratio $a/b = 0.5$ and $\alpha a = 0$, 1, 2 and 4, which reveal that the flexibility of the reinforcement decreases the bonding shear stress at the center but increases the maximum values at the edges.

The shear resultant $\tau(x, y)$ is defined as

$$\tau(x, y) = \sqrt{\tau_x^2(x, y) + \tau_y^2(x, y)} \tag{3.215}$$

The distribution of $\tau(x, y)\rho S/(E_b a)$ is plotted as a 3-D graph in Figure 3.42 for $\alpha a = 0.5$ and $a/b = 0.5$, which shows that the maximum shear resultant locates at $x = \pm a$ and $y = 0$. The normalized maximum shear resultant, $\tau(a, 0)\rho/(E_b a)$, is plotted in Figure 3.43 as a function of the stiffness ratio $k_f/(Gt)$ for $a/b = 0.5$ and several different a/t values, which shows that the maximum shear resultant decreases with increasing the stiffness ratio; the lower shape factor always has a higher shear resultant. The normalized maximum shear resultant plotted in Figure 3.44 is for $a/t = 10$ and $a/b = 0.1$, 0.2, 0.5 and 1, which shows that although the lower value of the aspect a/b has the smaller maximum shear resultant, the effect of the aspect ratio on the maximum shear resultant is negligible.

3.2.6 Solution for Rigid Reinforcement

Although the effective bending modulus of the rigid-reinforced elastomer is derived from the asymptotic solution of the flexible-reinforced elastomer by setting $\alpha \to 0$ in the previous sections, the effective bending modulus of the rigid-reinforced elastomer can be directly solved and is described in this section.

For a layer of elastomer in a rectangular isolator under a pure bending moment, as shown in Figure 3.25, if the top and bottom surfaces of the elastomeric layer are bonded to rigid reinforcements,

the displacements of the elastomer can be assumed as

$$u(x,y,z) = u_0(x,y)\left(1 - \frac{4z^2}{t^2}\right) \tag{3.216}$$

$$v(x,y,z) = v_0(x,y)\left(1 - \frac{4z^2}{t^2}\right) \tag{3.217}$$

$$w(x,y,z) = \frac{1}{\rho}xz \tag{3.218}$$

where ρ is the radius of the bending curvature defined in Eq. (3.143). Substituting these into the displacement constraint in Eq. (3.4), attributed to the assumption of incompressibility of the elastomer, and then taking the integration through the thickness lead to

$$\frac{2}{3}(u_{0,x} + v_{0,y}) = -\frac{1}{\rho}x \tag{3.219}$$

Substitution of Eqs. (3.216) to (3.218) into the shear stress components of elastomer σ_{xz} and σ_{xz} defined in Eqs. (3.13) and (3.14) gives

$$\sigma_{xz} = \left(-\frac{8G}{t^2}u_0 + \frac{G}{\rho}\right)z \tag{3.220}$$

$$\sigma_{yz} = -\frac{8G}{t^2}v_0 z \tag{3.221}$$

Bringing these into the equilibrium equations of elastomer in Eqs. (3.122) and (3.123), which are simplified by assuming that the pressure is dominated in the stress field of elastomer, leads to

$$p_{,x} = -\frac{8G}{t^2}u_0 + \frac{G}{\rho} \tag{3.222}$$

$$p_{,y} = -\frac{8G}{t^2}v_0 \tag{3.223}$$

Differentiating Eqs. (3.222) and (3.223) with respect to x and y, respectively, then adding them up and applying the relation in Eq. (3.219) yield

$$p_{,xx} + p_{,yy} = \frac{12G}{t^2\rho}x \tag{3.224}$$

According to the boundary condition $p(\pm a, y) = 0$ and the anti-symmetric property $p(x, y) = -p(-x, y)$, the pressure p can be assumed to be a sine series of x

$$p(x, y) = \sum_{n=1}^{\infty} f_n(y) \sin \tilde{\gamma}_n x \tag{3.225}$$

where the amplitude f_n is a function of y and $\tilde{\gamma}_n$ is defined in Eq. (3.171). Substitution of Eq. (3.225) into Eq. (3.224) gives

$$\sum_{n=1}^{\infty} \left(f_{n,yy} - \tilde{\gamma}_n^2 f_n \right) \sin \gamma_n x = \frac{12G}{t^2 \rho} x \tag{3.226}$$

which, by use of the orthogonal property in Eq. (3.179), can be reduced to

$$f_{n,yy} - \tilde{\gamma}_n^2 f_n = \frac{24Ga}{t^2 \rho} \frac{(-1)^{n-1}}{n\pi} \tag{3.227}$$

The boundary condition $p(x, \pm b) = 0$ and the symmetric property $p(x, y) = p(x, -y)$ give $f_n(\pm b) = 0$ and $f_n(y) = f_n(-y)$, from which $f_n(y)$ can be solved and the pressure p has the form

$$p(x, y) = \frac{a}{\rho} \frac{24GS^2}{\pi^3} \left(1 + \frac{a}{b} \right)^2 \sum_{n=1}^{\infty} \frac{(-1)^n}{n^3} \left(1 - \frac{\cosh \tilde{\gamma}_n y}{\cosh \tilde{\gamma}_n b} \right) \sin \tilde{\gamma}_n x \tag{3.228}$$

where S is the shape factor defined in Eq. (3.88). This series expression for the pressure distribution is different from the expression depicted in Eq. (3.208), but the numerical results of the two equations are the same. The series expression in Eq. (3.208) exhibits second-order convergence, whereas Eq. (3.228) has third-order convergence.

Using the pressure solution in Eq. (3.228), the effective bending modulus defined in Eq. (3.194) becomes

$$E_b = \frac{72GS^2}{\pi^4} \left(1 + \frac{a}{b} \right)^2 \sum_{n=1}^{\infty} \frac{1}{n^4} \left(1 - \frac{\tanh \tilde{\gamma}_n b}{\tilde{\gamma}_n b} \right) \tag{3.229}$$

Although the above series expression is different from the expression depicted in Eq. (3.201), the numerical results of the two equations are the same. To compare the convergence of the series solutions, the ratios of the values using the first 1 and 2 terms to the value of the first 50 terms are calculated from Eqs. (3.201) and (3.229) and are plotted in Figure 3.45 as a function of the

aspect ratio a/b. The figure reveals that, when a/b is small, the convergence rate of Eq. (3.229) is much faster than that of Eq. (3.201); when a/b is close to unity, the convergence rate of Eq. (3.201) becomes better than Eq. (3.229).

When the aspect ratio a/b tends to zero, $\tilde{\gamma}_n b \to \infty$. Using the following series equation

$$\sum_{n=1}^{\infty} \frac{1}{n^4} = \frac{\pi^4}{90} \tag{3.230}$$

Eq. (3.229) is reduced to

$$E_b = \frac{4}{5} G S^2 \tag{3.231}$$

which is the effective bending modulus of the infinitely long strip of elastomer bonded to rigid reinforcements shown in Eq. (2.83).

From Eqs. (3.220) to (3.223), we have the shear stresses on the bonding surface between the elastomer and the reinforcement

$$\tau_x(x,y) = \sigma_{xz}|_{z=-\frac{t}{2}} = -\frac{t}{2} p_{,x} \tag{3.232}$$

$$\tau_y(x,y) = \sigma_{yz}|_{z=-\frac{t}{2}} = -\frac{t}{2} p_{,y} \tag{3.233}$$

Substitution of Eq. (3.228) into these leads to

$$\tau_x(x,y) = \frac{a}{\rho} \frac{12GS}{\pi^2} \left(1 + \frac{a}{b}\right) \sum_{n=1}^{\infty} \frac{(-1)^{n-1}}{n^2} \left(1 - \frac{\cosh \tilde{\gamma}_n y}{\cosh \tilde{\gamma}_n b}\right) \cos \tilde{\gamma}_n x \tag{3.234}$$

$$\tau_y(x,y) = \frac{a}{\rho} \frac{12GS}{\pi^2} \left(1 + \frac{a}{b}\right) \sum_{n=1}^{\infty} \frac{(-1)^{n}}{n^2} \left(\frac{\sinh \tilde{\gamma}_n y}{\cosh \tilde{\gamma}_n b}\right) \sin \tilde{\gamma}_n x \tag{3.235}$$

Although the series expressions of the above two equations are different from the expressions depicted in Eqs. (3.213) and (3.214), the numerical results of the two sets of equations are the same.

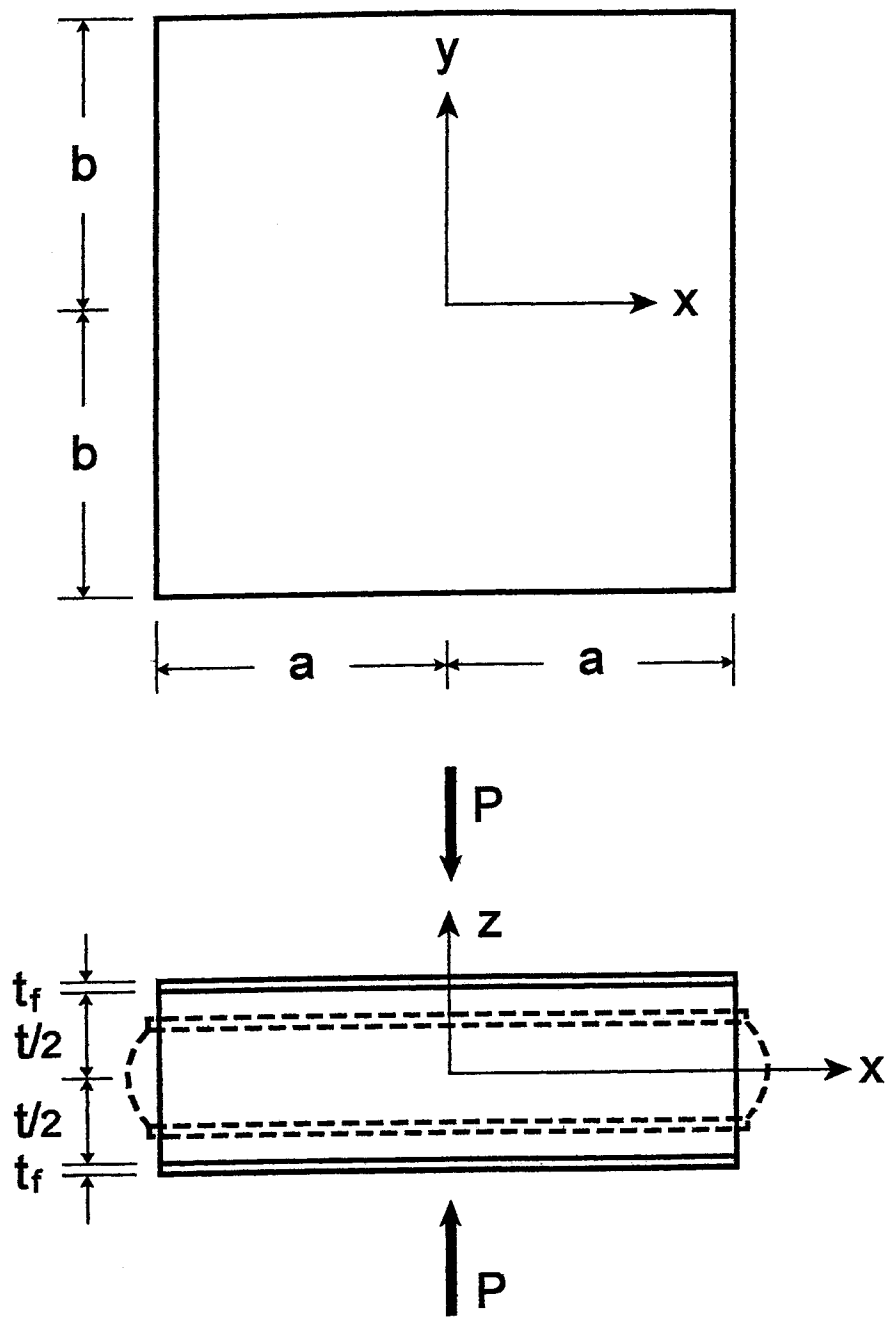

Figure 3.1: Rectangular layer of reinforced elastomer under compression load

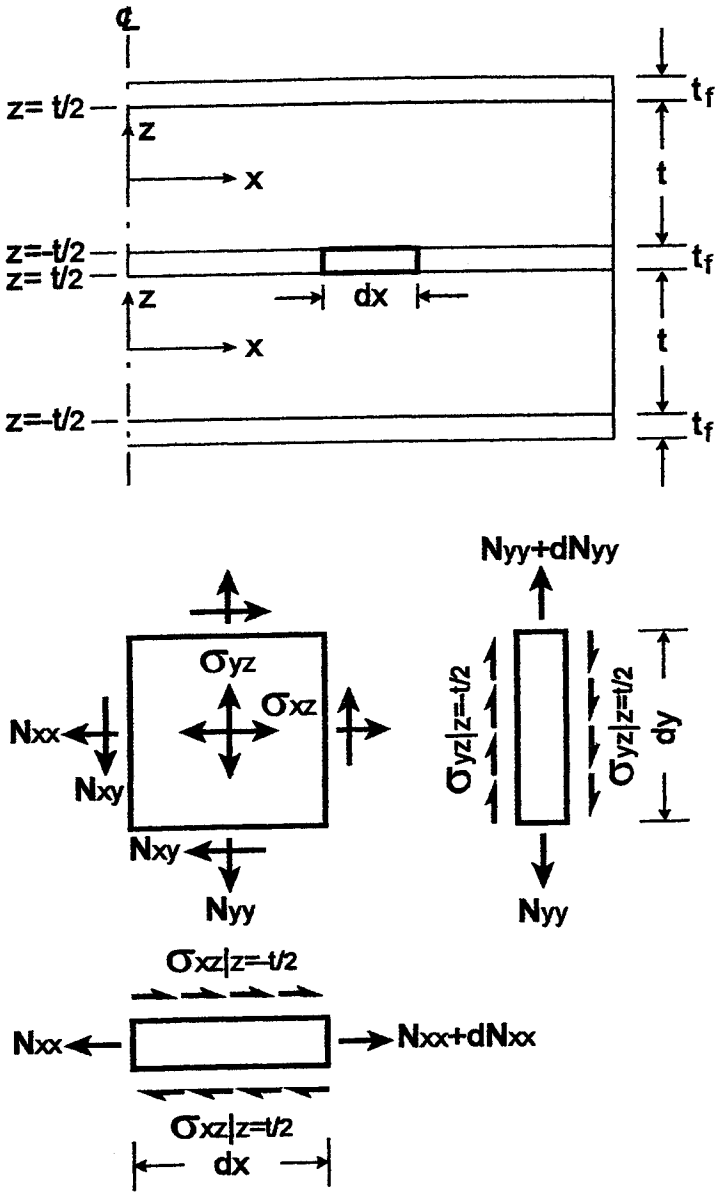

Figure 3.2: Forces in reinforcing sheet bonded to rectangular layers of elastomer

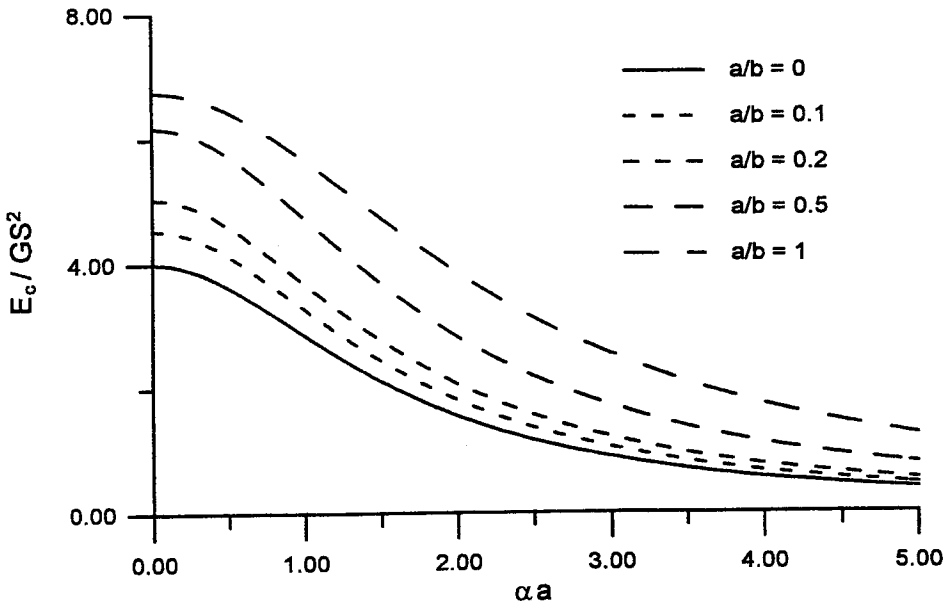

Figure 3.3: Variation of effective compressive modulus with αa in rectangular pad

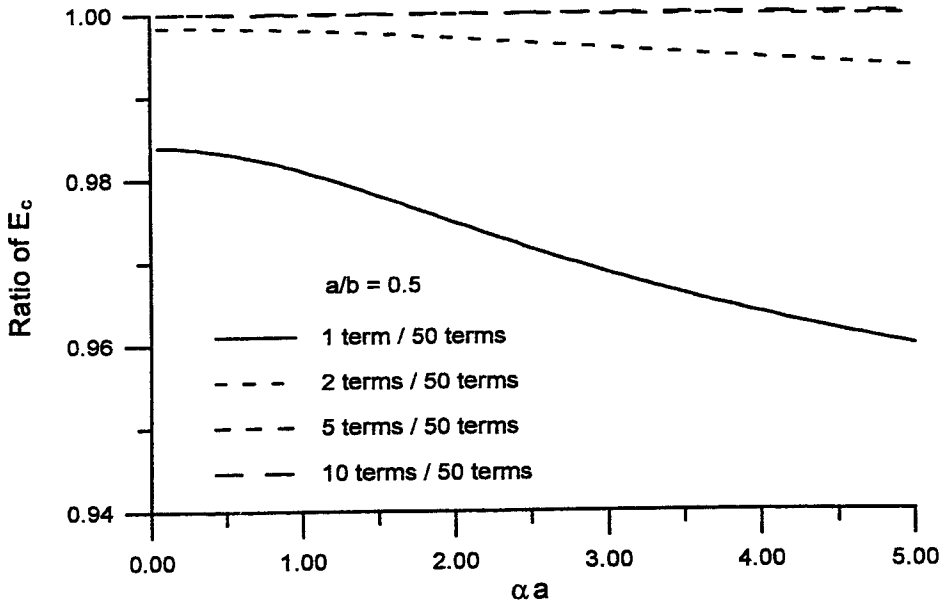

Figure 3.4: Convergence ratio of effective compressive modulus related with αa in rectangular pad of $a/b = 0.5$

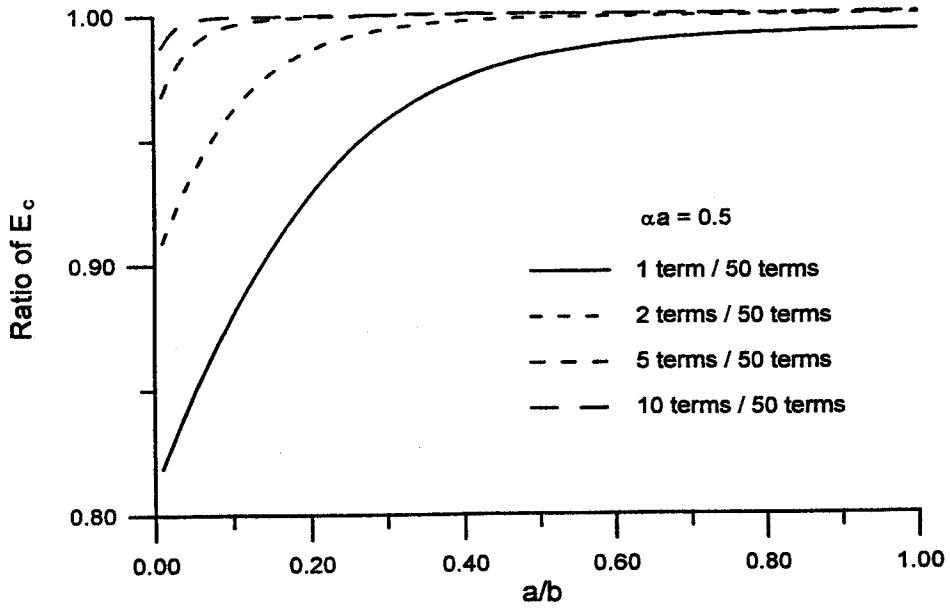

Figure 3.5: Convergence ratio of effective compressive modulus related with aspect ratio in rectangular pad of $\alpha a = 0.5$

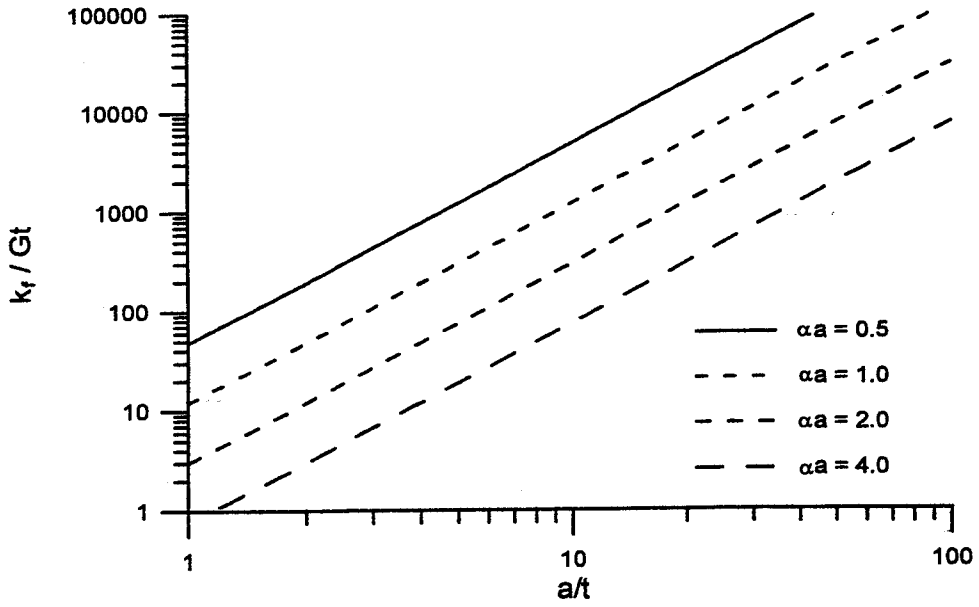

Figure 3.6: Relation between reinforcement stiffness and width-thickness ratio for different αa values in rectangular pad

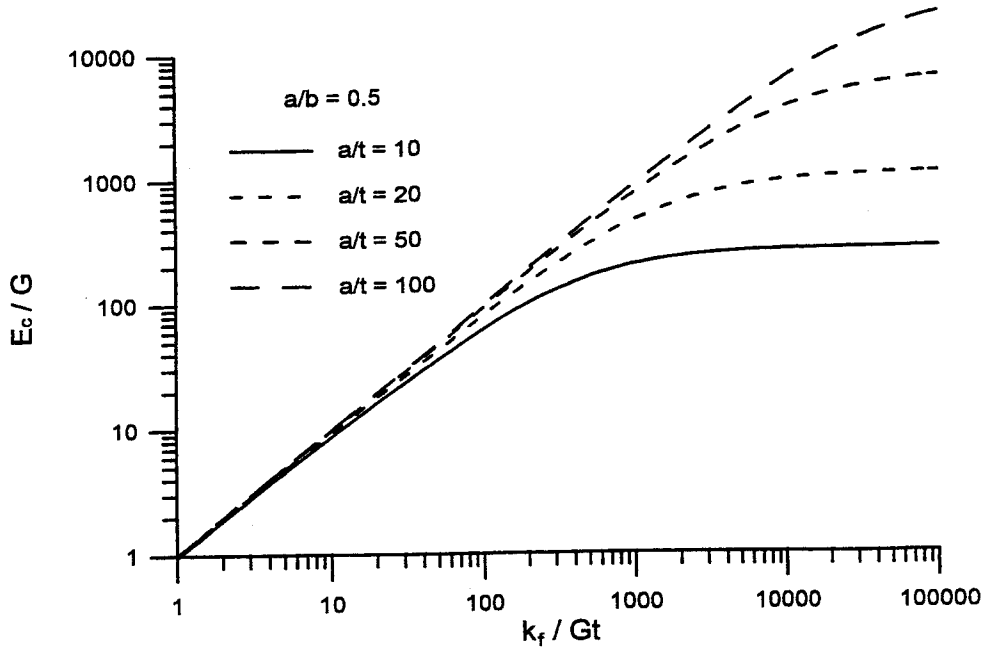

Figure 3.7: Variation of effective compressive modulus with reinforcement stiffness in rectangular pad of $a/b = 0.5$

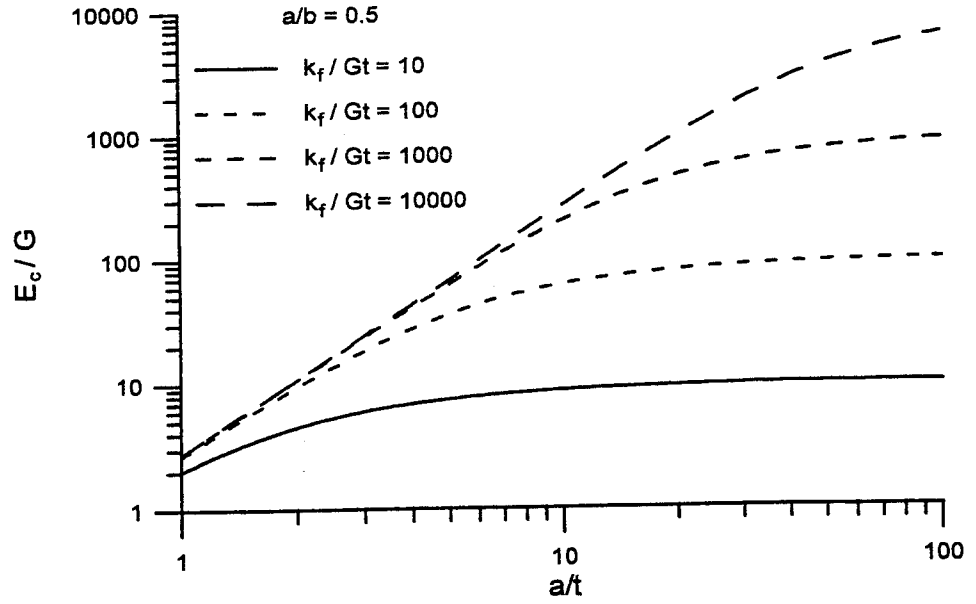

Figure 3.8: Variation of effective compressive modulus with width-thickness ratio in rectangular pad of $a/b = 0.5$

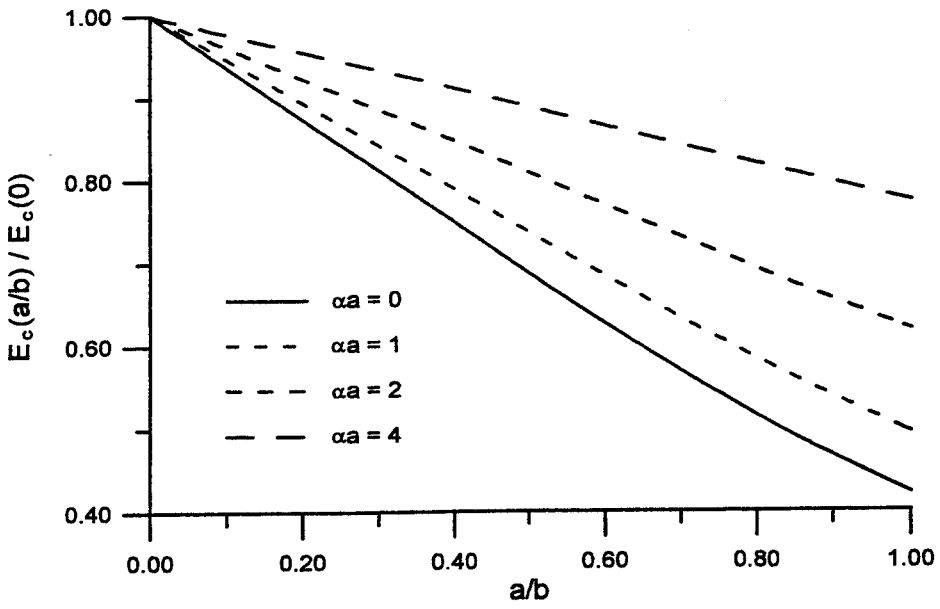

Figure 3.9: Ratio of effective compressive modulus of rectangular pad to infinite-long strip pad $(a/b = 0)$ versus aspect ratio

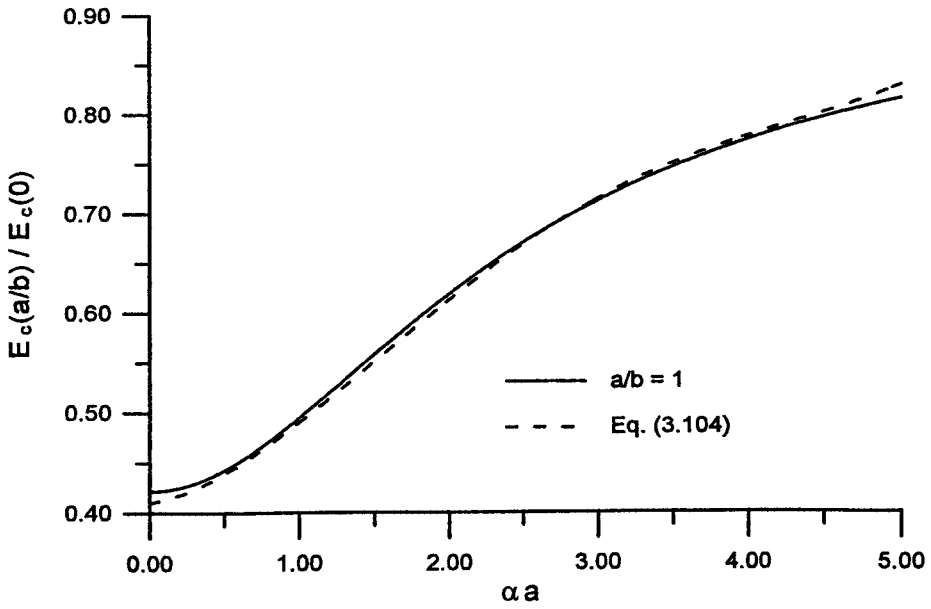

Figure 3.10: Ratio of effective compressive modulus of square pad $(a/b = 1)$ to infinite-long strip pad $(a/b = 0)$ versus αa and its regression curve

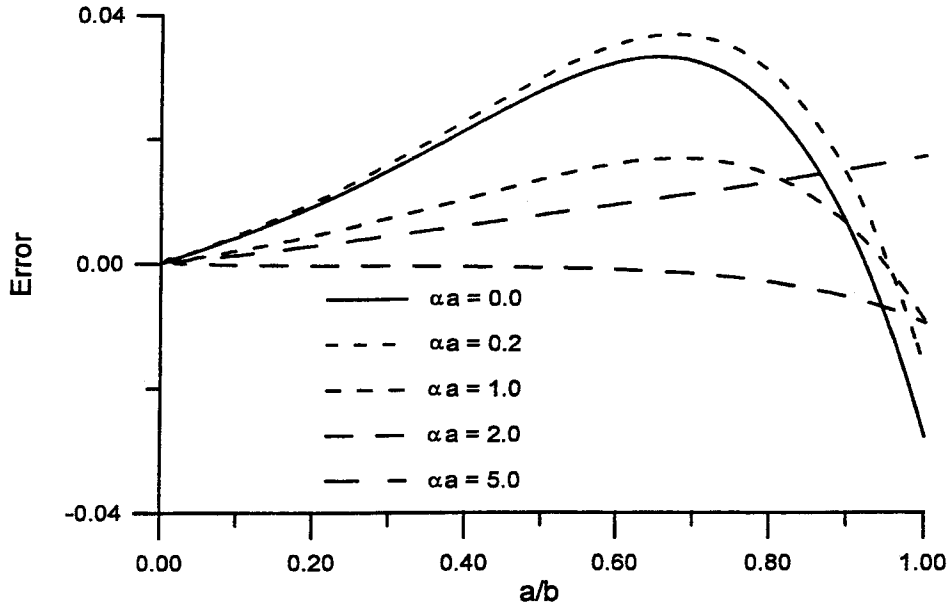

Figure 3.11: Error of empirical formula for effective compressive modulus of rectangular pad versus aspect ratio

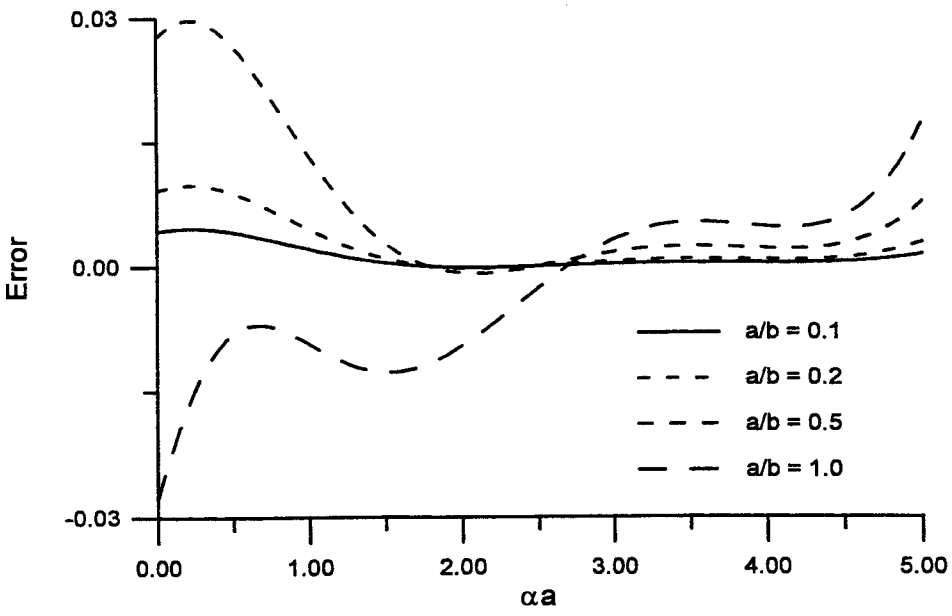

Figure 3.12: Error of empirical formula for effective compressive modulus of rectangular pad versus αa

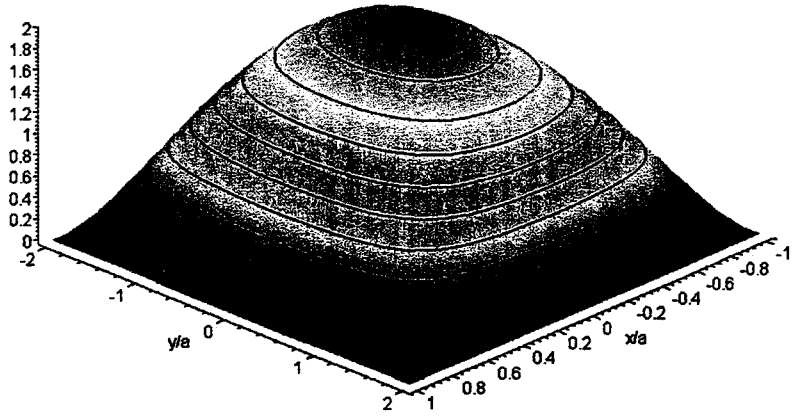

Figure 3.13: 3-D view on contour of normalized pressure in rectangular pad of $a/b = 0.5$ and $\alpha a = 0.5$ under compression load

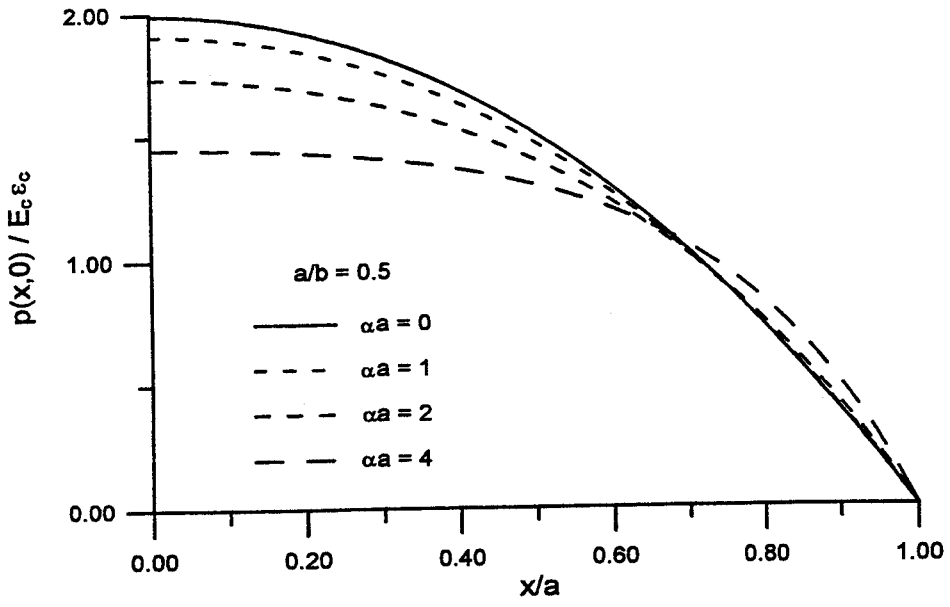

Figure 3.14: Distribution of normalized pressure along x axis in rectangular pad of different αa values and $a/b = 0.5$ under compression load

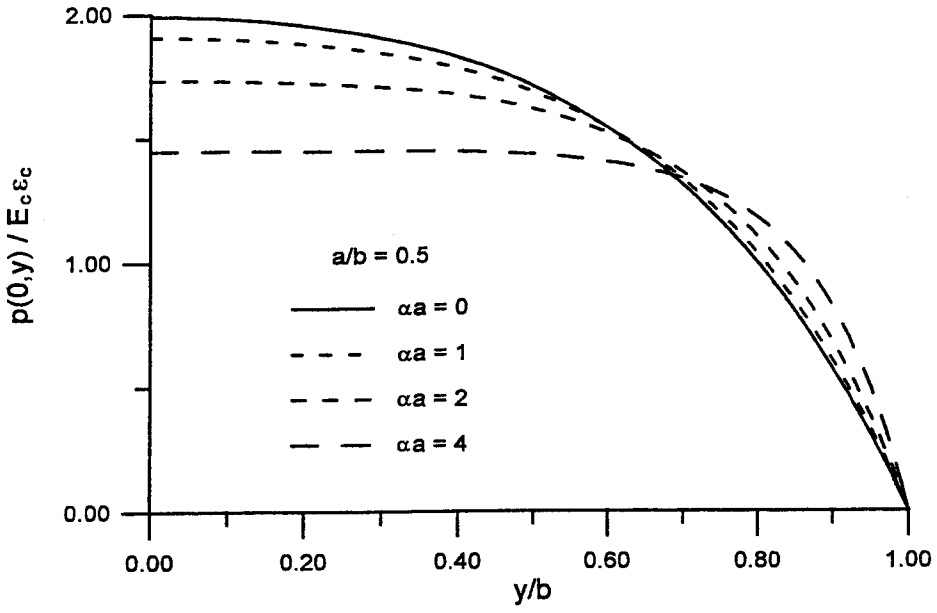

Figure 3.15: Distribution of normalized pressure along y axis in rectangular pad of different αa values and $a/b = 0.5$ under compression load

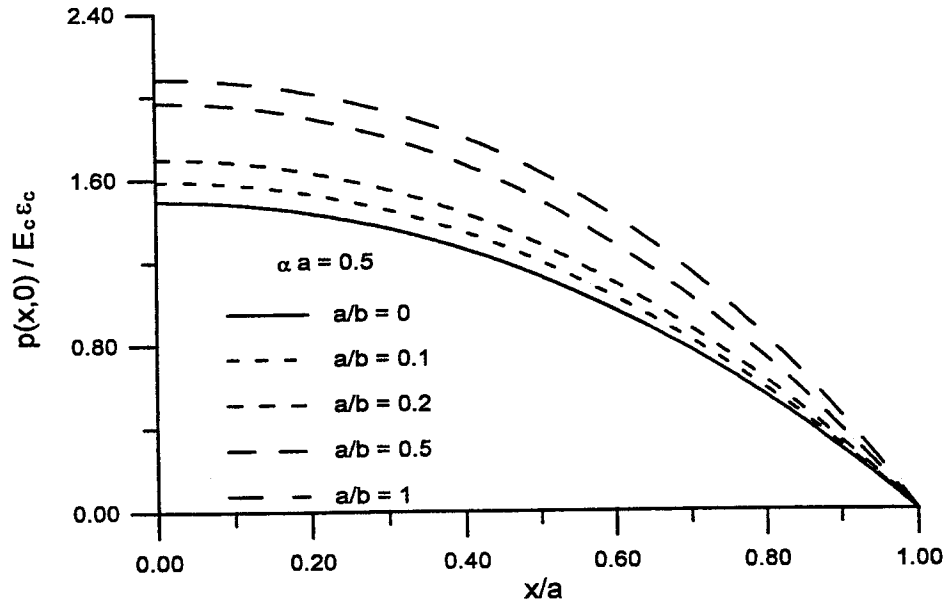

Figure 3.16: Distribution of normalized pressure along x axis in rectangular pad of different aspect ratios and $\alpha a = 0.5$ under compression load

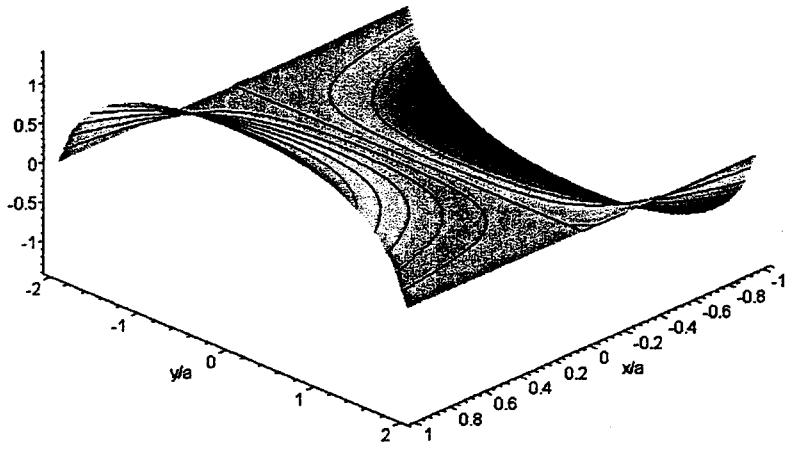

Figure 3.17: 3-D view on contour of bonding shear stress in x direction in rectangular pad of $a/b = 0.5$ and $\alpha a = 0.5$ under compression load

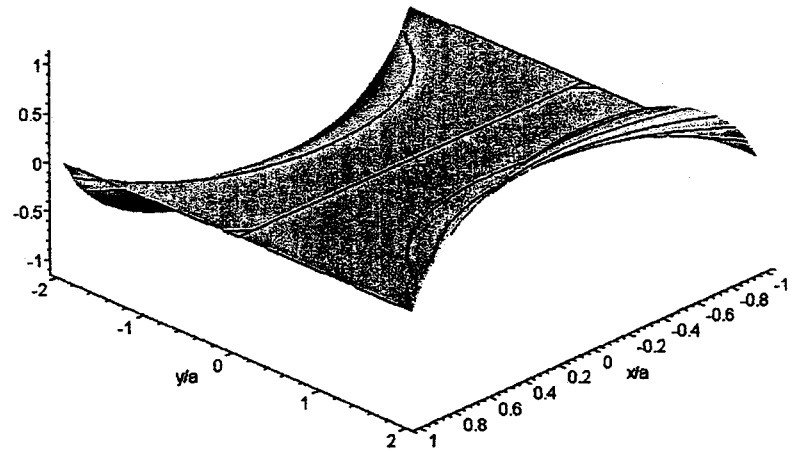

Figure 3.18: 3-D view on contour of bonding shear stress in y direction in rectangular pad of $a/b = 0.5$ and $\alpha a = 0.5$ under compression load

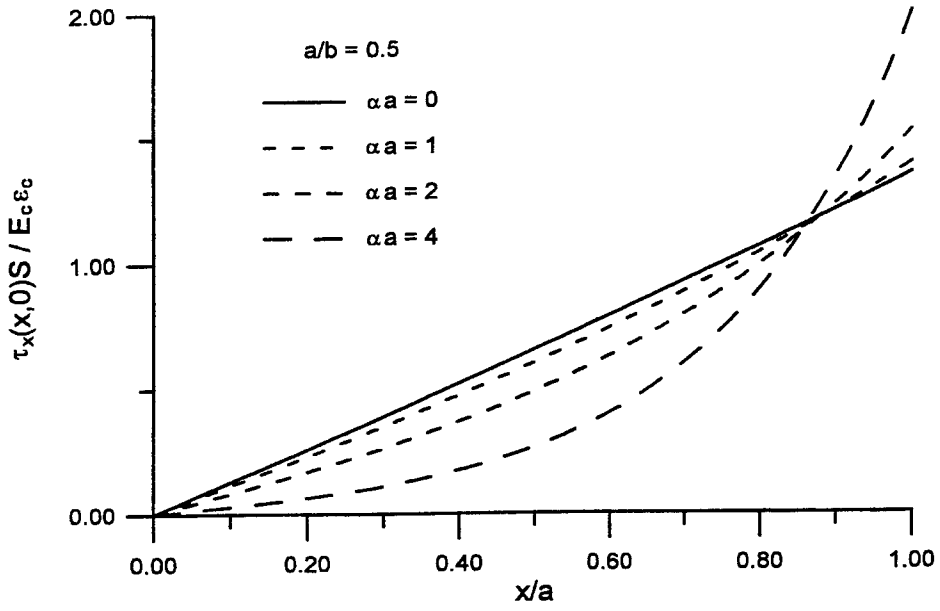

Figure 3.19: Distribution of bonding shear stress in x direction along x axis of rectangular pad under compression load

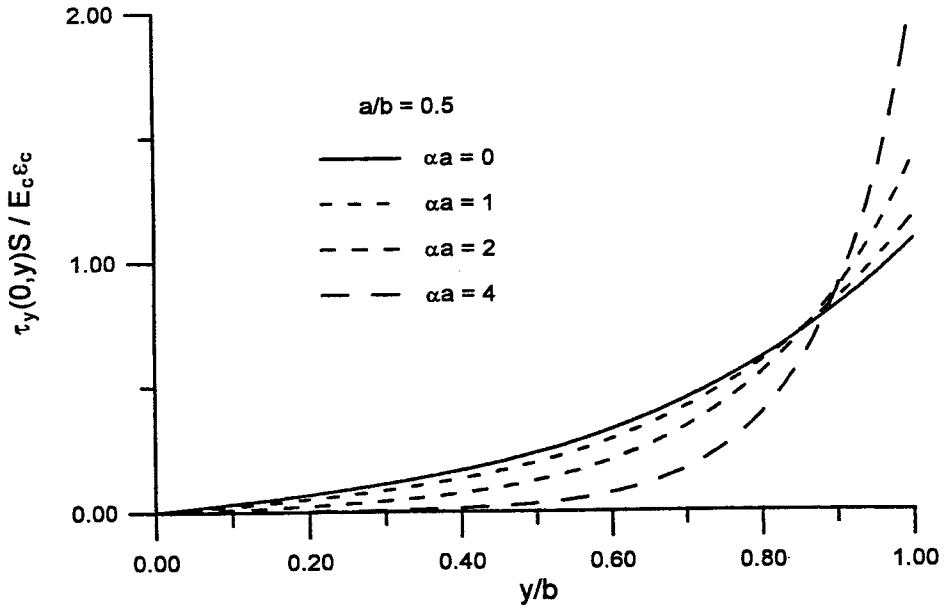

Figure 3.20: Distribution of bonding shear stress in y direction along y axis of rectangular pad under compression load

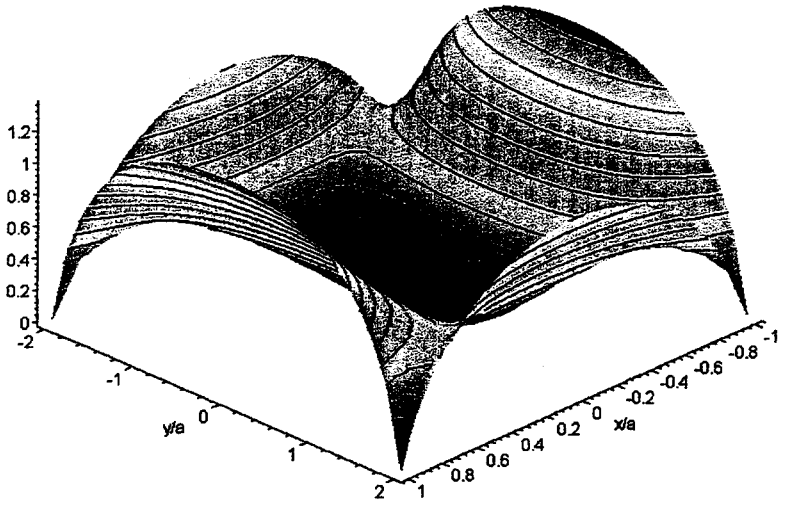

Figure 3.21: 3-D view on contour of bonding shear resultant in rectangular pad of $a/b = 0.5$ and $\alpha a = 0.5$ under compression load

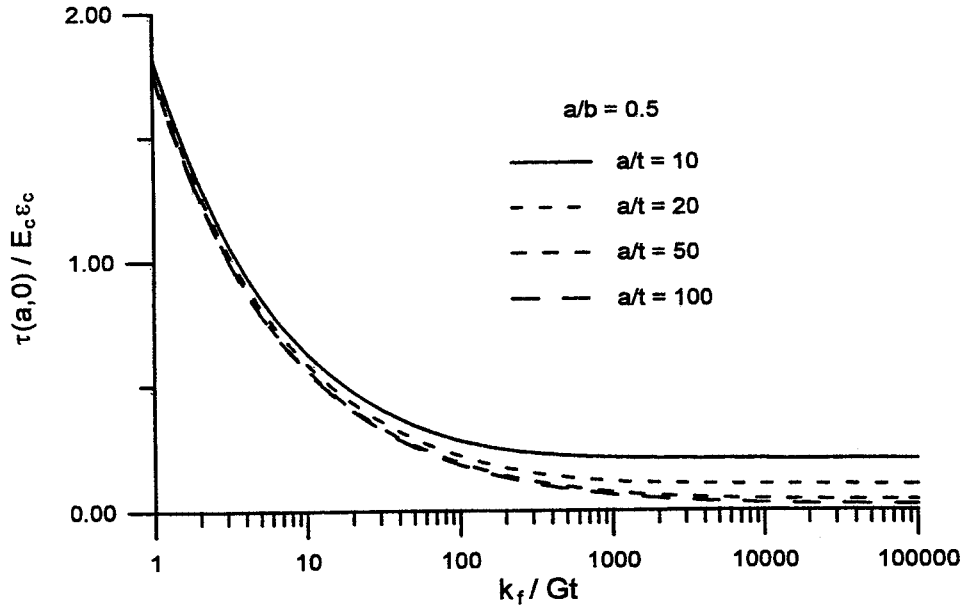

Figure 3.22: Variation of maximum bonding shear resultant with reinforcement stiffness in rectangular pad of different a/t values and $a/b = 0.5$ under compression load

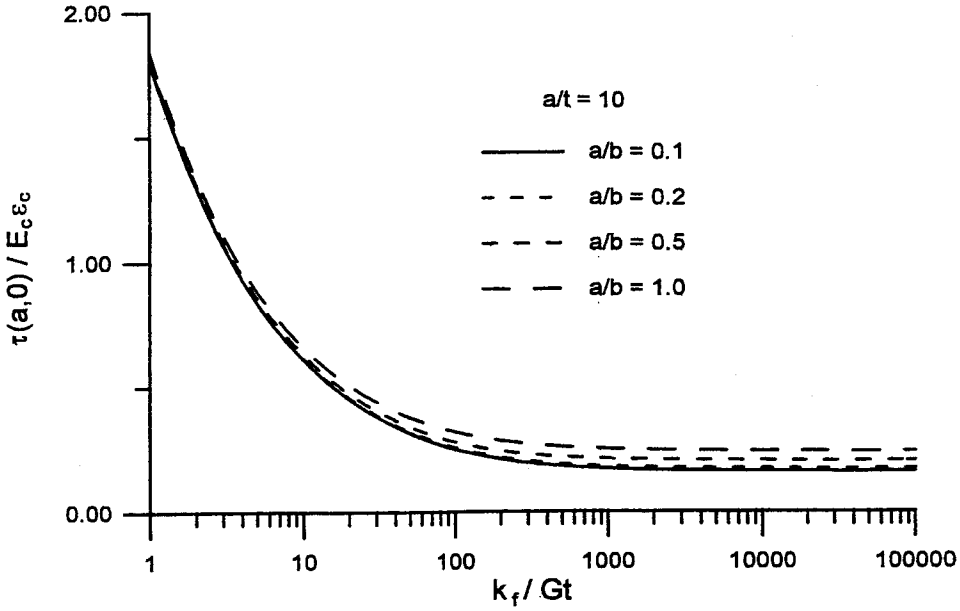

Figure 3.23: Variation of maximum bonding shear resultant with reinforcement stiffness in rectangular pad of different aspect ratios and $a/t = 10$ under compression load

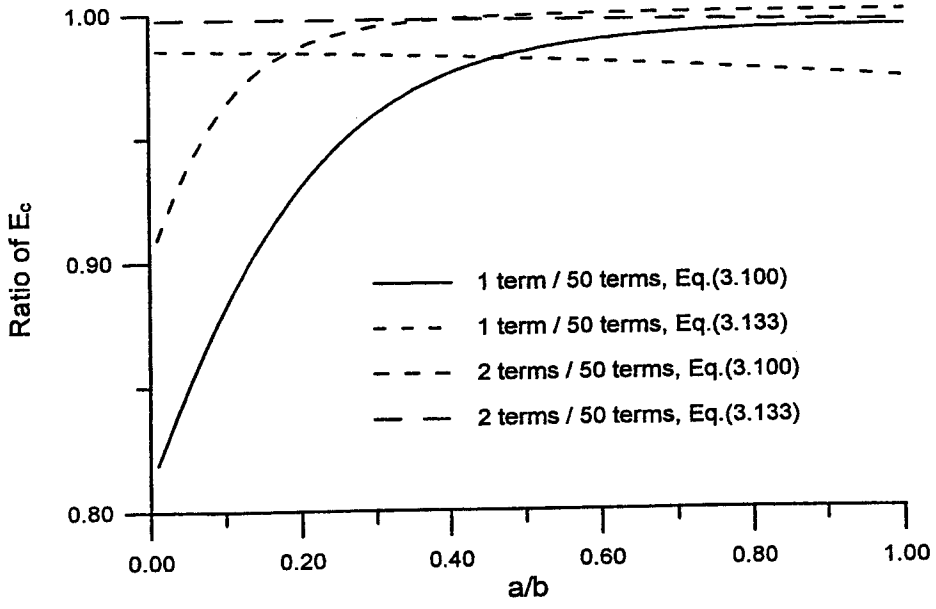

Figure 3.24: Convergence comparison between formulae for effective compressive stiffness of rigid-reinforced rectangular pad

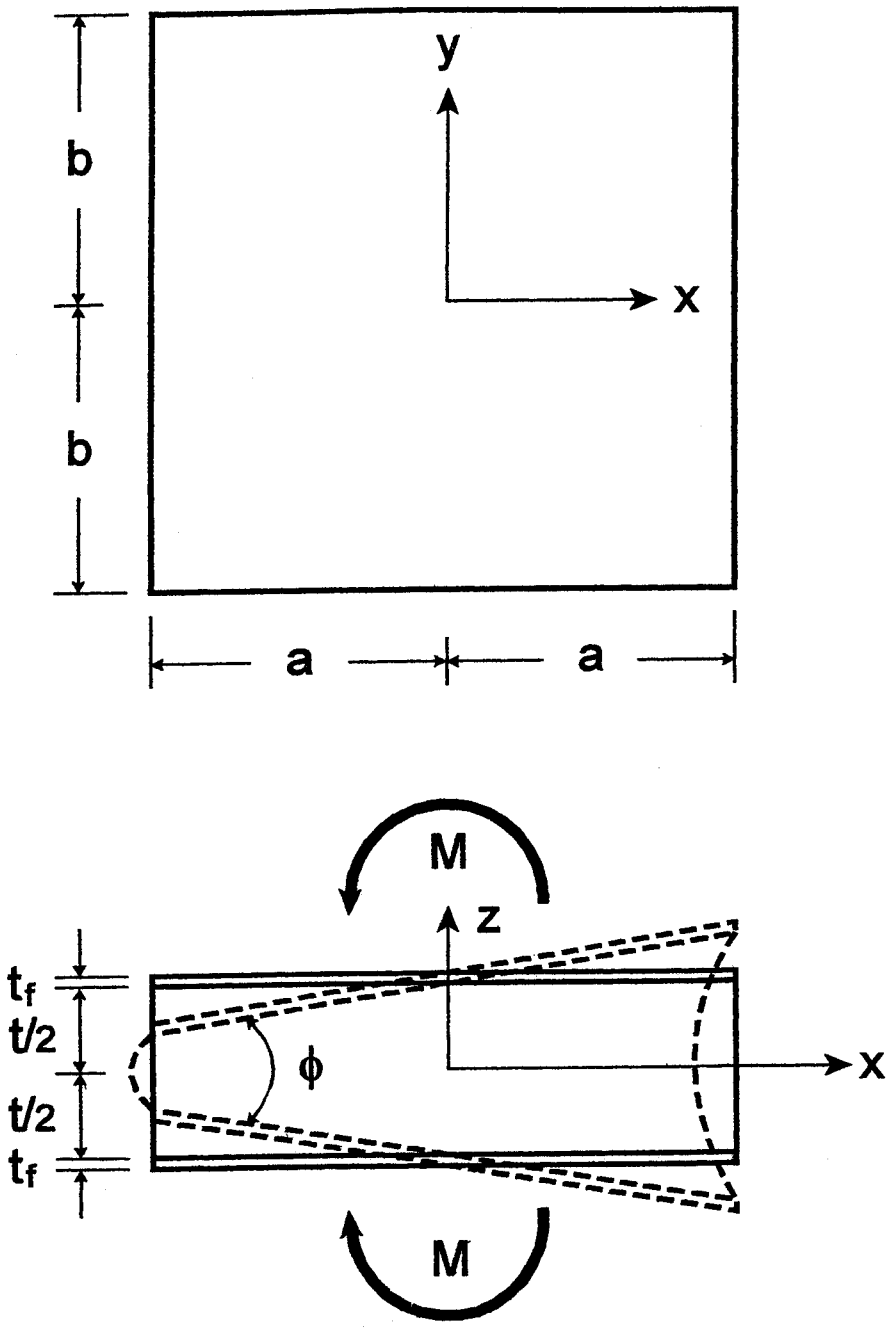

Figure 3.25: Rectangular layer of reinforced elastomer under pure bending load

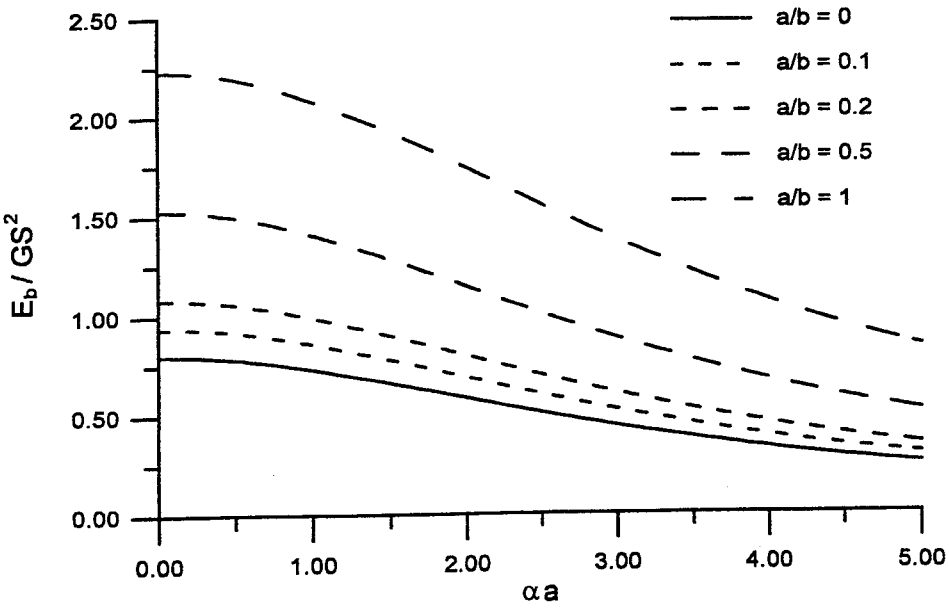

Figure 3.26: Variation of effective bending modulus with αa in rectangular pad

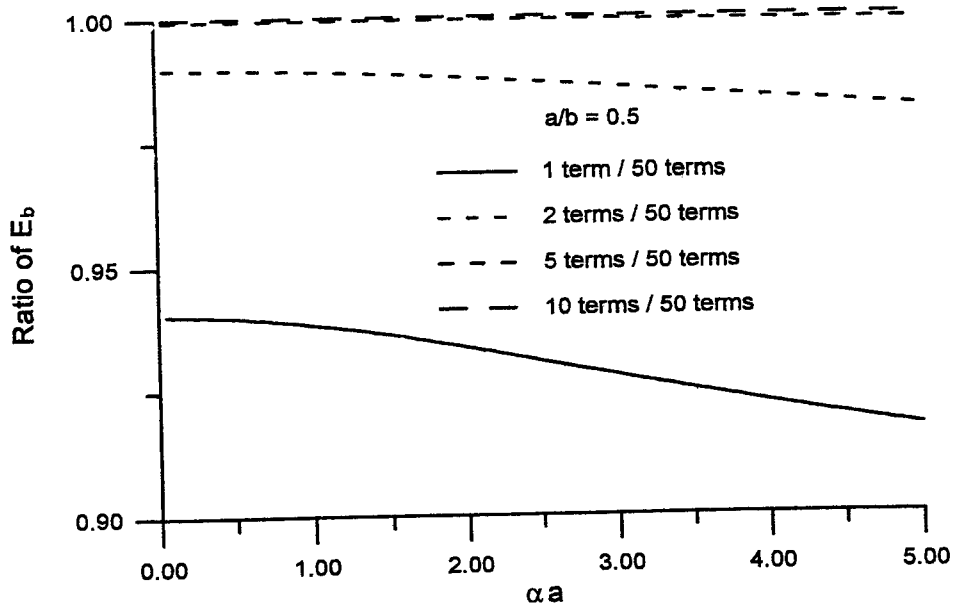

Figure 3.27: Convergence ratio of effective bending modulus related with αa in rectangular pad of $a/b = 0.5$

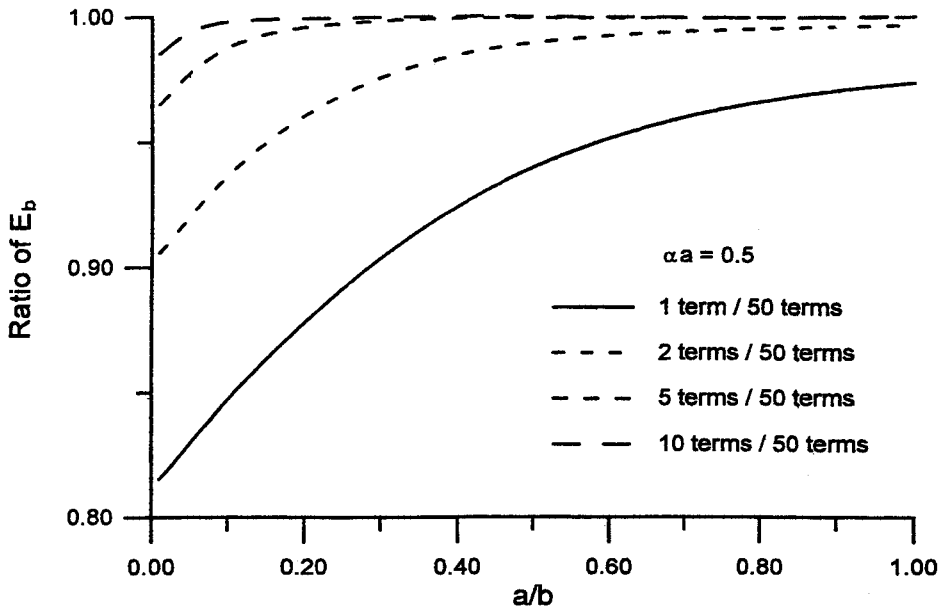

Figure 3.28: Convergence ratio of effective bending modulus related with aspect ratio in rectangular pad of $\alpha a = 0.5$

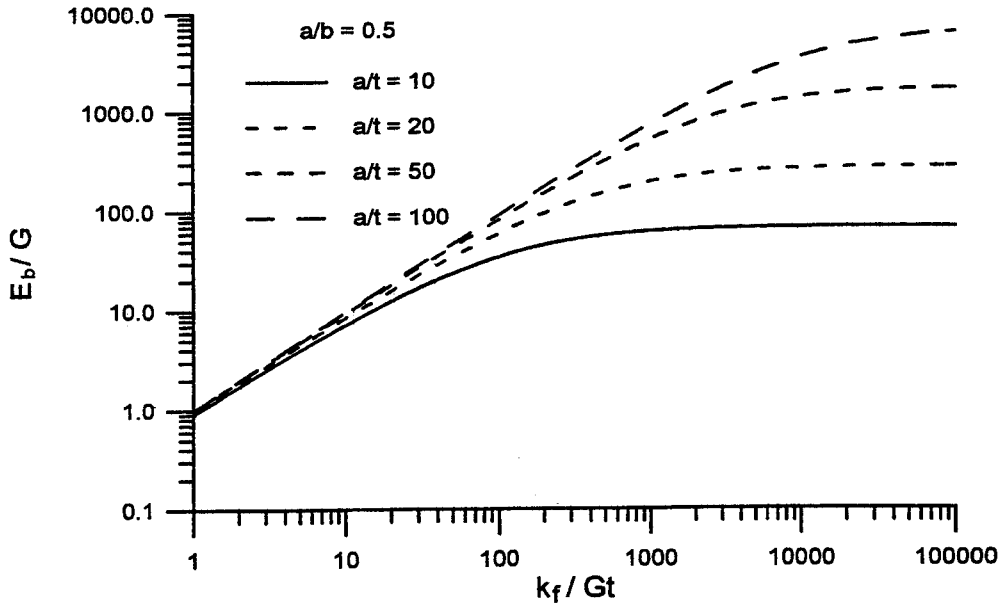

Figure 3.29: Variation of effective bending modulus with reinforcement stiffness in rectangular pad of $a/b = 0.5$

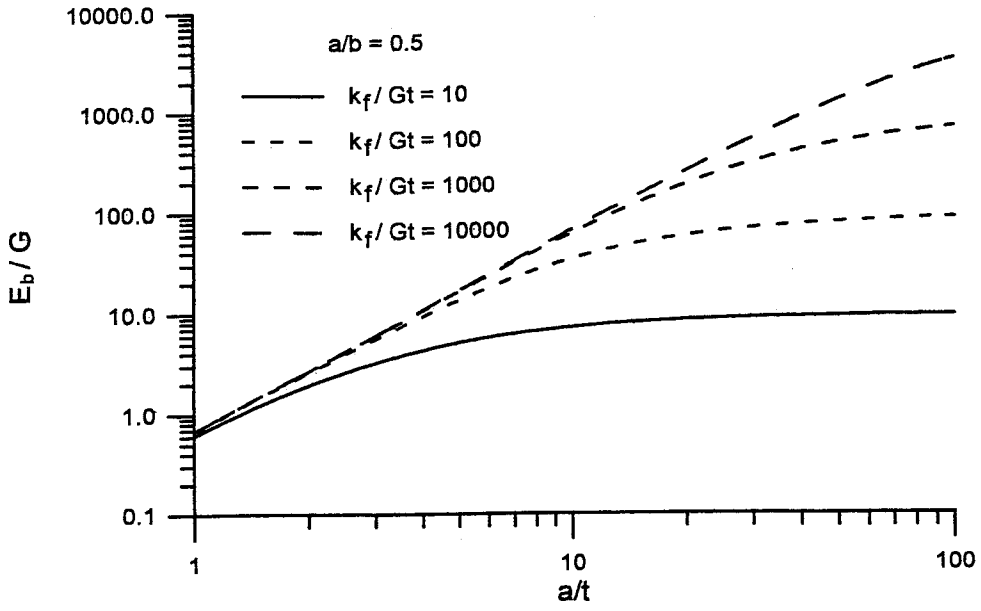

Figure 3.30: Variation of effective bending modulus with width-thickness ratio in rectangular pad of $a/b = 0.5$

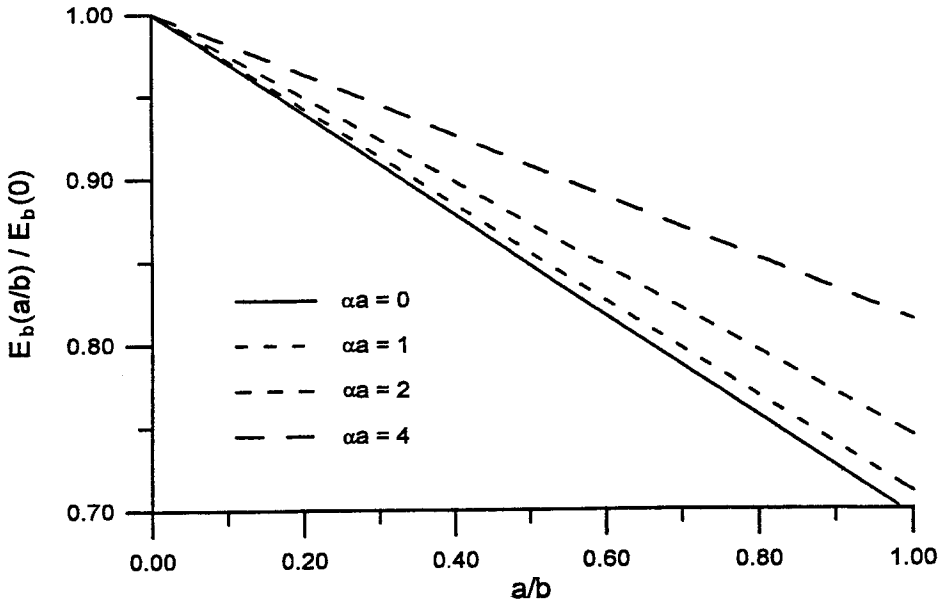

Figure 3.31: Ratio of effective bending modulus of rectangular pad to infinite-long strip pad ($a/b = 0$) versus aspect ratio

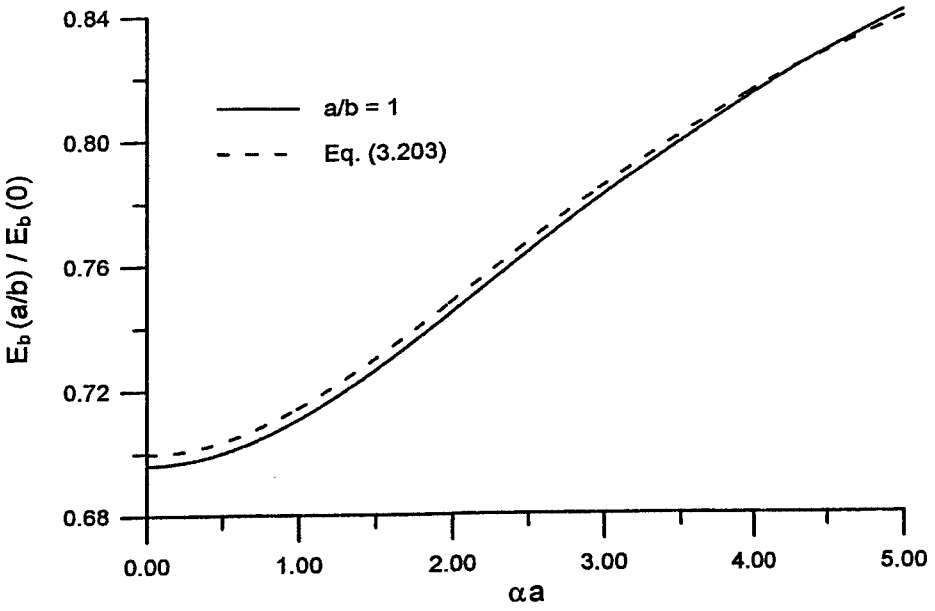

Figure 3.32: Ratio of effective bending modulus of square pad ($a/b = 1$) to infinite-long strip pad ($a/b = 0$) versus αa and its regression curve

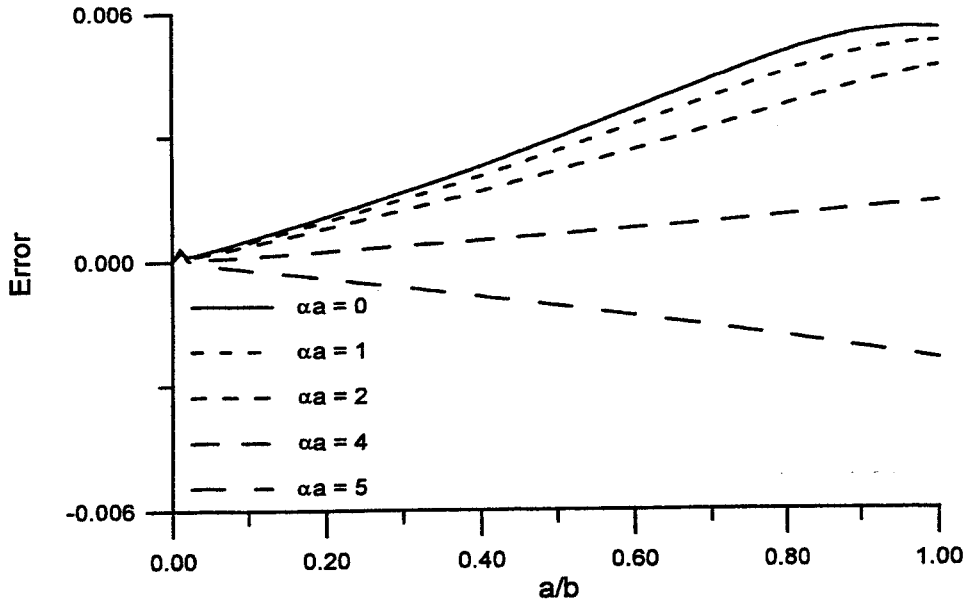

Figure 3.33: Error of empirical formula for effective bending modulus of rectangular pad versus aspect ratio

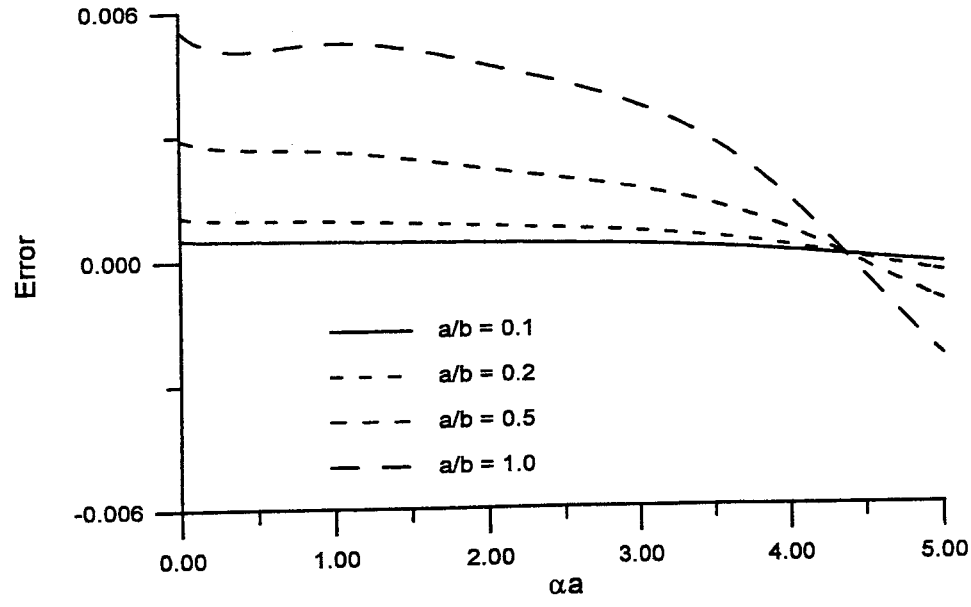

Figure 3.34: Error of empirical formula for effective bending modulus of rectangular pad versus αa

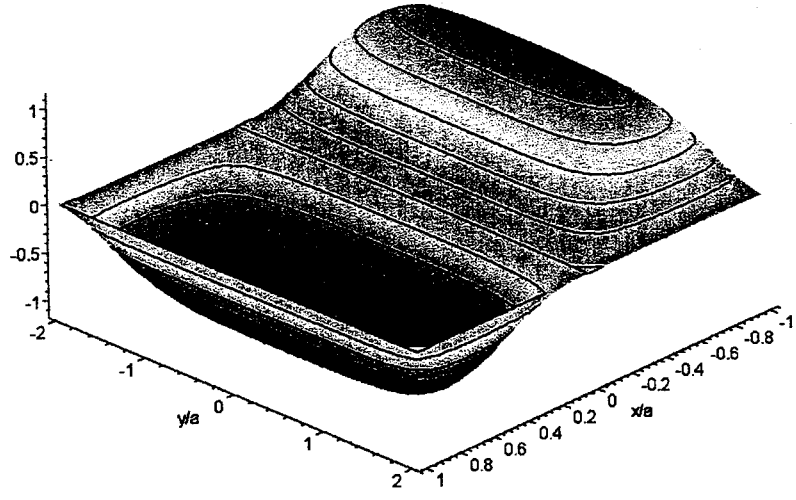

Figure 3.35: 3-D view on contour of normalized pressure in rectangular pad of $a/b = 0.5$ and $\alpha a = 0.5$ under pure bending load

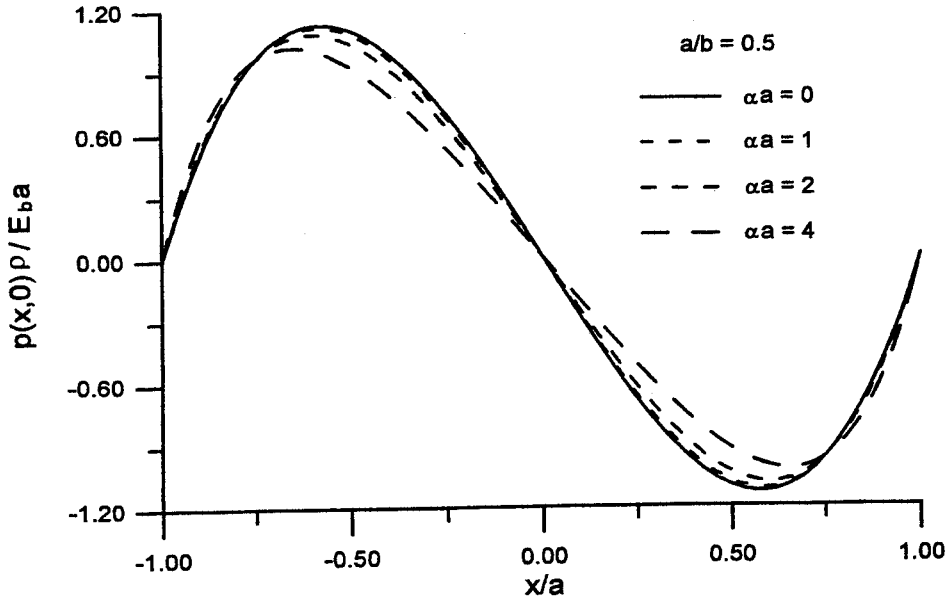

Figure 3.36: Distribution of normalized pressure along x axis in rectangular pad of different αa values and $a/b = 0.5$ under pure bending load

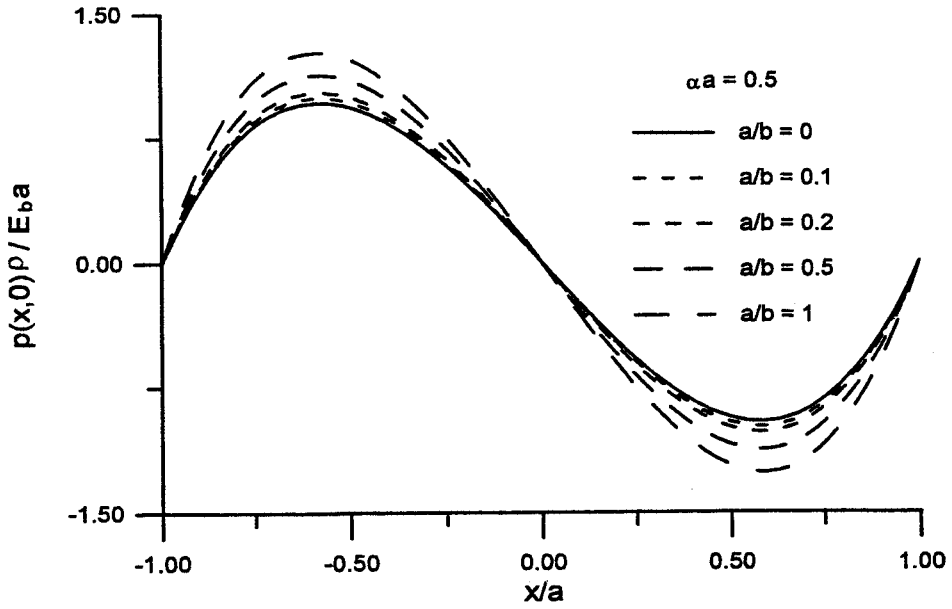

Figure 3.37: Distribution of normalized pressure along x axis in rectangular pad of different aspect ratios and $\alpha a = 0.5$ under pure bending load

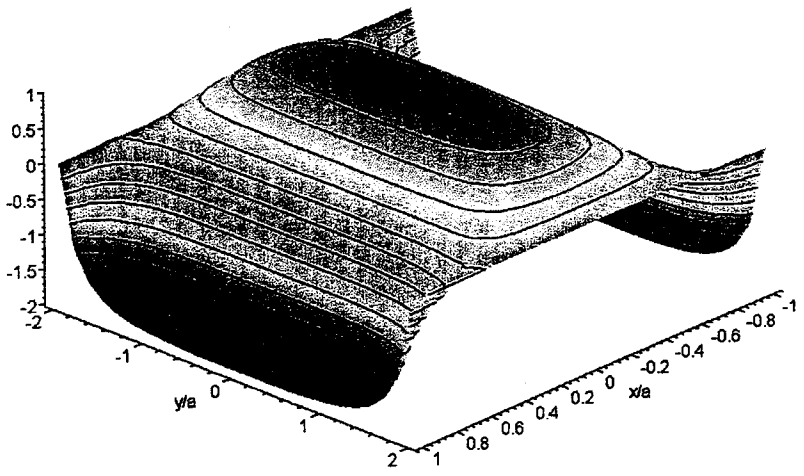

Figure 3.38: 3-D view on contour of bonding shear stress in x direction in rectangular pad of $a/b = 0.5$ and $\alpha a = 0.5$ under pure bending load

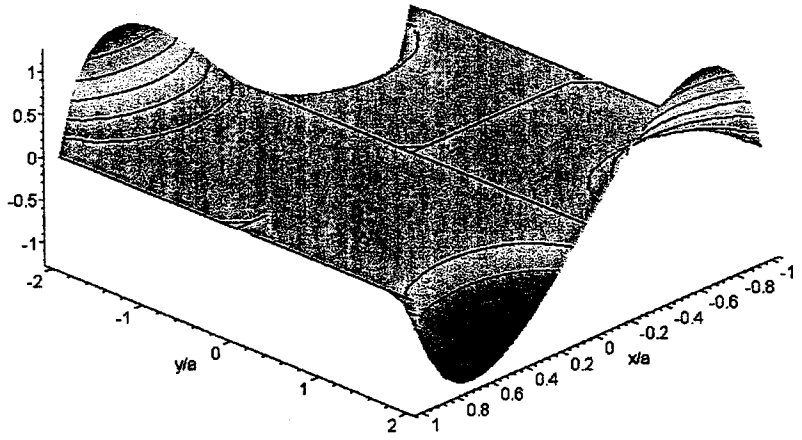

Figure 3.39: 3-D view on contour of bonding shear stress in y direction in rectangular pad of $a/b = 0.5$ and $\alpha a = 0.5$ under pure bending load

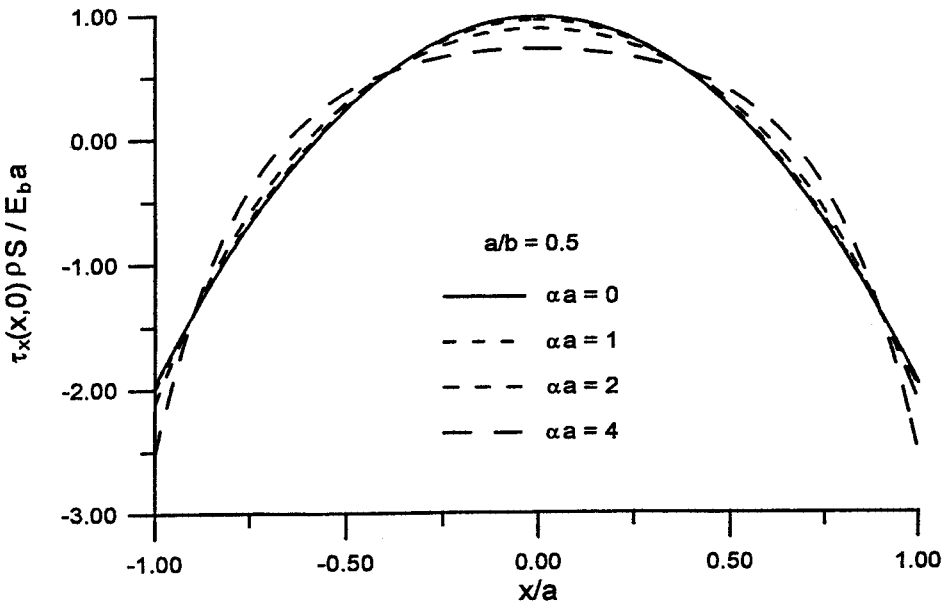

Figure 3.40: Distribution of bonding shear stress in x direction along x axis of rectangular pad under pure bending load

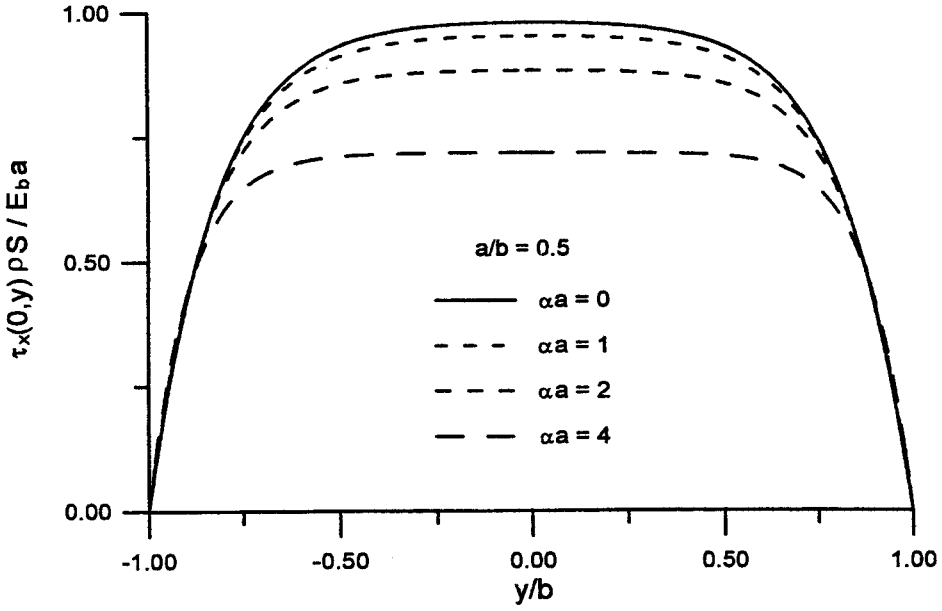

Figure 3.41: Distribution of bonding shear stress in x direction along y axis of rectangular pad under pure bending load

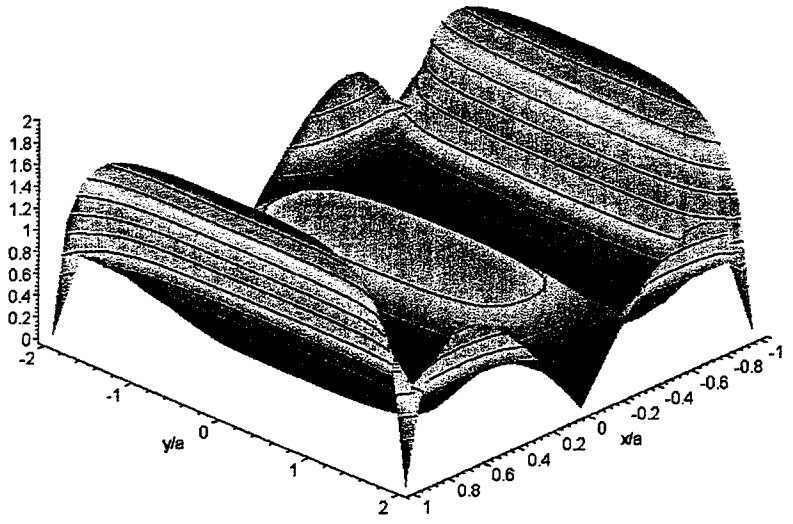

Figure 3.42: 3-D view on contour of bonding shear resultant in rectangular pad of $a/b = 0.5$ and $\alpha a = 0.5$ under pure bending load

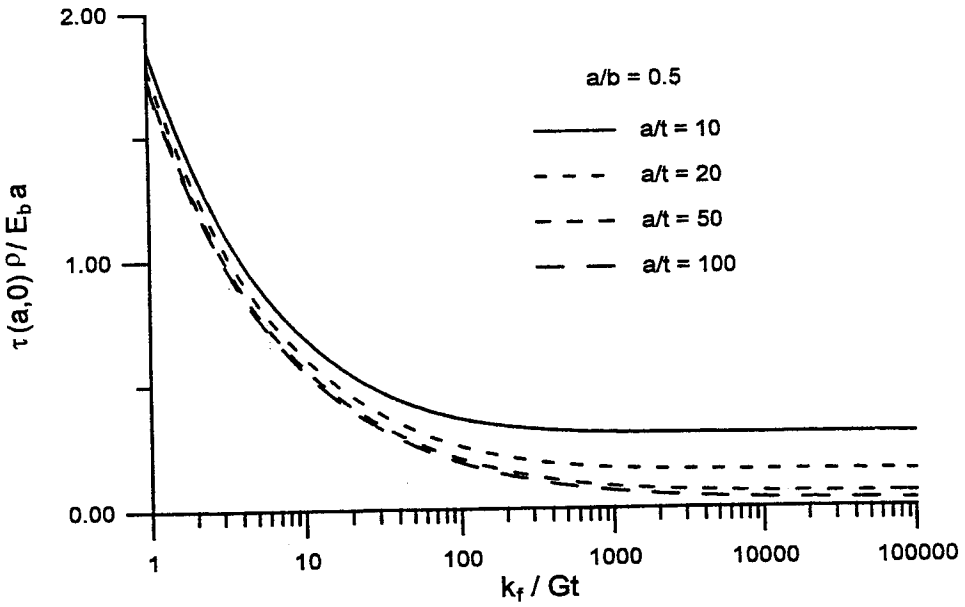

Figure 3.43: Variation of maximum bonding shear resultant with reinforcement stiffness in rectangular pad of different a/t values and $a/b = 0.5$ under pure bending load

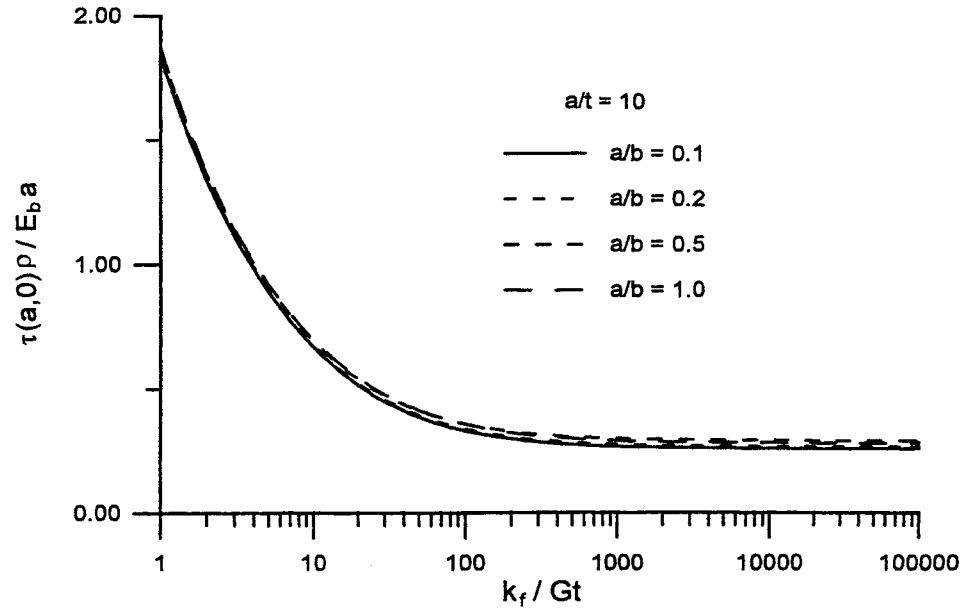

Figure 3.44: Variation of maximum bonding shear resultant with reinforcement stiffness in rectangular pad of different aspect ratios and $a/t = 10$ under pure bending load

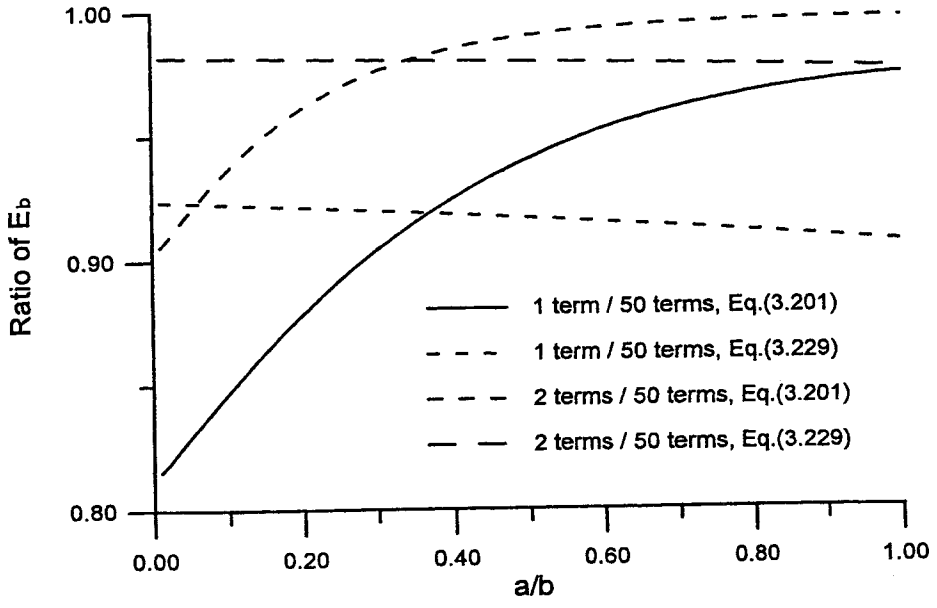

Figure 3.45: Convergence comparison between formulae for effective bending stiffness of rigid-reinforced rectangular pad

4 Analysis of Circular Isolators

4.1 Compression Stiffness of Circular Isolators

4.1.1 Equilibrium in Elastomer and Reinforcement

A layer of elastomer in a circular isolator is shown in Figure 4.1. The elastomeric layer has a radius of b and a thickness of t. Its top and bottom surfaces are perfectly bonded to flexible reinforcements which are modeled as an equivalent sheet of thickness t_f. A cylindrical coordinate system (r, θ, z) is established with the origin at the center of the layer. When the isolator sustains the compression load P along the z direction, the elastomeric layer and the reinforcing sheets are in the axisymmetric stress state, so that the displacement in the θ direction vanishes. The displacements of the elastomer along the r and z directions, denoted as u and w respectively, are assumed to have the forms

$$u(r,z) = u_0(r)\left(1 - \frac{4z^2}{t^2}\right) + u_1(r) \tag{4.1}$$

$$w(r,z) = w(z) \tag{4.2}$$

In Eq. (4.1), the term of u_0 represents the kinematic assumption of quadratically varied deformation of the vertical lines in the elastomer and is supplemented by additional displacement u_1 to accommodate the stretch of the reinforcement. Eq. (4.2) represents the assumption that horizontal planes remain planar in the elastomer.

The assumption of incompressibility in the elastomer means that the summation of the normal strains ϵ_{rr}, $\epsilon_{\theta\theta}$ and ϵ_{zz} in the r, θ and z directions, respectively, equals zero. Bringing the following

axisymmetric strain-displacement relations

$$\epsilon_{rr} = u_{,r} \quad ; \quad \epsilon_{\theta\theta} = \frac{u}{r} \quad ; \quad \epsilon_{zz} = w_{,z} \tag{4.3}$$

to this assumption gives a constraint on displacements in the form

$$u_{,r} + \frac{u}{r} + w_{,z} = 0 \tag{4.4}$$

where the commas imply partial differentiation with respect to the indicated coordinate. Substituting Eqs. (4.1) and (4.2) into the above equation and then taking integration through the thickness of the elastomer from $z = -t/2$ to $z = t/2$ give

$$\frac{2}{3}\left(u_{0,r} + \frac{u_0}{r}\right) + u_{1,r} + \frac{u_1}{r} = \epsilon_c \tag{4.5}$$

in which ϵ_c is the nominal compression strain defined as

$$\epsilon_c = -\frac{w(\frac{t}{2}) - w(-\frac{t}{2})}{t} \tag{4.6}$$

The stress state in the elastomer is assumed to be dominated by the internal pressure p, which gives the normal stress components of the elastomer, σ_{rr}, $\sigma_{\theta\theta}$ and σ_{zz}, as

$$\sigma_{rr} \approx \sigma_{\theta\theta} \approx \sigma_{zz} \approx -p \tag{4.7}$$

Under this stress assumption, the equilibrium equation in the r direction for the stresses in the elastomer

$$\sigma_{rr,r} + \sigma_{rz,z} + \frac{\sigma_{rr} - \sigma_{\theta\theta}}{r} = 0 \tag{4.8}$$

is reduced to

$$-p_{,r} + \sigma_{rz,z} = 0 \tag{4.9}$$

The assumption of linearly elastic behavior of the elastomer means that

$$\sigma_{rz} = G(u_{,z} + w_{,r}) \tag{4.10}$$

with G being the shear modulus of the elastomer. Using the displacement assumptions in Eqs. (4.1) and (4.2), the above equation becomes

$$\sigma_{rz} = -8Gu_0\frac{z}{t^2} \tag{4.11}$$

Substitution of this into the equilibrium equation in Eq. (4.9) leads to

$$p_{,r} = -\frac{8G}{t^2}u_0 \tag{4.12}$$

The internal forces acting in an infinitesimal sector of the reinforcing sheet with a length $\mathrm{d}r$ and an angle $\mathrm{d}\theta$ are shown in Figure 4.2, where N_{rr} and $N_{\theta\theta}$ are the normal forces per unit length in the r and θ directions, respectively. These internal forces are related to the shear stresses σ_{rz}, acting on the top and bottom surfaces of the reinforcement and generated by the deformation of the bonded layers of elastomer, through the equilibrium equation in the r direction

$$(N_{rr}+\mathrm{d}N_{rr})(r+\mathrm{d}r)\mathrm{d}\theta - N_{rr}r\mathrm{d}\theta - N_{\theta\theta}\mathrm{d}r\mathrm{d}\theta + \left(\sigma_{rz}|_{z=-\frac{t}{2}} - \sigma_{rz}|_{z=\frac{t}{2}}\right)[(r+\mathrm{d}r)^2 - r^2]\frac{\mathrm{d}\theta}{2} = 0 \tag{4.13}$$

By neglecting the higher-order derivative terms, the above equation becomes

$$N_{rr,r} + \frac{N_{rr}-N_{\theta\theta}}{r} + \sigma_{rz}|_{z=-\frac{t}{2}} - \sigma_{rz}|_{z=\frac{t}{2}} = 0 \tag{4.14}$$

From Eq. (4.11), we have the shear stresses acting on the top and bottom surfaces of the reinforcement, respectively,

$$\sigma_{rz}|_{z=-\frac{t}{2}} = \frac{4G}{t}u_0 \quad ; \quad \sigma_{rz}|_{z=\frac{t}{2}} = -\frac{4G}{t}u_0 \tag{4.15}$$

The equation of equilibrium in the reinforcing sheet in Eqs. (4.14) becomes

$$N_{rr,r} + \frac{N_{rr}-N_{\theta\theta}}{r} = -\frac{8G}{t}u_0 \tag{4.16}$$

The linearly elastic strain-stress relation in the reinforcement gives

$$u_{1,r} = \frac{1}{E_f}\left(\frac{N_{rr}}{t_f} - \nu\frac{N_{\theta\theta}}{t_f}\right) \tag{4.17}$$

$$\frac{u_1}{r} = \frac{1}{E_f}\left(\frac{N_{\theta\theta}}{t_f} - \nu\frac{N_{rr}}{t_f}\right) \tag{4.18}$$

where E_f is the elastic modulus of the reinforcement and ν is its Poisson's ratio. By inversion, we have the normal forces expressed in terms of displacement components in the reinforcement

$$N_{rr} = \frac{E_f t_f}{1-\nu^2}\left(u_{1,r} + \nu\frac{u_1}{r}\right) \tag{4.19}$$

$$N_{\theta\theta} = \frac{E_f t_f}{1-\nu^2}\left(\frac{u_1}{r} + \nu u_{1,r}\right) \tag{4.20}$$

Substitution of Eqs. (4.19) and (4.20) into Eq. (4.16) leads to

$$u_{1,rr} + \frac{u_{1,r}}{r} - \frac{u_1}{r^2} = -\frac{2}{3}\alpha^2 u_0 \tag{4.21}$$

in which α is defined as

$$\alpha = \sqrt{\frac{12G(1-\nu^2)}{E_f t_f t}} \tag{4.22}$$

4.1.2 Solution of Pressure

For clarification, we denote the function

$$q(r) = u_{1,r} + \frac{u_1}{r} = \frac{1}{r}(ru_1)_{,r} \tag{4.23}$$

Then, Eq. (4.21) becomes

$$u_0 = -\frac{3}{2\alpha^2}q_{,r} \tag{4.24}$$

and Eq. (4.5) becomes

$$u_{0,r} + \frac{u_0}{r} = \frac{3}{2}(\epsilon_c - q) \tag{4.25}$$

Substitution of Eq. (4.24) into Eq. (4.25) leads to

$$q_{,rr} + \frac{1}{r}q_{,r} - \alpha^2 q = -\alpha^2\epsilon_c \tag{4.26}$$

from which we have the expression for $q(r)$

$$q(r) = \epsilon_c + c_1 I_0(\alpha r) + c_2 K_0(\alpha r) \tag{4.27}$$

where c_1 and c_2 are constants to be determined; I_n and K_n are modified Bessel functions of the first and second kinds of order n, respectively. Since $K_0(0) = \infty$, we must have $c_2 = 0$.

Substitution of Eq. (4.27) into Eq. (4.23) gives

$$(ru_1)_{,r} = \epsilon_c r + c_1 r I_0(\alpha r) \tag{4.28}$$

from which we have the expression for u_1

$$u_1(r) = \frac{1}{2}\epsilon_c r + c_1 \frac{1}{\alpha} I_1(\alpha r) + c_3 \frac{1}{r} \tag{4.29}$$

where c_3 is the constant of integration. Since $u_1(0)$ is finite, we must have $c_3 = 0$. The constant c_1 can be determined from the requirement that the radial force vanishes at the edge of the reinforcing sheet, i.e., $N_{rr}(b) = 0$, which with Eq. (4.19) means

$$u_{1,r}(b) + \nu \frac{u_1(b)}{b} = 0 \tag{4.30}$$

Substitution of Eq. (4.29) into this gives

$$c_1 = -\frac{1}{2}\epsilon_c \left[\frac{(1+\nu)\alpha b}{\alpha b I_0(\alpha b) - (1-\nu) I_1(\alpha b)}\right] \tag{4.31}$$

from which

$$u_1(r) = \frac{1}{2}\epsilon_c b \left[\frac{r}{b} - \frac{(1+\nu) I_1(\alpha r)}{\alpha b I_0(\alpha b) - (1-\nu) I_1(\alpha b)}\right] \tag{4.32}$$

Substitution of Eq. (4.24) into Eq. (4.12) gives

$$p_{,r} = \frac{12G}{t^2 \alpha^2} q_{,r} \tag{4.33}$$

The requirement that the normal stress in the radial direction vanishes at the edge of the elastomeric layer means $p(b) = 0$, when applying the assumption in Eq. (4.7). The solution of Eq. (4.33) becomes

$$p(r) = \frac{12G}{t^2 \alpha^2}[q(r) - q(b)] \tag{4.34}$$

Substitution of Eq. (4.31) into Eq. (4.27) gives the solution of $q(r)$; then substituting $q(r)$ into the above equation, we have the solution of $p(r)$

$$p(r) = \epsilon_c \frac{6G(1+\nu)}{t^2\alpha^2} \left[\frac{\alpha b I_0(\alpha b) - \alpha b I_0(\alpha r)}{\alpha b I_0(\alpha b) - (1-\nu) I_1(\alpha b)} \right] \tag{4.35}$$

4.1.3 Effective Compressive Modulus

The compressive stiffness of the isolator is determined by the effective compressive modulus E_c defined as

$$E_c = \frac{\sigma_c}{\epsilon_c} \tag{4.36}$$

where σ_c is the nominal compression stress which is equal to the resultant compression load P divided by the area πb^2. By using the assumption in Eq. (4.7), the resultant compression load P has the form

$$P = -\int_0^b \int_0^{2\pi} \sigma_{zz}\, r \mathrm{d}\theta\, \mathrm{d}r \approx 2\pi \int_0^b p(r) r\, \mathrm{d}r \tag{4.37}$$

Thus, the effective compressive modulus becomes

$$E_c = \frac{2}{\epsilon_c b^2} \int_0^b p(r) r\, \mathrm{d}r \tag{4.38}$$

Substitution of the pressure solution in Eq. (4.35) into the above equation gives

$$E_c = GS^2 \frac{24(1+\nu)}{(\alpha b)^2} \left[\frac{\alpha b I_0(\alpha b) - 2 I_1(\alpha b)}{\alpha b I_0(\alpha b) - (1-\nu) I_1(\alpha b)} \right] \tag{4.39}$$

in which S is the shape factor of the circular layer defined as

$$S = \frac{b}{2t} \tag{4.40}$$

When α tends to zero, substituting the following power series for the Bessel functions

$$I_0(\alpha b) \approx 1 + \frac{(\alpha b)^2}{4} \quad ; \quad I_1(\alpha b) \approx \frac{\alpha b}{2} + \frac{(\alpha b)^3}{16} \tag{4.41}$$

into Eq. (4.39) and neglecting the higher-order terms of αb

$$E_c = 6GS^2 \tag{4.42}$$

which is the effective compressive modulus for the circular layer of elastomer bonded to the rigid reinforcement (Kelly, 1997).

The ratio $E_c/(GS^2)$ is plotted in Figure 4.3 as a function of αb for $\nu = 0, 0.3$ and 0.5, which shows that the effective compressive modulus decreases with increasing αb. To have high compressive modulus, we must keep the value of αb as low as possible. The figure also reveals that a higher Poisson's ratio of the reinforcement tends to have higher modulus, but the difference becomes negligible when αb is small.

If k_f denotes the in-plane stiffness of the reinforcing sheet,

$$k_f = \frac{E_f t_f}{1-\nu^2} \tag{4.43}$$

from Eq. (4.22)

$$\alpha b = S\sqrt{48\frac{Gt}{k_f}} \tag{4.44}$$

Figure 4.4 plots the ratio of the in-plane stiffness of reinforcement to the shear stiffness of elastomer, $K_f/(Gt)$, versus the shape factor S for several αb values, which shows that small αb value is not necessary to mean high reinforcement stiffness. Using the relation in Eq. (4.44), Eq. (4.39) can be rewritten as

$$E_c = \frac{(1+\nu)k_f}{2t}\left[\frac{1-2\frac{I_1(\alpha b)}{\alpha b I_0(\alpha b)}}{1-(1-\nu)\frac{I_1(\alpha b)}{\alpha b I_0(\alpha b)}}\right] \tag{4.45}$$

As αb becomes infinite, the term of the Bessel function $I_1(\alpha b)/[\alpha b I_0(\alpha b)]$ tends to zero, so that

$$E_c = \frac{(1+\nu)k_f}{2t} \tag{4.46}$$

Substituting αb in Eq. (4.44) into Eq. (4.39), we have the normalized effective compressive modulus E_c/G expressed as a function of the shape factor S and the stiffness ratio of the reinforcement to the elastomer $k_f/(Gt)$. The curves of E_c/G versus $k_f/(Gt)$ are plotted in Figure 4.5

for $\nu = 0.3$ and several S values, which shows that the effective compressive modulus increases with increasing the reinforcement stiffness until reaching the asymptotic value in Eq. (4.42). The curve of the smaller shape factor reaches the plateau at the smaller value of $k_f/(Gt)$. The curves of E_c/G versus S are plotted in Figure 4.6 for $\nu = 0.3$ and several $k_f/(Gt)$ values, which shows that the effective compressive modulus increases with increasing the shape factor until reaching the asymptotic value in Eq. (4.46). The curve of the smaller value of $k_f/(Gt)$ reaches the plateau at the smaller shape factor.

4.1.4 Stresses in Elastomer and Reinforcement

Normalized to the nominal compression stress $\sigma_c = E_c\epsilon_c$, the pressure distribution of the elastomer in Eq. (4.35) becomes

$$\frac{p(r)}{E_c\epsilon_c} = \alpha b \left[\frac{I_0(\alpha b) - I_0(\alpha r)}{\alpha b I_0(\alpha b) - 2I_1(\alpha b)}\right] \tag{4.47}$$

When α tends to zero, applying the power series approximation in Eq. (4.41) to the above equation gives

$$\frac{p(r)}{E_c\epsilon_c} = 2\left(1 - \frac{r^2}{b^2}\right) \tag{4.48}$$

which is the pressure distribution in the elastomeric layer bonded to the rigid reinforcement. The distribution of the normalized pressure along the r axis is plotted in Figure 4.7 for $\alpha b = 0$, 1, 2 and 4, which reveals that the effect of the flexibility of the reinforcement is to make the pressure distribution more uniform and to decrease the maximum value at the center. It should be noted that the normalized pressure distribution in Eq. (4.47) is independent of the Poisson's ratio of the reinforcement ν.

If τ_r denotes the shear stress in the radial direction on the bonding surface between the elastomer and the reinforcement, from Eqs. (4.12) and (4.15)

$$\tau_r(r) = \sigma_{rz}|_{z=-\frac{t}{2}} = -\frac{t}{2}p_{,r} \tag{4.49}$$

Substitution of Eq. (4.47) into the above equation gives the normalized shear stress as

$$\frac{\tau_r(r)}{E_c\epsilon_c} = \frac{1}{4S}\left[\frac{(\alpha b)^2 I_1(\alpha r)}{\alpha b I_0(\alpha b) - 2I_1(\alpha b)}\right] \tag{4.50}$$

which shows that the normalized bonding shear stress distribution is independent of the Poisson's ratio of the reinforcement ν. Substituting Eq. (4.48) into Eq. (4.49),

$$\frac{\tau_r(r)}{E_c\epsilon_c} = \frac{1}{S}\left(\frac{r}{b}\right) \tag{4.51}$$

which is the bonding shear stress for the rigid reinforcement. The curves of $\tau_r(r)S/(E_c\epsilon_c)$ versus r/b are plotted in Figure 4.8 for $\alpha b = 0$, 1, 2 and 4 to show the distribution of the bonding shear stress along the r axis. The figure demonstrates that the effect of the flexibility of the reinforcement is to make the shear stress distribution more concentrated on the edge and to increase the maximum value at the edge. The normalized shear stress at the edge, $\tau_r(b)/(E_c\epsilon_c)$, is plotted in Figure 4.9 as a function of the stiffness ratio $k_f/(Gt)$ for several S values. The figure shows that, under the same compressive load, increasing the reinforcement stiffness or the shape factor will reduce the maximum bonding shear stress in the radial direction.

To depict the reinforcement displacement pattern under the compressive load, the curves of $u_1(r)/(b\epsilon_c)$ versus r/b, calculated from Eq. (4.32), are plotted in Figure 4.10 for $\nu = 0.3$ and several αb values. The figure demonstrates that the radial displacement of the reinforcement increases with increasing the value of αb, i.e., with increasing the reinforcement stiffness or decreasing the shape factor.

The radial force N_{rr} and the hoop force $N_{\theta\theta}$ in the reinforcement can be derived by substituting Eq. (4.32) into Eqs. (4.19) and (4.20), respectively, which gives

$$\frac{N_{rr}(r)}{E_c\epsilon_c t} = \frac{I_0(\alpha b) - I_0(\alpha r) - (1-\nu)\left[\frac{I_1(\alpha b)}{\alpha b} - \frac{I_1(\alpha r)}{\alpha r}\right]}{I_0(\alpha b) - 2\frac{I_1(\alpha b)}{\alpha b}} \tag{4.52}$$

and

$$\frac{N_{\theta\theta}(r)}{E_c\epsilon_c t} = \frac{I_0(\alpha b) - \nu I_0(\alpha r) - (1-\nu)\left[\frac{I_1(\alpha b)}{\alpha b} + \frac{I_1(\alpha r)}{\alpha r}\right]}{I_0(\alpha b) - 2\frac{I_1(\alpha b)}{\alpha b}} \tag{4.53}$$

The distributions of the radial force and the hoop force along the r axis are plotted in Figure 4.11 and Figure 4.12, respectively, for $\nu = 0.3$ and several αb values, which show that increasing αb value reduces the maximum values of the radial force and the hoop force at the center. At the center, the radial force is equal to the hoop force, $N_{rr}(0) = N_{\theta\theta}(0)$. At the edge,

$$\frac{N_{\theta\theta}(b)}{E_c \epsilon_c t} = 1 - \nu \tag{4.54}$$

which is independent of αb.

4.2 Bending Stiffness of Circular Isolators

4.2.1 Equilibrium in Elastomeric Layer

For a layer of elastomer in a circular isolator shown in Figure 4.13, the elastomeric layer has a radius of b and a thickness of t. Its top and bottom surfaces are perfectly bonded to flexible reinforcements, which are modeled as an equivalent sheet of thickness t_f. When a pure bending moment M is applied to the top and bottom reinforcing sheets, assuming the reinforcing sheets remain planar, the two sheets rotate about the y axis and form an angle ϕ. A cylindrical coordinate system (r, θ, z) is established with the origin at the center of the layer, so that the angle ϕ is symmetric to the r-θ plane at $z = 0$. Let u, v and w denote the displacements of the elastomer along the r, θ and z directions, respectively, which are assumed to have the form

$$u(r, \theta, z) = u_0(r, \theta)\left(1 - \frac{4z^2}{t^2}\right) + u_1(r, \theta) \tag{4.55}$$

$$v(r, \theta, z) = v_0(r, \theta)\left(1 - \frac{4z^2}{t^2}\right) + v_1(r, \theta) \tag{4.56}$$

$$w(r, \theta, z) = \frac{1}{\rho} z r \cos\theta \tag{4.57}$$

in which ρ is the radius of the bending curvature defined as

$$\rho = \frac{t}{\phi} \tag{4.58}$$

In Eqs. (4.55) and (4.56), the terms of u_0 and v_0 represents the kinematic assumption of quadratically varied displacements and are supplemented by additional displacements u_1 and v_1, respectively, which are constant through the thickness and are intended to accommodate the stretch of the reinforcement. Eq. (4.57) represents the assumption that horizontal planes in the elastomer remain planar.

The assumption of incompressibility of the elastomer means that the summation of three normal strain components, ϵ_{rr}, $\epsilon_{\theta\theta}$ and ϵ_{zz}, equals zero. Bringing the strain-displacement relations

$$\epsilon_{rr} = u_{,r} \quad ; \quad \epsilon_{\theta\theta} = \frac{u + v_{,\theta}}{r} \quad ; \quad \epsilon_{zz} = w_{,z} \tag{4.59}$$

gives a constraint on displacements in the form

$$u_{,r} + \frac{u}{r} + \frac{v_{,\theta}}{r} + w_{,z} = 0 \tag{4.60}$$

where the commas imply partial differentiation with respect to the indicated coordinate. Substituting Eqs. (4.55) to (4.57) into the above equation and then taking integration through the thickness from $z = -t/2$ to $z = t/2$ give

$$\frac{2}{3}(u_{0,r} + \frac{u_0}{r} + \frac{v_{0,\theta}}{r}) + u_{1,r} + \frac{u_1}{r} + \frac{v_{1,\theta}}{r} = -\frac{1}{\rho} r \cos\theta \tag{4.61}$$

For clarification, the form is denoted

$$q = u_{1,r} + \frac{1}{r} u_1 + \frac{1}{r} v_{1,\theta} \tag{4.62}$$

Eq. (4.61) becomes

$$\frac{2}{3}(u_{0,r} + \frac{u_0}{r} + \frac{v_{0,\theta}}{r}) = -q - \frac{1}{\rho} r \cos\theta \tag{4.63}$$

The stress state in the elastomer is assumed to be dominated by the internal pressure p, such that the normal stress components σ_{rr}, $\sigma_{\theta\theta}$ and σ_{zz} differ from $-p$ only by terms of order pt^2/b^2. The shear stress components σ_{rz} and $\sigma_{\theta z}$ which are generated by the constraint of the reinforcement

are assumed to be of order pt/b; the in-plane shear stress $\sigma_{r\theta}$ is assumed to be of the order pt^2/b^2. The thickness of a single elastomeric layer, t, in an isolator is generally much smaller than the radius of the isolator, b. Therefore, we can neglect the terms of order pt^2/b^2, which gives the stress components of the elastomer as

$$\sigma_{rr} \approx \sigma_{\theta\theta} \approx \sigma_{zz} \approx -p \quad ; \quad \sigma_{r\theta} \approx 0 \tag{4.64}$$

Under these stress assumptions, the equilibrium equation in the r direction

$$\sigma_{rr,r} + \frac{1}{r}\sigma_{r\theta,\theta} + \sigma_{rz,z} + \frac{1}{r}(\sigma_{rr} - \sigma_{\theta\theta}) = 0 \tag{4.65}$$

is reduced to

$$-p_{,r} + \sigma_{rz,z} = 0 \tag{4.66}$$

The equilibrium equation in the θ direction

$$\sigma_{r\theta,r} + \frac{1}{r}\sigma_{\theta\theta,\theta} + \sigma_{\theta z,z} + \frac{2}{r}\sigma_{r\theta} = 0 \tag{4.67}$$

becomes

$$-\frac{1}{r}p_{,\theta} + \sigma_{\theta z,z} = 0 \tag{4.68}$$

The assumption of linearly elastic behavior in the elastomer means that

$$\sigma_{rz} = G(u_{,z} + w_{,r}) \tag{4.69}$$

$$\sigma_{\theta z} = G(v_{,z} + \frac{1}{r}w_{,\theta}) \tag{4.70}$$

with G being the shear modulus of the elastomer. Using the displacement assumptions in Eqs. (4.55) to (4.57), the above equations become

$$\sigma_{rz} = G\left(-\frac{8}{t^2}u_0 z + \frac{1}{\rho}z\cos\theta\right) \tag{4.71}$$

$$\sigma_{\theta z} = G\left(-\frac{8}{t^2}v_0 z - \frac{1}{\rho}z\sin\theta\right) \tag{4.72}$$

Substitution of these into the equilibrium equations in Eqs. (4.66) and (4.68), respectively, leads to

$$p_{,r} = G\left(-\frac{8}{t^2}u_0 + \frac{1}{\rho}\cos\theta\right) \tag{4.73}$$

$$p_{,\theta} = Gr\left(-\frac{8}{t^2}v_0 - \frac{1}{\rho}\sin\theta\right) \tag{4.74}$$

From these,

$$(rp_{,r})_{,r} + \left(\frac{1}{r}p_{,\theta}\right)_{,\theta} = G\left[\left(-\frac{8}{t^2}ru_0 + \frac{1}{\rho}r\cos\theta\right)_{,r} + \left(-\frac{8}{t^2}v_0 - \frac{1}{\rho}\sin\theta\right)_{,\theta}\right] \tag{4.75}$$

which can be simplified as

$$rp_{,rr} + p_{,r} + \frac{1}{r}p_{,\theta\theta} = -\frac{8G}{t^2}(ru_{0,r} + u_0 + v_{0,\theta}) \tag{4.76}$$

Subtracting the differentiation of Eq. (4.73) with respect to θ from the differentiation of Eq. (4.74) with respect to r,

$$v_{0,r} + \frac{1}{r}v_0 - \frac{1}{r}u_{0,\theta} = 0 \tag{4.77}$$

4.2.2 Equilibrium in Reinforcing Sheet

The internal forces acting in an infinitesimal sector of the reinforcing sheet with a length $\mathrm{d}r$ and an angle $\mathrm{d}\theta$ are shown in Figure 4.14, where N_{rr} and $N_{\theta\theta}$ are the normal forces per unit length in the r and θ directions, respectively. $N_{r\theta}$ is the in-plane shear force per unit length. These internal forces are related to the bonding shear stresses σ_{rz} and $\sigma_{\theta z}$, created by the elastomeric layers bonded on the top and bottom surfaces of the reinforcing sheet, through two equilibrium equations in the r and θ directions

$$N_{rr,r} + \frac{1}{r}(N_{rr} - N_{\theta\theta}) + \frac{1}{r}N_{r\theta,\theta} + \left(\sigma_{rz}|_{z=-\frac{t}{2}} - \sigma_{rz}|_{z=\frac{t}{2}}\right) = 0 \tag{4.78}$$

$$\frac{1}{r}N_{\theta\theta,\theta} + N_{r\theta,r} + \frac{2}{r}N_{r\theta} + \left(\sigma_{\theta z}|_{z=-\frac{t}{2}} - \sigma_{\theta z}|_{z=\frac{t}{2}}\right) = 0 \tag{4.79}$$

After making use of Eqs. (4.71) and (4.72) to calculate the bonding shear stresses, these equilibrium equations in the reinforcement become

$$N_{rr,r} + \frac{1}{r}(N_{rr} - N_{\theta\theta}) + \frac{1}{r}N_{r\theta,\theta} = -G\left(\frac{8}{t}u_0 - \frac{t}{\rho}\cos\theta\right) \tag{4.80}$$

$$\frac{1}{r}N_{\theta\theta,\theta} + N_{r\theta,r} + \frac{2}{r}N_{r\theta} = -G\left(\frac{8}{t}v_0 + \frac{t}{\rho}\sin\theta\right) \tag{4.81}$$

The displacements in the reinforcement are related to the internal normal forces through the linearly elastic strain-stress relation such that

$$u_{1,r} = \frac{1}{E_f}\left(\frac{N_{rr}}{t_f} - \nu\frac{N_{\theta\theta}}{t_f}\right) \tag{4.82}$$

$$\frac{1}{r}(u_1 + v_{1,\theta}) = \frac{1}{E_f}\left(\frac{N_{\theta\theta}}{t_f} - \nu\frac{N_{rr}}{t_f}\right) \tag{4.83}$$

where E_f is the elastic modulus of the reinforcement and ν is the Poisson's ratio of the reinforcement. By inversion, we have the normal forces expressed in terms of displacement components

$$N_{rr} = \frac{E_f t_f}{1-\nu^2}\left(u_{1,r} + \nu\frac{v_{1,\theta} + u_1}{r}\right) \tag{4.84}$$

$$N_{\theta\theta} = \frac{E_f t_f}{1-\nu^2}\left(\frac{v_{1,\theta} + u_1}{r} + \nu u_{1,x}\right) \tag{4.85}$$

The in-plane shear force has the following relation with the displacements

$$N_{r\theta} = \frac{E_f t_f}{2(1+\nu)}\left(\frac{u_{1,\theta}}{r} + v_{1,r} - \frac{v_1}{r}\right) \tag{4.86}$$

Substitution of Eqs. (4.84) to (4.86) into Eqs. (4.80) and (4.81) leads to

$$q_{,r} - \frac{(1-\nu)}{2}\frac{s_{,\theta}}{r} = -\frac{t^2\alpha^2}{12}\left(\frac{8}{t^2}u_0 - \frac{1}{\rho}\cos\theta\right) \tag{4.87}$$

$$\frac{q_{,\theta}}{r} + \frac{(1-\nu)}{2}s_{,r} = -\frac{t^2\alpha^2}{12}\left(\frac{8}{t^2}v_0 + \frac{1}{\rho}\sin\theta\right) \tag{4.88}$$

where α is defined in Eq. (4.22) and s is defined as

$$s = v_{1,r} + \frac{1}{r}v_1 - \frac{1}{r}u_{1,\theta} \tag{4.89}$$

To eliminate the s terms in Eqs. (4.87) and (4.88), multiply Eq. (4.87) by r and differentiate the result with respect to r; then add this to the differentiation of Eq. (4.88) with respect to θ, which gives

$$rq_{,rr} + q_{,r} + \frac{1}{r}q_{,\theta\theta} = -\frac{2}{3}\alpha^2(ru_{0,r} + u_0 + v_{0,\theta}) \tag{4.90}$$

Substitution of Eq. (4.63) into the above equation yields

$$q_{,rr} + \frac{1}{r}q_{,r} + \frac{1}{r^2}q_{,\theta\theta} - \alpha^2 q = \frac{1}{\rho}\alpha^2 r\cos\theta \tag{4.91}$$

To eliminate the q terms in Eqs. (4.87) and (4.88), multiply Eq. (4.88) by r and differentiate the result with respect to r; then subtract this from the differentiation of Eq. (4.87) with respect to θ, which gives

$$-\frac{1-\nu}{2}(rs_{,rr} + s_{,r} + \frac{1}{r}s_{,\theta\theta}) = \frac{2}{3}\alpha^2(rv_{0,r} + v_0 - u_{0,\theta}) \tag{4.92}$$

Substitution of Eq. (4.77) into the above equation yields

$$s_{,rr} + \frac{1}{r}s_{,r} + \frac{1}{r^2}s_{,\theta\theta} = 0 \tag{4.93}$$

4.2.3 Series Solutions of Governing Equations

Under the pure bending moment, the pressure and displacements have the following symmetric and anti-symmetric properties

$$p(r,\theta) = p(r,-\theta) = -p(r,\pi-\theta) \tag{4.94}$$

$$u_1(r,\theta) = u_1(r,-\theta) = -u_1(r,\pi-\theta) \tag{4.95}$$

$$v_1(r,\theta) = -v_1(r,-\theta) = v_1(r,\pi-\theta) \tag{4.96}$$

According to the definitions of q in Eq. (4.62) and s in Eq. (4.89),

$$q(r,\theta) = q(r,-\theta) = -q(r,\pi-\theta) \tag{4.97}$$

$$s(r,\theta) = -s(r,-\theta) = s(r,\pi-\theta) \tag{4.98}$$

The method of separation of variables is applied to solve the partial differential equation in Eq. (4.91). By defining the complementary solution of $q(r,\theta)$ equal to $R(r)\Theta(\theta)$, the functions $R(r)$ and $\Theta(\theta)$ must satisfy the following relation

$$\frac{R_{,rr}+\frac{1}{r}R_{,r}-\alpha^2 R}{\frac{1}{r^2}R}=-\frac{\Theta_{,\theta\theta}}{\Theta}=c \tag{4.99}$$

where c is a constant. Since $q(r,\theta)$ is a periodic function of θ, i.e. $q(r,\theta)=q(r,\theta+2\pi)$, we can set $c=n^2$ where n is an integer. The solution of Θ for a particular n value is

$$\Theta_n=c_1\cos n\theta+c_2\sin n\theta \tag{4.100}$$

with c_1 and c_2 being constants. The symmetric property in Eq. (4.97) means $c_2=0$, and the anti-symmetric property in Eq. (4.97) implies that n has to be an odd integer. The differential equation for R becomes

$$R_{,rr}+\frac{1}{r}R_{,r}-\left(\alpha^2+\frac{n^2}{r^2}\right)R=0 \tag{4.101}$$

The solution of R for a particular n value is

$$R_n(r)=c_3I_n(\alpha r)+c_4K_n(\alpha r) \tag{4.102}$$

where I_n and K_n are modified Bessel functions of the first and second kinds of order n, respectively, and c_3 and c_4 are constants. Since $q(r,\theta)$ is finite at $r=0$ and $K_n(0)=\infty$, we must have $c_4=0$. Including the particular solution of $q(r,\theta)$ in Eq. (4.91), we have the series solution of q

$$q(r,\theta)=-\frac{1}{\rho}r\cos\theta+\sum_{n=1,3,5,\ldots}^{\infty}A_nI_n(\alpha r)\cos n\theta \tag{4.103}$$

where A_n is a constant to be determined.

Combining Eqs. (4.76) with (4.90) to eliminate the terms of $ru_{0,r}+u_0+v_{0,\theta}$ yields

$$\left(q-\frac{t^2\alpha^2}{12G}p\right)_{,rr}+\frac{1}{r}\left(q-\frac{t^2\alpha^2}{12G}p\right)_{,r}+\frac{1}{r^2}\left(q-\frac{t^2\alpha^2}{12G}p\right)_{,\theta\theta}=0 \tag{4.104}$$

When the method of separation of variables is applied to solve this equation, the symmetric properties in Eqs. (4.94) and (4.97) for p and q indicate that we can assume that

$$q - \frac{t^2\alpha^2}{12G}p = \sum_{n=1,3,5,\ldots}^{\infty} \bar{R}_n(r)\cos n\theta \tag{4.105}$$

Substitution of this into Eq. (4.104) gives

$$\bar{R}_{n,rr} + \frac{1}{r}\bar{R}_{n,r} - \frac{n^2}{r^2}\bar{R}_n = 0 \tag{4.106}$$

which has a solution

$$\bar{R}_n(r) = c_3 r^n + c_4 r^{-n} \tag{4.107}$$

To keep $\bar{R}_n$ being finite at $r = 0$, it must be $c_4 = 0$, so that

$$q - \frac{t^2\alpha^2}{12G}p = \sum_{n=1,3,5,\ldots}^{\infty} B_n r^n \cos n\theta \tag{4.108}$$

where B_n is a constant to be determined. Substitution of Eq. (4.103) into the above equation gives

$$p(r,\theta) = \frac{12G}{t^2\alpha^2}\left\{-\frac{1}{\rho}r\cos\theta + \sum_{n=1,3,5,\ldots}^{\infty}[A_n I_n(\alpha r) - B_n r^n]\cos n\theta\right\} \tag{4.109}$$

The method of separation of variables is also applied to solve $s(r,\theta)$ in Eq. (4.93). Using the anti-symmetric property in Eq. (4.98), we can assume that

$$s(r,\theta) = \sum_{n=1,3,5,\ldots}^{\infty} s^{(n)}(r)\sin n\theta \tag{4.110}$$

in which $s^{(n)}(r)$ is the amplitude of the nth term. Substitution of this into Eq. (4.93) gives

$$s^{(n)}_{,rr} + \frac{1}{r}s^{(n)}_{,r} - \frac{n^2}{r^2}s^{(n)} = 0 \tag{4.111}$$

To keep $s^{(n)}$ being finite at $r = 0$, the solution of $s^{(n)}(r)$ is

$$s^{(n)}(r) = C_n r^n \tag{4.112}$$

where C_n is a constant to be determined, so that

$$s(r,\theta) = \sum_{n=1,3,5,\ldots}^{\infty} C_n r^n \sin n\theta \tag{4.113}$$

4.2.4 Constants in Series Solutions

There are three sets of constants, A_n, B_n and C_n, to be determined in the series solutions, which requires three equations to show the relations among these constants. In this section, we establish the first two equations. The third equation will be derived in the next section.

Combination of Eq. (4.73), which represents the elastomer equilibrium in the r direction, and Eq. (4.87), which represents the reinforcement equilibrium in the r direction, yields

$$q_{,r} - \frac{(1-\nu)}{2}\frac{s_{,\theta}}{r} = \frac{t^2\alpha^2}{12G}p_{,r} \tag{4.114}$$

Substituting of the series solutions in Eqs. (4.103), (4.109) and (4.113) into the above equation,

$$\sum_{n=1,3,5,\ldots}^{\infty}\left[B_n - \frac{(1-\nu)}{2}C_n\right] nr^{n-1}\cos n\theta = 0 \tag{4.115}$$

which gives

$$C_n = \frac{2}{(1-\nu)}B_n \qquad \text{for } n = 1,3,5,\ldots \tag{4.116}$$

Combination of Eq. (4.74), which represents the elastomer equilibrium in the θ direction, and Eq. (4.88), which represents the reinforcement equilibrium in the θ direction, yields

$$\frac{q_{,\theta}}{r} + \frac{(1-\nu)}{2}s_{,r} = \frac{t^2\alpha^2}{12G}\frac{p_{,\theta}}{r} \tag{4.117}$$

Substitution of the series solutions in Eqs. (4.103), (4.109) and (4.113) into the above equation will give the same result in Eq. (4.116).

Based on the assumption of pressure domination in Eq. (4.64), the boundary condition that the normal stress in the radial direction is zero at the edge of the elastomeric layer means $p(b,\theta) = 0$, which with Eq. (4.109) gives

$$-\frac{1}{\rho}b\cos\theta + \sum_{n=1,3,5,\ldots}^{\infty}[A_nI_n(\alpha b) - B_nb^n]\cos n\theta = 0 \tag{4.118}$$

so that,

$$B_1 = -\frac{1}{\rho} + \frac{1}{b} A_1 I_1(\alpha b) \tag{4.119}$$

and

$$B_n = \frac{1}{b^n} A_n I_n(\alpha b) \qquad \text{for } n = 3, 5, 7, ... \tag{4.120}$$

4.2.5 Displacements in Reinforcing Sheet

Since the solution of $q(r, \theta)$ in Eq. (4.103) is a cosine series and the solution of $s(r, \theta)$ in Eq. (4.113) is a sine series, the definitions of q in Eq. (4.62) and s in Eq. (4.89) imply that we can assume u_1 be a cosine series, according to the symmetric properties in Eq. (4.95),

$$u_1(r, \theta) = \sum_{n=1,3,5,...}^{\infty} u_1^{(n)}(r) \cos n\theta \tag{4.121}$$

and v_1 be a sine series, according to the anti-symmetric properties in Eq. (4.96),

$$v_1(r, \theta) = \sum_{n=1,3,5,...}^{\infty} v_1^{(n)}(r) \sin n\theta \tag{4.122}$$

where $u_1^{(n)}(r)$ and $v_1^{(n)}(r)$ are the amplitudes of the nth term in $u_1(r, \theta)$ and $v_1(r, \theta)$, respectively. Using these series forms of u_1 and v_1 and the series expression of q in Eq. (4.103), the definition of q in Eq. (4.62) gives

$$u_{1,r}^{(1)} + \frac{1}{r} u_1^{(1)} + \frac{1}{r} v_1^{(1)} = -\frac{1}{\rho} r + A_1 I_1(\alpha r) \tag{4.123}$$

and

$$u_{1,r}^{(n)} + \frac{1}{r} u_1^{(n)} + \frac{n}{r} v_1^{(1)} = A_n I_n(\alpha r) \qquad \text{for } n = 3, 5, 7, ... \tag{4.124}$$

Using the series expression of s in Eq. (4.113) and the series forms of u_1 and v_1, the definition of s in Eq. (4.89) gives

$$v_{1,r}^{(n)} + \frac{1}{r} v_1^{(n)} + \frac{n}{r} u_1^{(n)} = C_n r^n \qquad \text{for } n = 1, 3, 5, ... \tag{4.125}$$

Summation of Eqs. (4.123) and (4.125) with $n = 1$ yields

$$\left(u_1^{(1)} + v_1^{(1)}\right)_{,r} + \frac{2}{r}\left(u_1^{(1)} + v_1^{(1)}\right) = \left(C_1 - \frac{1}{\rho}\right) r + A_1 I_1(\alpha r) \tag{4.126}$$

It is known that the modified Bessel function has the relation

$$I_2(r)_{,r} + \frac{2}{r} I_2(r) = I_1(r) \tag{4.127}$$

so that the particular solution of Eq. (4.126) is

$$u_1^{(1)} + v_1^{(1)} = \frac{1}{4}\left(C_1 - \frac{1}{\rho}\right) r^2 + \frac{1}{\alpha} A_1 I_2(\alpha r) \tag{4.128}$$

The complementary solution of Eq. (4.126) is

$$u_1^{(1)} + v_1^{(1)} = cr^{-2} \tag{4.129}$$

which is infinite at $r = 0$, unless the constant $c = 0$. Subtraction of Eq. (4.123) from Eq. (4.125) with $n = 1$ yields

$$\left(u_1^{(1)} - v_1^{(1)}\right)_{,r} = -\left(C_1 + \frac{1}{\rho}\right) r + A_1 I_1(\alpha r) \tag{4.130}$$

Since $I_0(r)_{,r} = I_1(r)$, this equation has the solution

$$u_1^{(1)} - v_1^{(1)} = -\frac{1}{2}\left(C_1 + \frac{1}{\rho}\right) r^2 + \frac{1}{\alpha} A_1 I_0(\alpha r) + D_1 \tag{4.131}$$

where D_1 is the integration constant. From Eqs. (4.128) and (4.131),

$$u_1^{(1)}(r) = -\frac{1}{8}\left(C_1 + 3\frac{1}{\rho}\right) r^2 + \frac{1}{2\alpha} A_1 [I_2(\alpha r) + I_0(\alpha r)] + \frac{1}{2} D_1 \tag{4.132}$$

$$v_1^{(1)}(r) = \frac{1}{8}\left(3C_1 + \frac{1}{\rho}\right) r^2 + \frac{1}{2\alpha} A_1 [I_2(\alpha r) - I_0(\alpha r)] - \frac{1}{2} D_1 \tag{4.133}$$

so that

$$u_{1,r}^{(1)}(r) = -\frac{1}{4}\left(C_1 + 3\frac{1}{\rho}\right) r + A_1 \left[I_1(\alpha r) - \frac{1}{\alpha r} I_2(\alpha r)\right] \tag{4.134}$$

$$v_{1,r}^{(1)}(r) = \frac{1}{4}\left(3C_1 + \frac{1}{\rho}\right) r - A_1 \frac{1}{\alpha r} I_2(\alpha r) \tag{4.135}$$

For the terms of $n > 1$, summation of Eqs. (4.124) and (4.125) yields

$$\left(u_1^{(n)} + v_1^{(n)}\right)_{,r} + \frac{n+1}{r}\left(u_1^{(n)} + v_1^{(n)}\right) = C_n r^n + A_n I_n(\alpha r) \tag{4.136}$$

Since the modified Bessel function has the relation

$$I_{n+1}(r)_{,r} + \frac{n+1}{r} I_{n+1}(r) = I_n(r) \tag{4.137}$$

the particular solution of Eq. (4.136) can be

$$u_1^{(n)} + v_1^{(n)} = \frac{1}{2(n+1)} C_n r^{n+1} + \frac{1}{\alpha} A_n I_{n+1}(\alpha r) \tag{4.138}$$

The complementary solution of Eq. (4.136) is

$$u_1^{(n)} + v_1^{(n)} = c r^{-(n+1)} \tag{4.139}$$

which is infinite at $r = 0$, unless the constant $c = 0$. Subtraction of Eq. (4.124) from Eq. (4.125) with $n > 1$ yields

$$\left(u_1^{(n)} - v_1^{(n)}\right)_{,r} - \frac{(n-1)}{r}\left(u_1^{(n)} - v_1^{(n)}\right) = -C_n r^n + A_n I_n(\alpha r) \tag{4.140}$$

Applying the following relation of the modified Bessel functions

$$I_{n-1}(r)_{,r} - \frac{(n-1)}{r} I_{n-1}(r) = I_n(r) \tag{4.141}$$

the solution is

$$u_1^{(n)} - v_1^{(n)} = -\frac{1}{2} C_n r^{n+1} + \frac{1}{\alpha} A_n I_{n-1}(\alpha r) + D_n r^{n-1} \tag{4.142}$$

where D_n is the integration constant. From Eqs. (4.138) and (4.142)

$$u_1^{(n)}(r) = -\frac{n}{4(n+1)} C_n r^{n+1} + \frac{1}{2\alpha} A_n [I_{n+1}(\alpha r) + I_{n-1}(\alpha r)] + \frac{1}{2} D_n r^{n-1} \tag{4.143}$$

$$v_1^{(n)}(r) = \frac{(n+2)}{4(n+1)} C_n r^{n+1} + \frac{1}{2\alpha} A_n [I_{n+1}(\alpha r) - I_{n-1}(\alpha r)] - \frac{1}{2} D_n r^{n-1} \tag{4.144}$$

so that

$$u_{1,r}^{(n)}(r) = -\frac{n}{4}C_n r^n + \frac{1}{2}A_n\left[2I_n(\alpha r) - (n+1)\frac{I_{n+1}(\alpha r)}{\alpha r} + (n-1)\frac{I_{n-1}(\alpha r)}{\alpha r}\right] + \frac{(n-1)}{2}D_n r^{n-2} \tag{4.145}$$

$$v_{1,r}^{(n)}(r) = \frac{(n+2)}{4}C_n r^n - \frac{1}{2}A_n\left[(n+1)\frac{I_{n+1}(\alpha r)}{\alpha r} + (n-1)\frac{I_{n-1}(\alpha r)}{\alpha r}\right] - \frac{(n-1)}{2}D_n r^{n-2} \tag{4.146}$$

The requirement that the radial force in the reinforcement is zero at the edge $r = b$ means $N_{rr}(b,\theta) = 0$, which with Eq. (4.84) gives

$$u_{1,r}(b,\theta) + \frac{\nu}{b}[v_{1,\theta}(b,\theta) + u_1(b,\theta)] = 0 \tag{4.147}$$

This can be expressed as an equation of cosine series, of which the nth term gives

$$u_{1,r}^{(n)}(b) + \frac{\nu}{b}[nv_1^{(n)}(b) + u_1^{(n)}(b)] = 0 \tag{4.148}$$

For $n = 1$, substitution of Eqs. (4.132), (4.133) and (4.134) with $r = b$ into Eq. (4.148) leads to

$$A_1\left[\frac{1}{(1-\nu)}I_1(\alpha b) - \frac{1}{\alpha b}I_2(\alpha b)\right] - \frac{1}{4}C_1 b = \left(\frac{3}{4} + \frac{\nu}{1-\nu}\right)\frac{b}{\rho} \tag{4.149}$$

For $n > 1$, substitution of Eqs. (4.143), (4.144) and (4.145) with $r = b$ into Eq. (4.148) yields

$$A_n\left[\frac{2}{(1-\nu)}I_n(\alpha b) - \frac{n+1}{\alpha b}I_{n+1}(\alpha b) + \frac{n-1}{\alpha b}I_{n-1}(\alpha b)\right] - \frac{n}{2}C_n b^n + (n-1)D_n b^{n-2} = 0 \tag{4.150}$$

The requirement that the in-plane shear force in the reinforcement is zero at the edge $r = b$ means $N_{r\theta}(b,\theta) = 0$, which with Eq. (4.86) gives

$$v_{1,r}(b,\theta) + \frac{1}{b}[u_{1,\theta}(b,\theta) - v_1(b,\theta)] = 0 \tag{4.151}$$

This can be expressed as an equation of sine series, of which the nth term gives

$$v_{1,r}^{(n)}(b) - \frac{1}{b}\left[nu_1^{(n)}(b) + v_1^{(n)}(b)\right] = 0 \tag{4.152}$$

For $n = 1$, substitution of Eqs. (4.132), (4.133) and (4.135) with $r = b$ into Eq. (4.152) leads to

$$A_1\frac{1}{\alpha b}I_2(\alpha b) - \frac{1}{4}C_1 b = \frac{1}{4}\frac{b}{\rho} \tag{4.153}$$

For $n > 1$, substitution of Eqs. (4.143), (4.144) and (4.146) with $r = b$ into Eq. (4.152) yields

$$A_n \left[\frac{(n+1)}{\alpha b} I_{n+1}(\alpha b) + \frac{(n-1)}{\alpha b} I_{n-1}(\alpha b) \right] - \frac{n}{2} C_n b^n + (n-1) D_n b^{n-2} = 0 \tag{4.154}$$

Substitution of Eq. (4.116) with $n = 1$ into Eq. (4.119) gives

$$A_1 \frac{1}{(1-\nu)} I_1(\alpha b) - \frac{1}{2} C_1 b = \frac{1}{(1-\nu)} \frac{b}{\rho} \tag{4.155}$$

Eqs. (4.149), (4.153) and (4.155) are the linear equations of A_1 and C_1, but only two of them are independent. Select any two of these equations to solve A_1 and C_1

$$A_1 = \frac{b}{\rho} \frac{(1+\nu)}{2} \left[\frac{\alpha b}{\alpha b I_1(\alpha b) - 2(1-\nu) I_2(\alpha b)} \right] \tag{4.156}$$

$$C_1 = \frac{1}{\rho} \left[-\frac{2}{(1-\nu)} + \left(\frac{1+\nu}{1-\nu} \right) \frac{\alpha b I_1(\alpha b)}{\alpha b I_1(\alpha b) - 2(1-\nu) I_2(\alpha b)} \right] \tag{4.157}$$

Then we have, from Eq. (4.116),

$$B_1 = \frac{1}{\rho} \left[-1 + \left(\frac{1+\nu}{2} \right) \frac{\alpha b I_1(\alpha b)}{\alpha b I_1(\alpha b) - 2(1-\nu) I_2(\alpha b)} \right] \tag{4.158}$$

For $n > 1$, subtraction of Eqs. (4.150) from (4.154) gives

$$A_n = 0 \tag{4.159}$$

Then, from Eqs. (4.120), (4.116) and (4.150), we have

$$B_n = 0 \quad ; \quad C_n = 0 \quad ; \quad D_n = 0 \tag{4.160}$$

Therefore, all the $n > 1$ terms in the series solutions vanish.

If we assume the displacement of the reinforcement at the center to be zero, $u_1^{(1)}(0) = v_1^{(1)}(0) = 0$, which gives, from Eq. (4.132) or (4.133),

$$D_1 = -\frac{1}{\alpha} A_1 \tag{4.161}$$

By substituting this and the solutions of A_1 in Eq. (4.156) and C_1 in Eq. (4.157) into Eqs. (4.132) and (4.133), the displacements of the reinforcement in Eqs. (4.121) and (4.122) have the forms

$$u_1(r,\theta) = \frac{b^2}{4\rho}\left[-\frac{r^2}{b^2} + (1+\nu)\frac{I_2(\alpha r) + I_0(\alpha r) - 1 - I_2(\alpha b)\left(\frac{r}{b}\right)^2}{\alpha b I_1(\alpha b) - 2(1-\nu)I_2(\alpha b)}\right]\cos\theta \tag{4.162}$$

$$v_1(r,\theta) = \frac{b^2}{4\rho}\left[-\frac{r^2}{b^2} + (1+\nu)\frac{I_2(\alpha r) - I_0(\alpha r) + 1 + 3I_2(\alpha b)\left(\frac{r}{b}\right)^2}{\alpha b I_1(\alpha b) - 2(1-\nu)I_2(\alpha b)}\right]\sin\theta \tag{4.163}$$

4.2.6 Effective Bending Modulus

The effective bending stiffness of a single layer of the reinforced elastomer $(EI)_{eff}$ is defined as

$$(EI)_{eff} = \rho M \tag{4.164}$$

in which M is the resultant bending moment. Using the assumption of pressure dominating in Eq. (4.64), the bending moment M has the form

$$M = \int_0^{2\pi}\int_0^b \sigma_{zz} r^2 \cos\theta \; \mathrm{d}r\mathrm{d}\theta \approx -\int_0^{2\pi}\int_0^b p(r,\theta) r^2 \cos\theta \; \mathrm{d}r\mathrm{d}\theta \tag{4.165}$$

Substituting the expression of $p(r,\theta)$ in Eq. (4.109) into the above equation, the effective bending stiffness becomes

$$(EI)_{eff} = 12\pi G S^2 \frac{b^2}{\alpha^2}\left[1 + \rho B_1 - \rho A_1 \frac{4I_2(\alpha b)}{\alpha b^2}\right] \tag{4.166}$$

where S is the shape factor defined in Eq. (4.40) . Using the solutions of A_1 in Eq. (4.156) and B_1 in Eq. (4.158), the above equation becomes

$$(EI)_{eff} = 6\pi G S^2 (1+\nu)\frac{b^2}{\alpha^2}\left[\frac{\alpha b I_1(\alpha b) - 4I_2(\alpha b)}{\alpha b I_1(\alpha b) - 2(1-\nu)I_2(\alpha b)}\right] \tag{4.167}$$

For clarification, we define the effective bending modulus as

$$E_b = \frac{(EI)_{eff}}{I_r} \tag{4.168}$$

in which I_r is the moment of inertia of the cross-section area about the r axis. For the circular pad, $I_r = \pi b^4/4$, so that

$$E_b = 24GS^2 \frac{(1+\nu)}{(\alpha b)^2} \left[\frac{\alpha b I_1(\alpha b) - 4I_2(\alpha b)}{\alpha b I_1(\alpha b) - 2(1-\nu) I_2(\alpha b)} \right] \tag{4.169}$$

When α tends to zero, substituting the following power series for the Bessel functions

$$I_1(\alpha b) \approx \frac{\alpha b}{2} + \frac{(\alpha b)^3}{16} \quad ; \quad I_2(\alpha b) \approx \frac{(\alpha b)^2}{8} + \frac{(\alpha b)^4}{96} \tag{4.170}$$

into Eq. (4.169) and neglecting the higher order terms of αb,

$$E_b = 2GS^2 \tag{4.171}$$

which is the effective bending modulus for the circular layer of elastomer bonded to the rigid reinforcement. The ratio $E_b/(GS^2)$ is plotted in Figure 4.15 as a function of αb for $\nu = 0$, 0.3 and 0.5. The figure shows that the effective bending modulus decreases with increasing αb; higher Poisson's ratio of the reinforcement tends to produce higher modulus, but the difference becomes negligible when αb is small.

Using the relation in Eq. (4.44), Eq. (4.169) can be rewritten as

$$E_b = \frac{(1+\nu)k_f}{2t} \left[\frac{1 - 4\frac{I_2(\alpha b)}{\alpha b I_1(\alpha b)}}{1 - 2(1-\nu)\frac{I_2(\alpha b)}{\alpha b I_1(\alpha b)}} \right] \tag{4.172}$$

in which k_f is the in-plane stiffness of the reinforcement defined in Eq. (4.43). As αb tends to infinity, the term of the Bessel function $I_2(\alpha b)/[\alpha b I_1(\alpha b)]$ tends to zero, so that

$$E_b = \frac{(1+\nu)k_f}{2t} \tag{4.173}$$

Substituting αb in Eq. (4.44) into Eq. (4.169), we have the normalized effective bending modulus E_b/G expressed as a function of the shape factor S and the stiffness ratio of the reinforcement to the elastomer $k_f/(Gt)$. The curves of E_b/G versus $k_f/(Gt)$ are plotted in Figure 4.16 for $\nu = 0.3$ and several S values, which shows that the effective bending modulus increases with increasing

reinforcement stiffness until reaching the asymptotic value in Eq. (4.171). The curve of the smaller shape factor reaches a plateau at the smaller value of $k_f/(Gt)$. The curves of E_b/G versus S are plotted in Figure 4.17 for $\nu = 0.3$ and several $k_f/(Gt)$ values, which shows that the effective bending modulus increases with increasing shape factor until reaching the asymptotic value in Eq. (4.173). The curve of the smaller value of $k_f/(Gt)$ reaches a plateau at the smaller shape factor.

4.2.7 Stresses in Elastomer and Reinforcement

The nominal bending stress σ_b is the maximum normal stress in the elastomer created by the moment M. From Eqs. (4.164) and (4.168)

$$\sigma_b = \frac{Mb}{I_r} = E_b \frac{b}{\rho} \tag{4.174}$$

The pressure distribution can be solved by substituting the constants A_1 and B_1 in Eqs. (4.156) and (4.158) into Eq. (4.109)

$$p(r,\theta) = \frac{b}{\rho} 24GS^2 \frac{(1+\nu)}{(\alpha b)^2} \left[\frac{\alpha b I_1(\alpha r) - \alpha r I_1(\alpha b)}{\alpha b I_1(\alpha b) - 2(1-\nu) I_2(\alpha b)} \right] \cos\theta \tag{4.175}$$

which becomes, after normalized with respect to the nominal bending stress,

$$\frac{p(r,\theta)\rho}{E_b b} = \frac{\alpha b I_1(\alpha r) - \alpha r I_1(\alpha b)}{\alpha b I_1(\alpha b) - 4 I_2(\alpha b)} \cos\theta \tag{4.176}$$

When α tends to zero, applying the power series approximation in Eq. (4.170) to the above equation

$$\frac{p(r,\theta)\rho}{E_b b} = -3 \left(\frac{r}{b} - \frac{r^3}{b^3} \right) \cos\theta \tag{4.177}$$

which is the pressure distribution in the elastomeric layer bonded to the rigid reinforcement. The distribution of the normalized pressure along the r axis at $\theta = 0$ is plotted in Figure 4.18 for $\alpha b = 0$, 1, 2 and 4, which shows that the effect of the flexibility of the reinforcement is to decrease the maximum pressure and make the location of the maximum pressure closer to the edge. It should

be noted that the normalized pressure distribution in Eq. (4.176) is independent of the Poisson's ratio of the reinforcement ν.

If τ_r and τ_θ denote the shear stresses in the radial and hoop directions, respectively, on the bonding surface between the elastomer and the reinforcement, from Eqs. (4.71) and (4.73), we have

$$\tau_r(r,\theta) = \sigma_{rz}|_{z=-\frac{t}{2}} = -\frac{t}{2}p_{,r} \tag{4.178}$$

and, from Eqs. (4.72) and (4.74),

$$\tau_\theta(r,\theta) = \sigma_{\theta z}|_{z=-\frac{t}{2}} = -\frac{t}{2r}p_{,\theta} \tag{4.179}$$

Substituting Eq. (4.176) into Eqs. (4.178) and (4.179), the normalized shear stresses are

$$\frac{\tau_r(r,\theta)\rho}{E_b b} = \frac{(\alpha b)^2}{4S}\left[\frac{\frac{I_1(\alpha b)}{\alpha b} - \frac{I_1(\alpha r)}{\alpha r} - I_2(\alpha r)}{\alpha b I_1(\alpha b) - 4I_2(\alpha b)}\right]\cos\theta \tag{4.180}$$

$$\frac{\tau_\theta(r,\theta)\rho}{E_b b} = -\frac{(\alpha b)^2}{4S}\left[\frac{\frac{I_1(\alpha b)}{\alpha b} - \frac{I_1(\alpha r)}{\alpha r}}{\alpha b I_1(\alpha b) - 4I_2(\alpha b)}\right]\sin\theta \tag{4.181}$$

which show that the normalized bonding shear stresses are independent of the Poisson's ratio of the reinforcement ν. When α tends to zero, substituting the power series approximation in Eq. (4.170) into the above two equations,

$$\frac{\tau_r(r,\theta)\rho}{E_b b} = \frac{3}{4S}\left(1 - 3\frac{r^2}{b^2}\right)\cos\theta \tag{4.182}$$

$$\frac{\tau_\theta(r,\theta)\rho}{E_b b} = -\frac{3}{4S}\left(1 - \frac{r^2}{b^2}\right)\sin\theta \tag{4.183}$$

which are the bonding shear stresses for the rigid reinforcement. The distribution of the bonding shear stress in the radial direction along the r axis at $\theta = 0$ is plotted in Figure 4.19 for $\alpha b = 0$, 1, 2 and 4, which demonstrates that the effect of the flexibility of the reinforcement is to decrease the magnitude at the center but to increase the maximum value at the edge. The distribution of the bonding shear stress in the hoop direction along the r axis at $\theta = \pi/2$ is plotted in Figure 4.20

for $\alpha b = 0$, 1, 2 and 4, which demonstrates that the effect of the flexibility of the reinforcement is to decrease the maximum value at the center.

The shear resultant on the bonding surface $\tau(r,\theta)$ which is defined as

$$\tau(r,\theta) = \sqrt{\tau_r^2(r,\theta) + \tau_\theta^2(r,\theta)} \tag{4.184}$$

has the maximum value at $r = b$ and $\theta = 0$ or π which has the form, after normalization,

$$\frac{\tau(b,0)\rho}{E_b b} = \frac{1}{4S}\left[\frac{(\alpha b)^2 I_2(\alpha b)}{\alpha b I_1(\alpha b) - 4I_2(\alpha b)}\right] \tag{4.185}$$

By using the expression of αb in Eq. (4.44), the above equation becomes a function of the stiffness ratio $k_f/(Gt)$ and the shape factor S, which is plotted in Figure 4.21. The figure shows that, under the same bending moment, the maximum shear resultant at the edge decreases with increasing stiffness ratio or shape factor. At the center $r = 0$, the normalized shear resultant is

$$\frac{\tau(0,\theta)\rho}{E_b b} = \frac{1}{8S}\left[\frac{2\alpha b I_1(\alpha b) - (\alpha b)^2}{\alpha b I_1(\alpha b) - 4I_2(\alpha b)}\right] \tag{4.186}$$

To demonstrate the displacement pattern in the reinforcement under the bending moment, the radial displacement u_1 in Eq. (4.162) is plotted in Figure 4.22 along the r axis at $\theta = 0$, and the hoop displacement v_1 in Eq. (4.163) is plotted in Figure 4.23 along the r axis at $\theta = \pi/2$ for $\nu = 0.3$ and $\alpha b = 0.5$, 1, 2 and 4. The deformed shapes of the reinforcing sheet for different values of αb are plotted in Figure 4.24. The shape for $\alpha b = 0$ is an undeformed circular shape. The reinforcing sheet does not move at the center because $u_1 = v_1 = 0$ at the center of the reinforcing sheet is assumed in deriving Eqs. (4.162) and (4.163).

The in-plane force components in the reinforcing sheet, N_{rr}, $N_{\theta\theta}$ and $N_{r\theta}$, can be derived by substituting Eqs. (4.162) and (4.163) into Eqs. (4.84) to (4.86), which give, after being normalized with respect to the nominal bending stress in Eqs. (4.175),

$$\frac{N_{rr}(r,\theta)\rho}{E_b b t} = \frac{\alpha b I_1(\alpha r) - \alpha r I_1(\alpha b) + (1-\nu)\left[\frac{r}{b} I_2(\alpha b) - \frac{b}{r} I_2(\alpha r)\right]}{\alpha b I_1(\alpha b) - 4I_2(\alpha b)} \cos\theta \tag{4.187}$$

$$\frac{N_{\theta\theta}(r,\theta)\rho}{E_b bt} = \frac{\nu\alpha b I_1(\alpha r) - \alpha r I_1(\alpha b) + (1-\nu)\left[3\frac{r}{b}I_2(\alpha b) + \frac{b}{r}I_2(\alpha r)\right]}{\alpha b I_1(\alpha b) - 4I_2(\alpha b)}\cos\theta \tag{4.188}$$

$$\frac{N_{r\theta}(r,\theta)\rho}{E_b bt} = (1-\nu)\frac{\frac{r}{b}I_2(\alpha b) - \frac{b}{r}I_2(\alpha r)}{\alpha b I_1(\alpha b) - 4I_2(\alpha b)}\sin\theta \tag{4.189}$$

The distributions of N_{rr} and $N_{\theta\theta}$ along the r axis at $\theta = 0$, and $N_{r\theta}$ along the r axis at $\theta = \pi/2$ are plotted in Figures 4.25 to 4.27, respectively, for $\nu = 0.3$ and several αb values. At the edge $r = b$,

$$\frac{N_{\theta\theta}(b,\theta)\rho}{E_b bt} = -(1-\nu)\cos\theta \tag{4.190}$$

which is independent of αb.

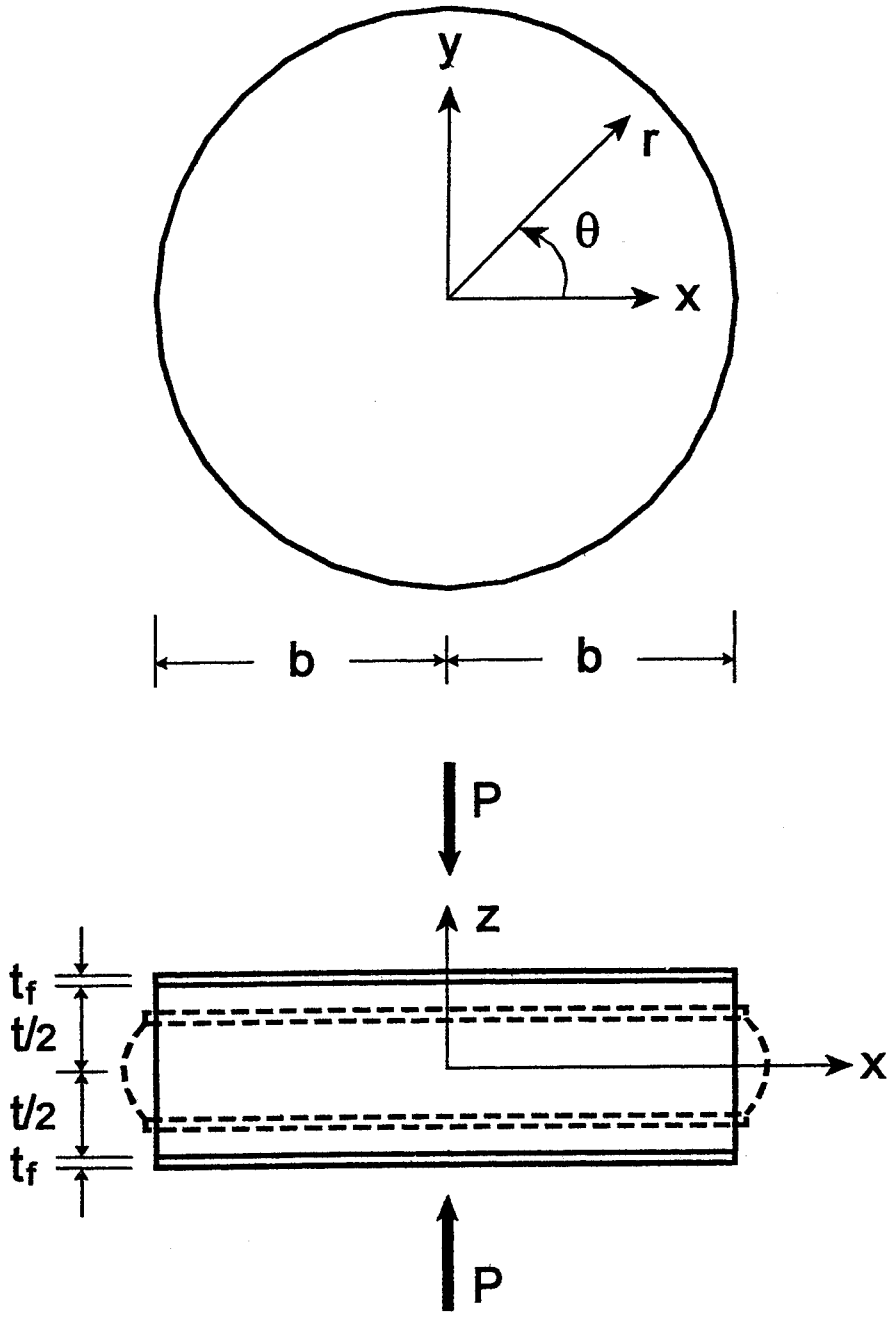

Figure 4.1: Circular layer of reinforced elastomer under compression load

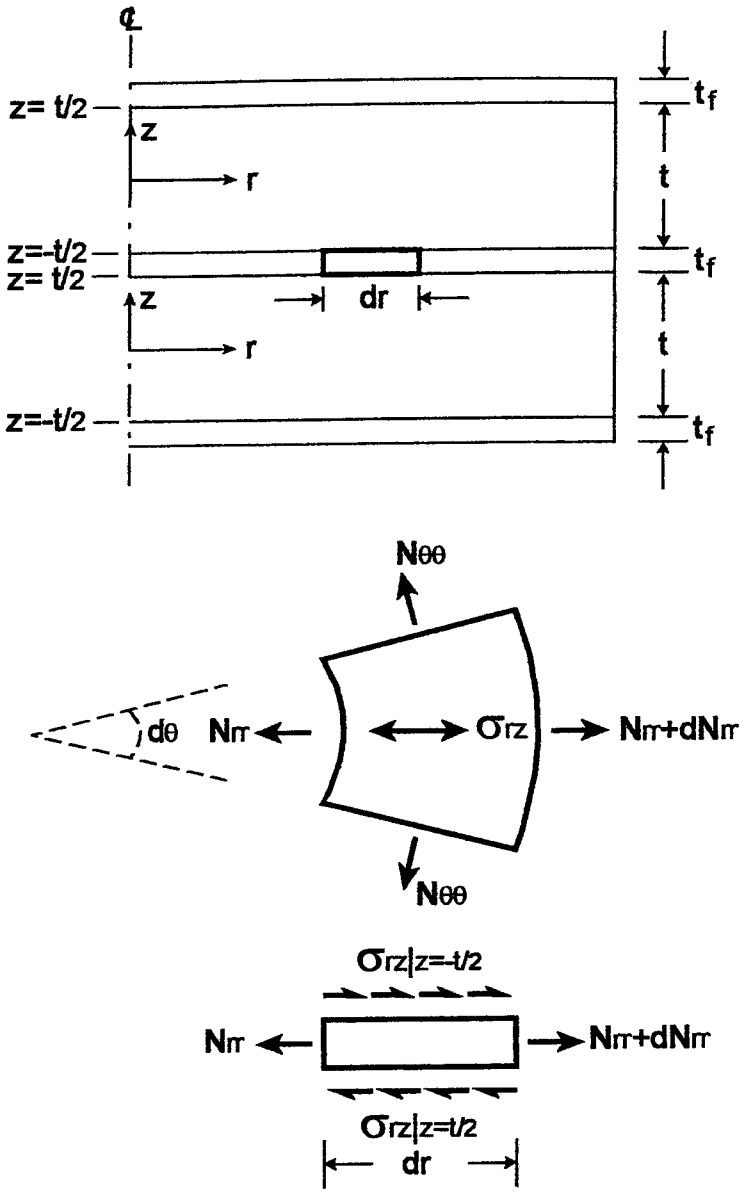

Figure 4.2: Forces in reinforcing sheet bonded to circular layers of elastomer under compression load

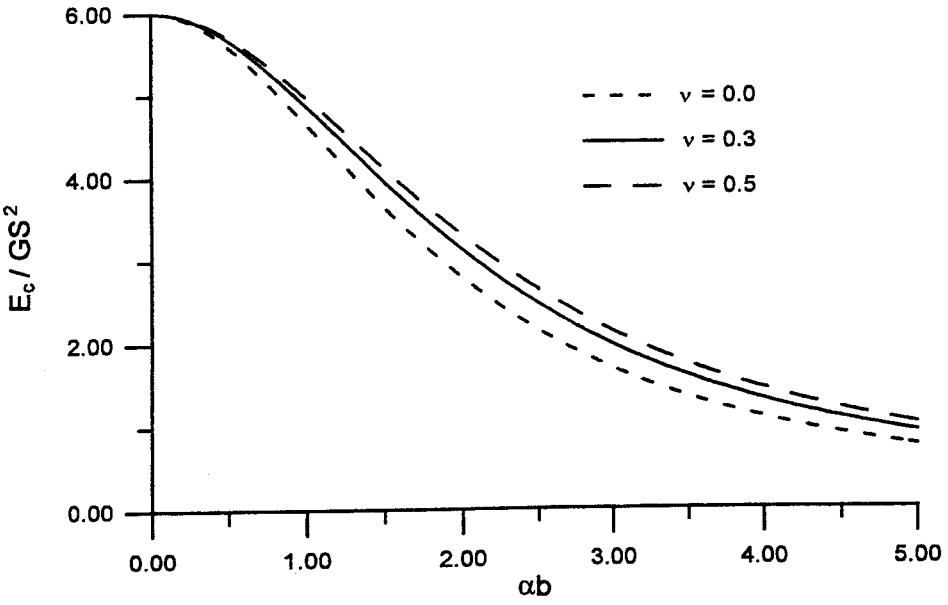

Figure 4.3: Variation of effective compressive modulus with αb in circular pad

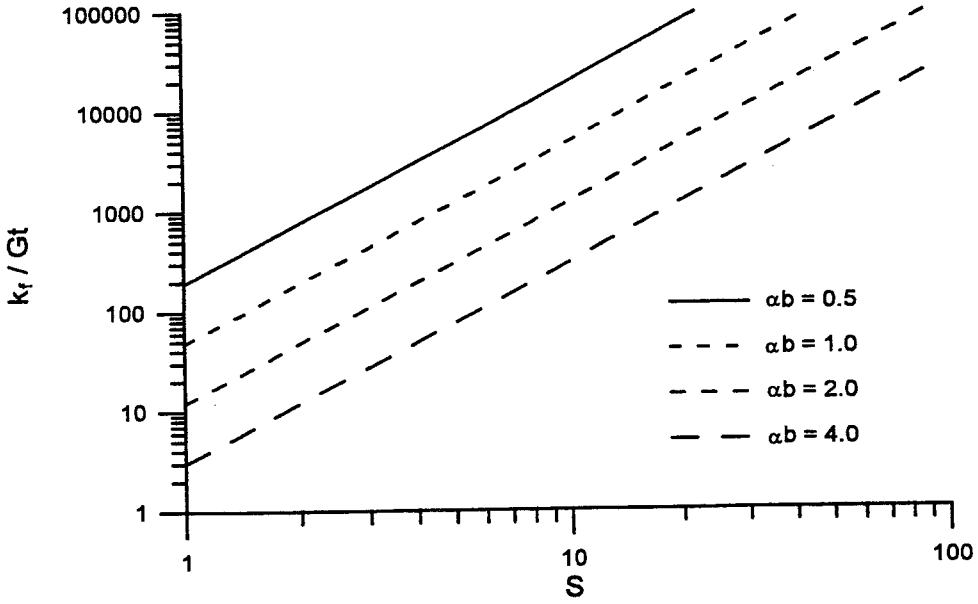

Figure 4.4: Relation between reinforcement stiffness and shape factor for different αb values in circular pad

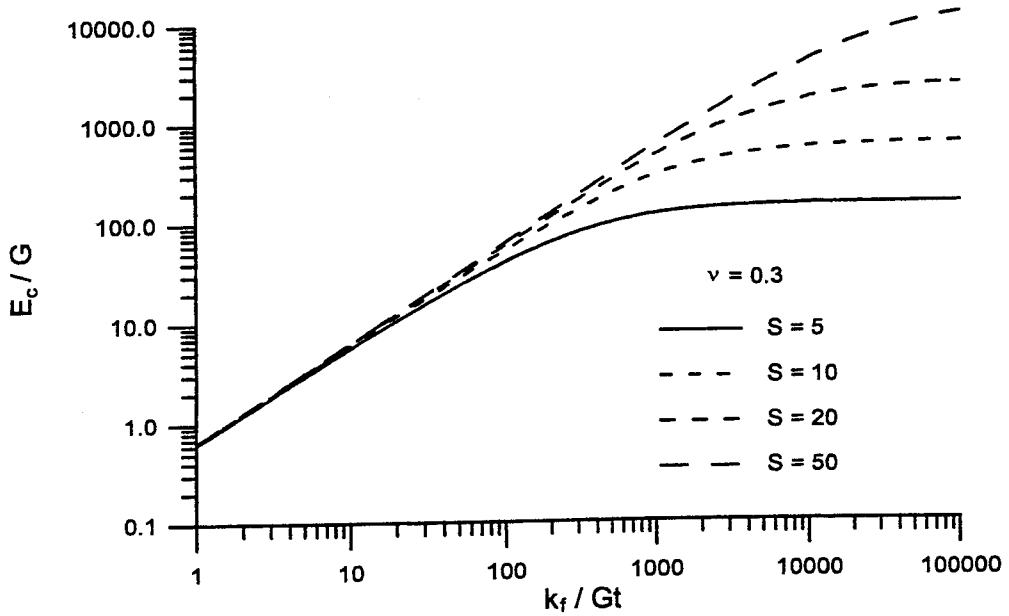

Figure 4.5: Variation of effective compressive modulus with reinforcement stiffness in circular pad

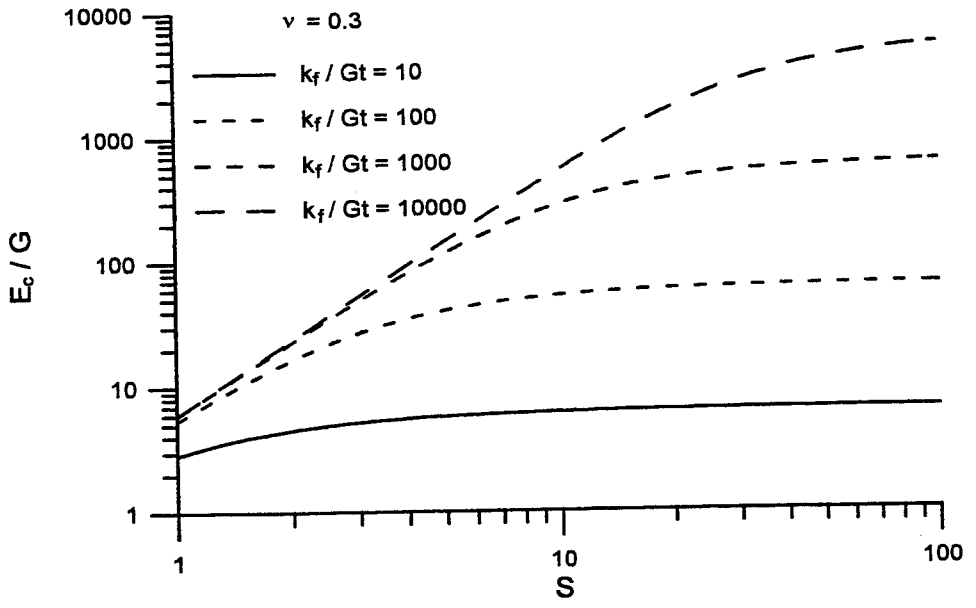

Figure 4.6: Variation of effective compressive modulus with shape factor in circular pad

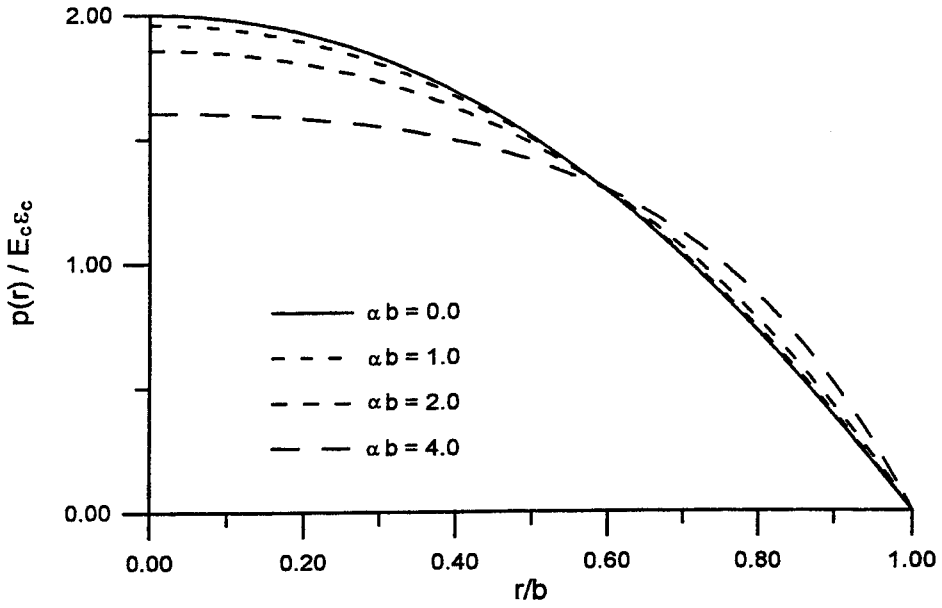

Figure 4.7: Distribution of normalized pressure in circular pad under compression load

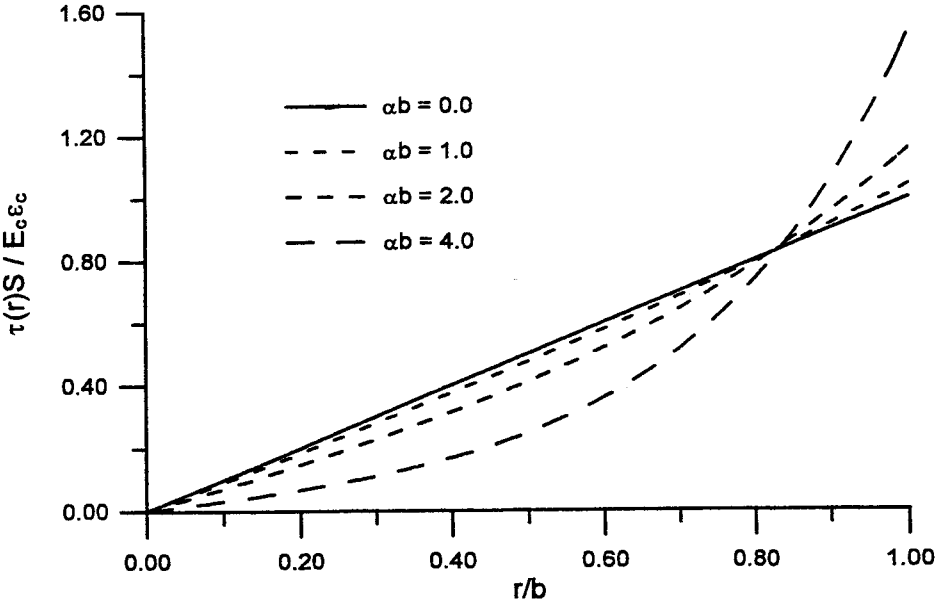

Figure 4.8: Distribution of bonding shear stress in circular pad under compression load

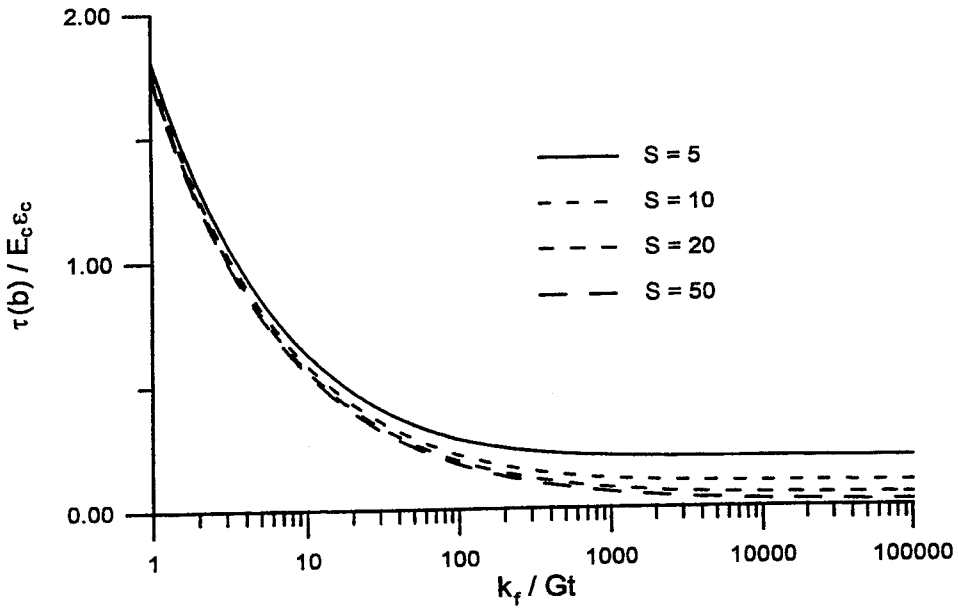

Figure 4.9: Variation of maximum bonding shear stress with reinforcement stiffness in circular pad under compression load

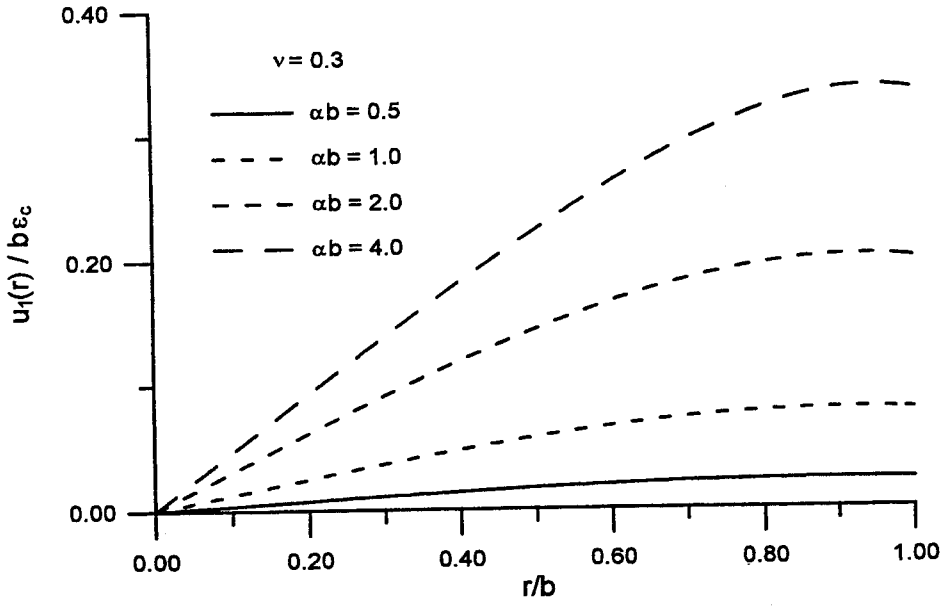

Figure 4.10: Displacement pattern in reinforcement of circular pad under compression load

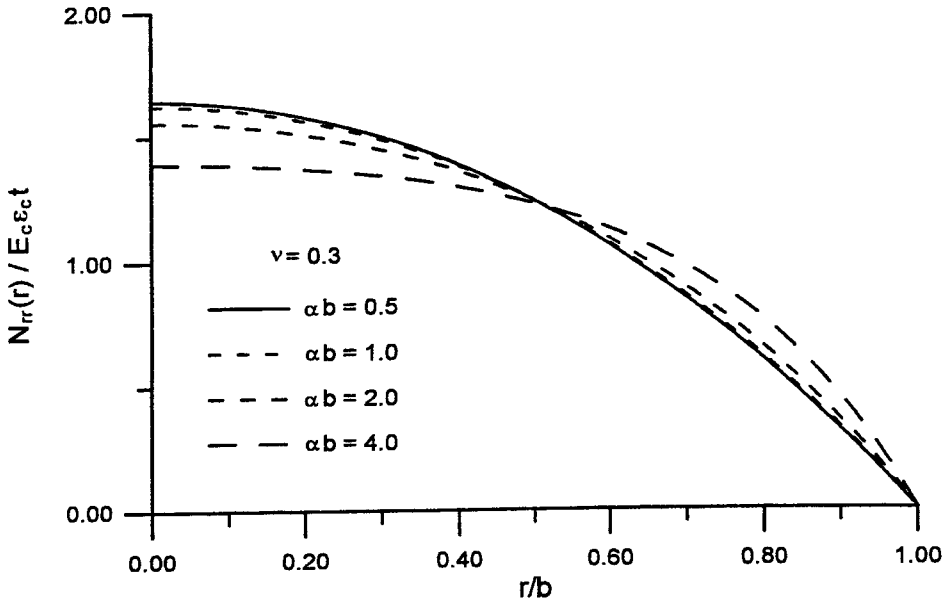

Figure 4.11: Distribution of radial force in reinforcement of circular pad under compression load

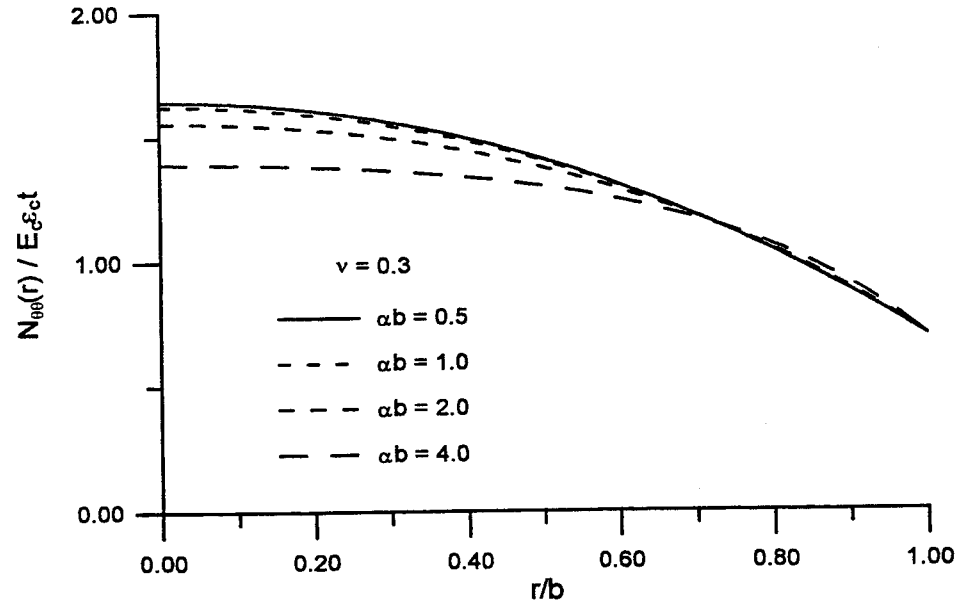

Figure 4.12: Distribution of hoop force in reinforcement of circular pad under compression load

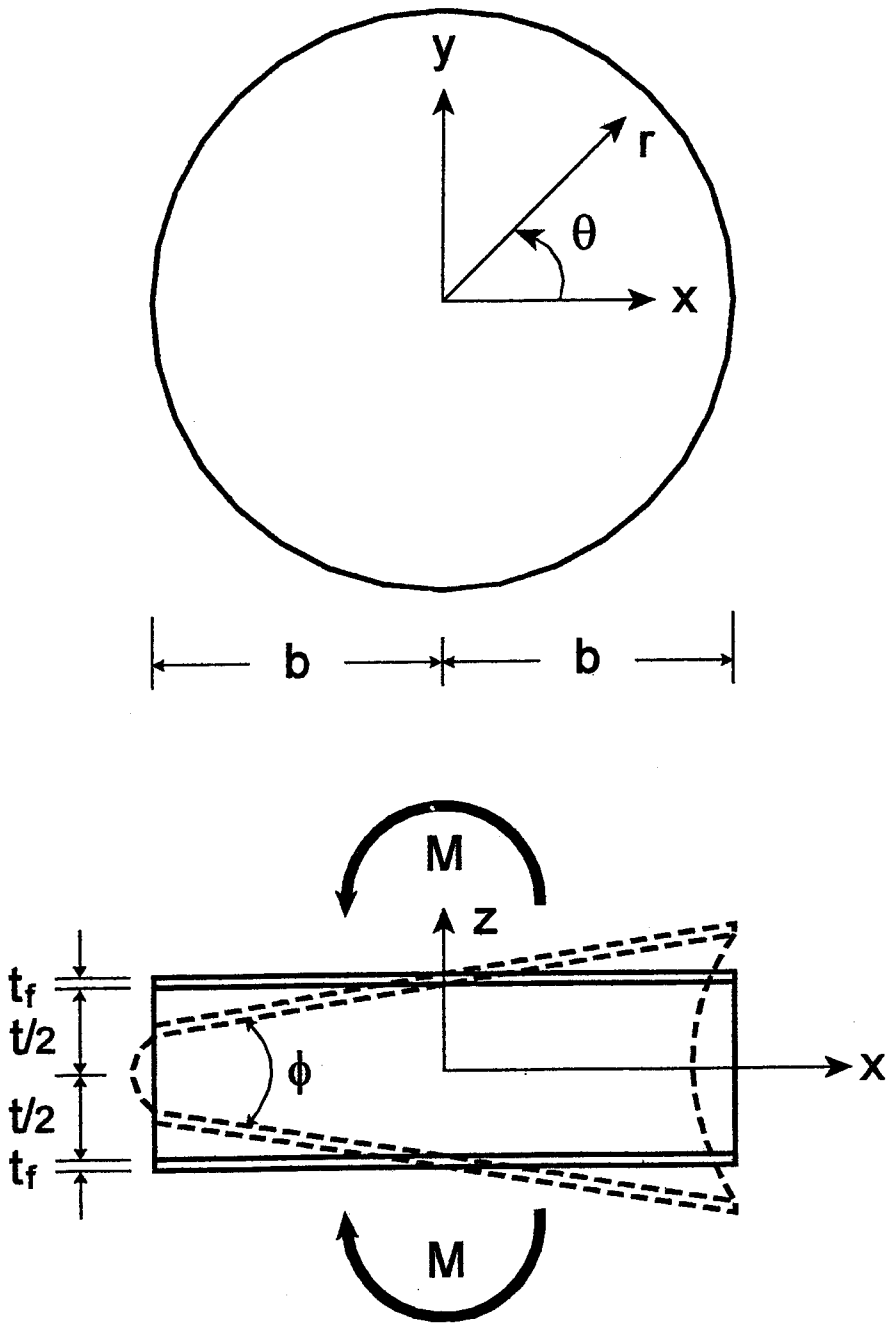

Figure 4.13: Circular layer of reinforced elastomer under pure bending load

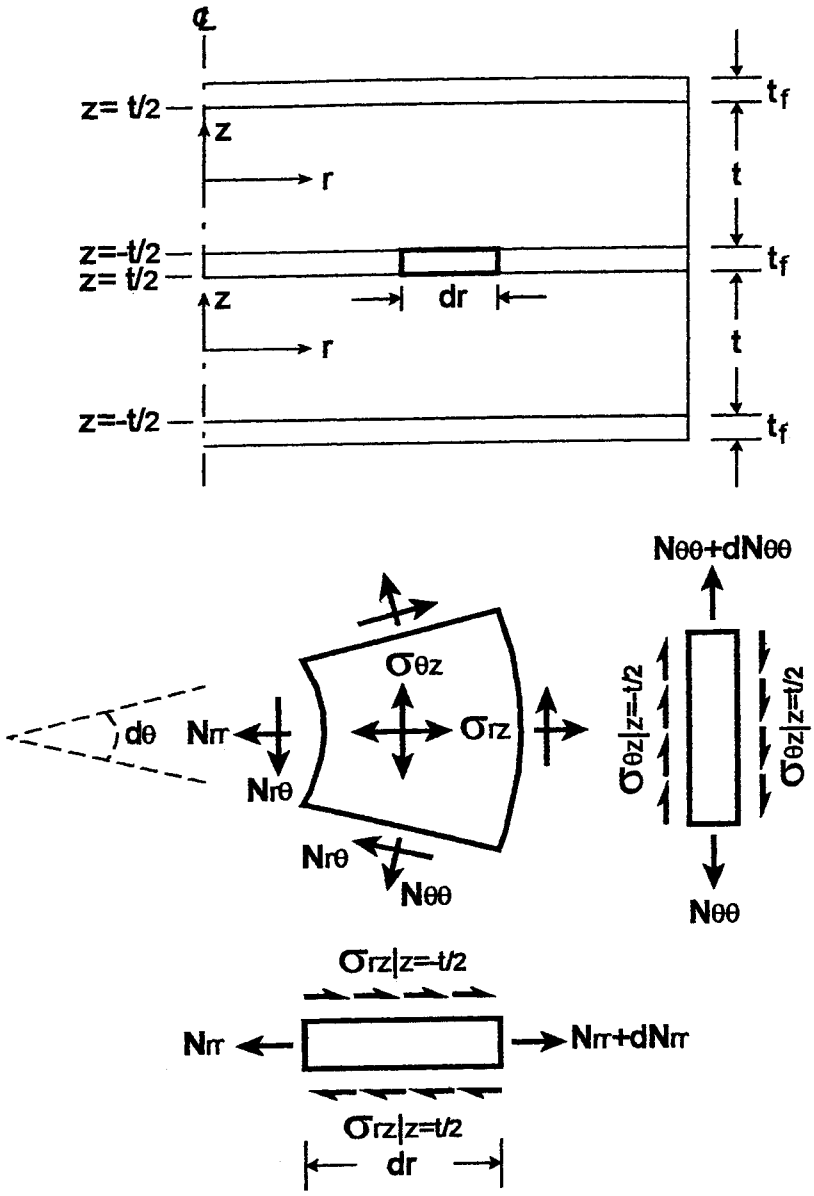

Figure 4.14: Forces in reinforcing sheet bonded to circular layers of elastomer under pure bending load

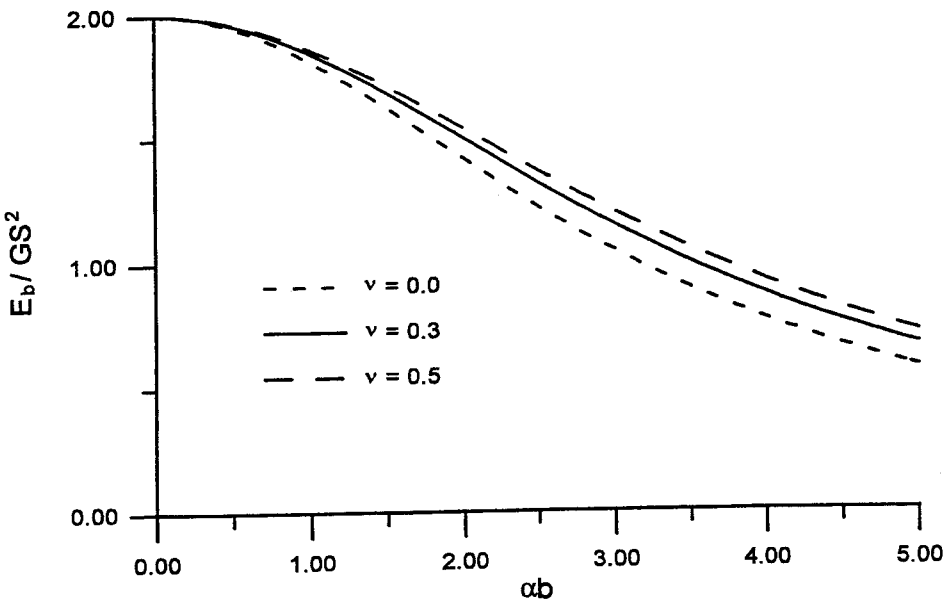

Figure 4.15: Variation of effective bending modulus with αb in circular pad

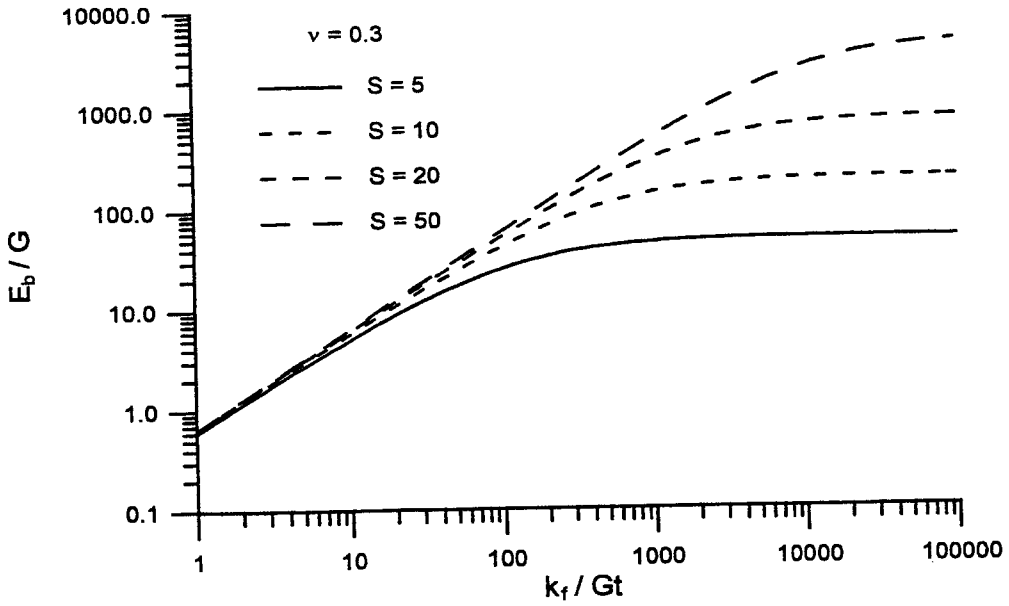

Figure 4.16: Variation of effective bending modulus with reinforcement stiffness in circular pad

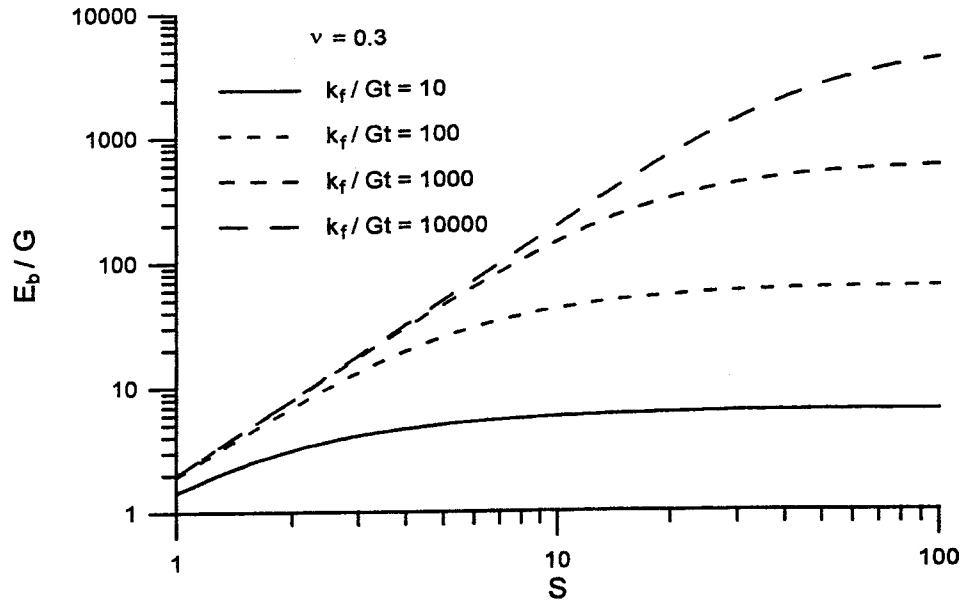

Figure 4.17: Variation of effective bending modulus with shape factor in circular pad

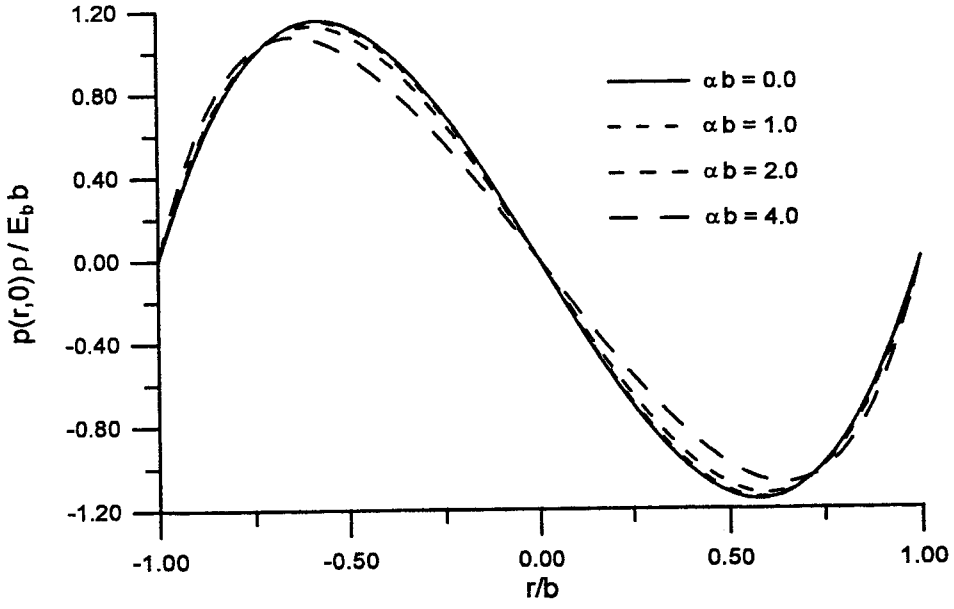

Figure 4.18: Distribution of normalized pressure in circular pad under pure bending load

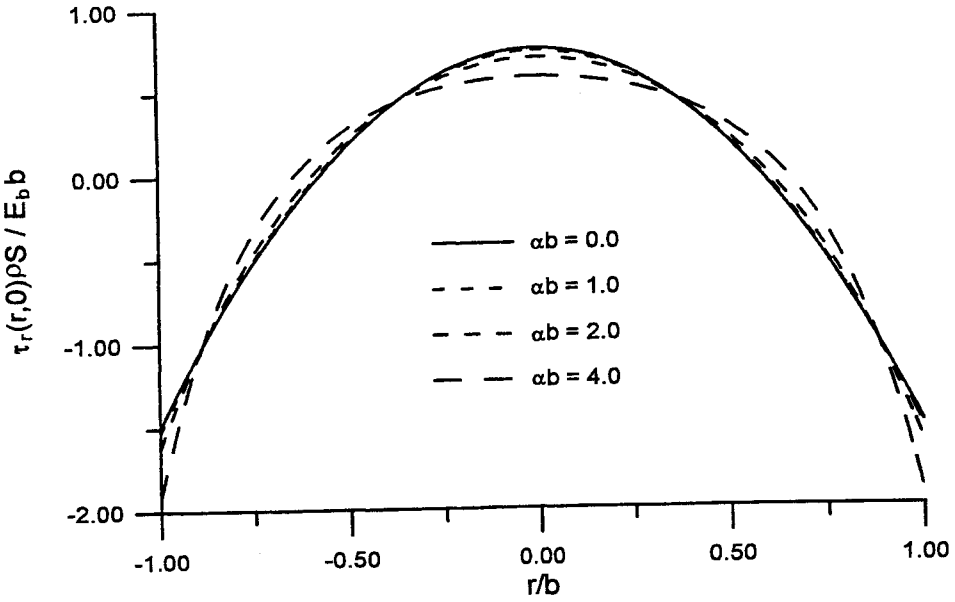

Figure 4.19: Distribution of bonding shear stress in radial direction of circular pad under pure bending load

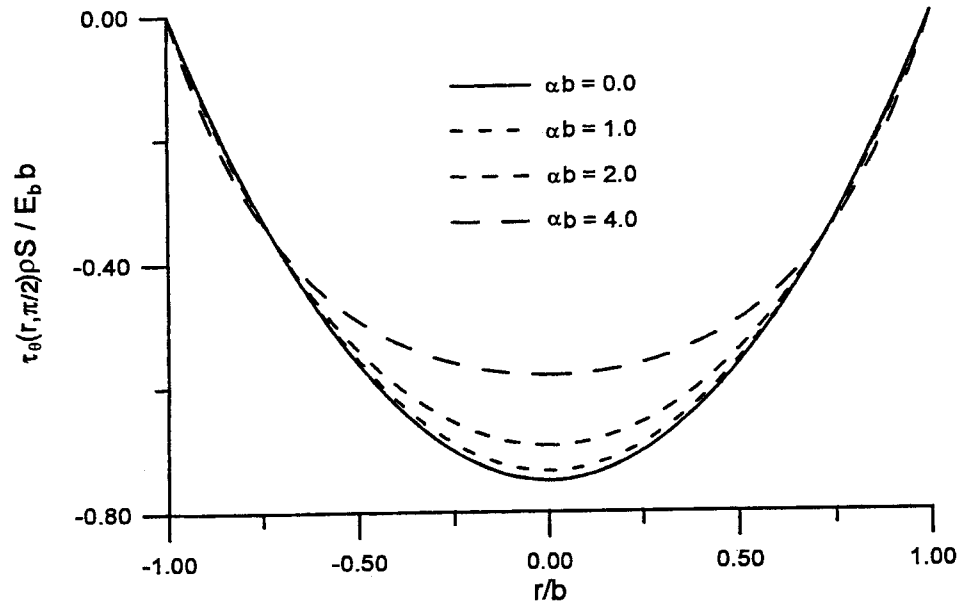

Figure 4.20: Distribution of bonding shear stress in hoop direction of circular pad under pure bending load

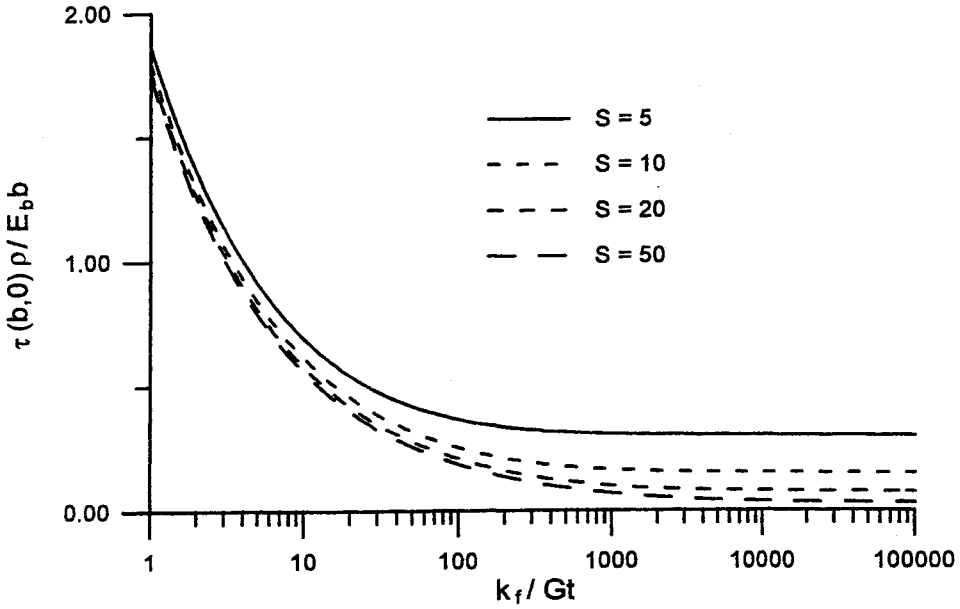

Figure 4.21: Variation of maximum bonding shear resultant with reinforcement stiffness in circular pad under pure bending load

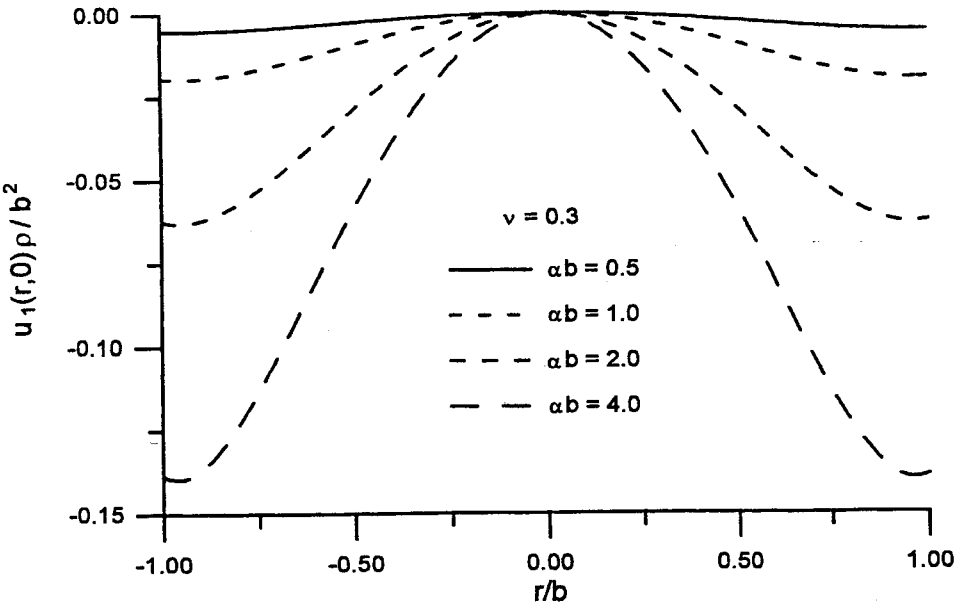

Figure 4.22: Radial displacement pattern in reinforcement of circular pad under pure bending load

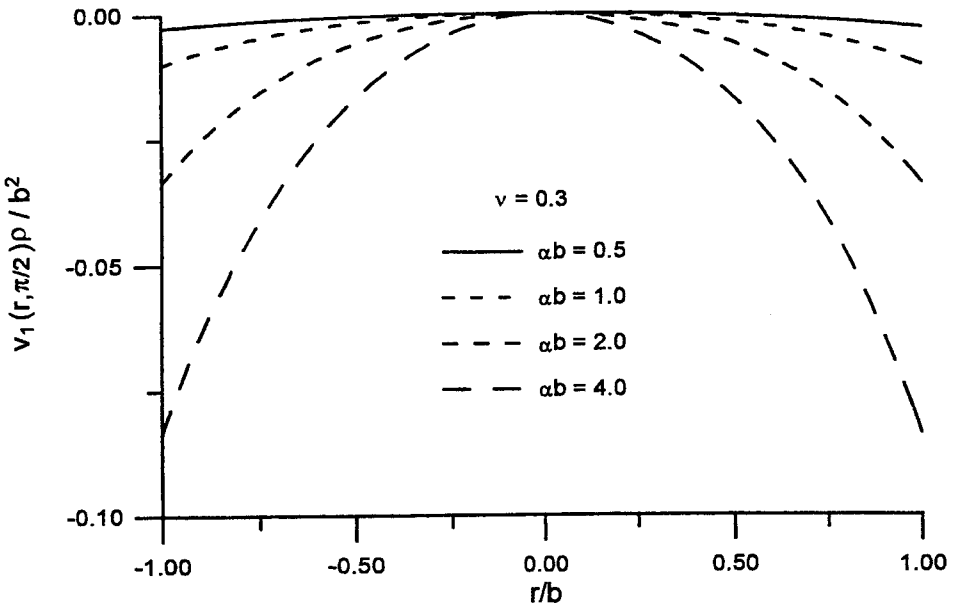

Figure 4.23: Hoop displacement pattern in reinforcement of circular pad under pure bending load

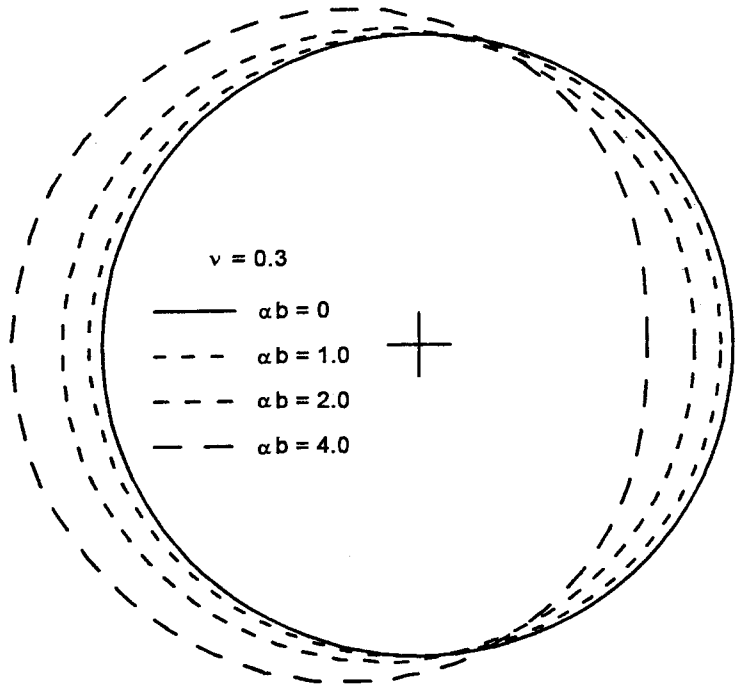

Figure 4.24: Deformed shapes of reinforcement in circular pad under pure bending load

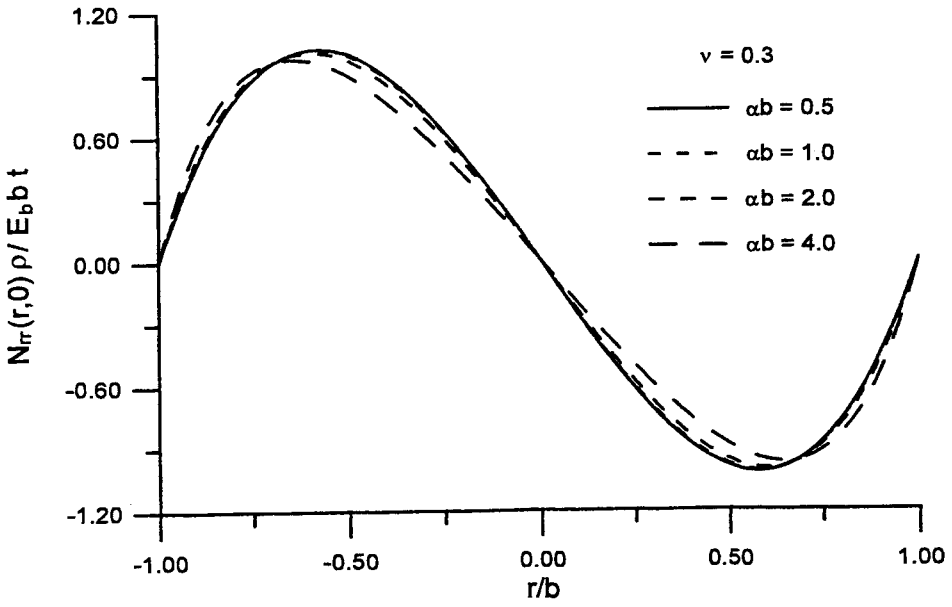

Figure 4.25: Distribution of radial force in reinforcement of circular pad under pure bending load

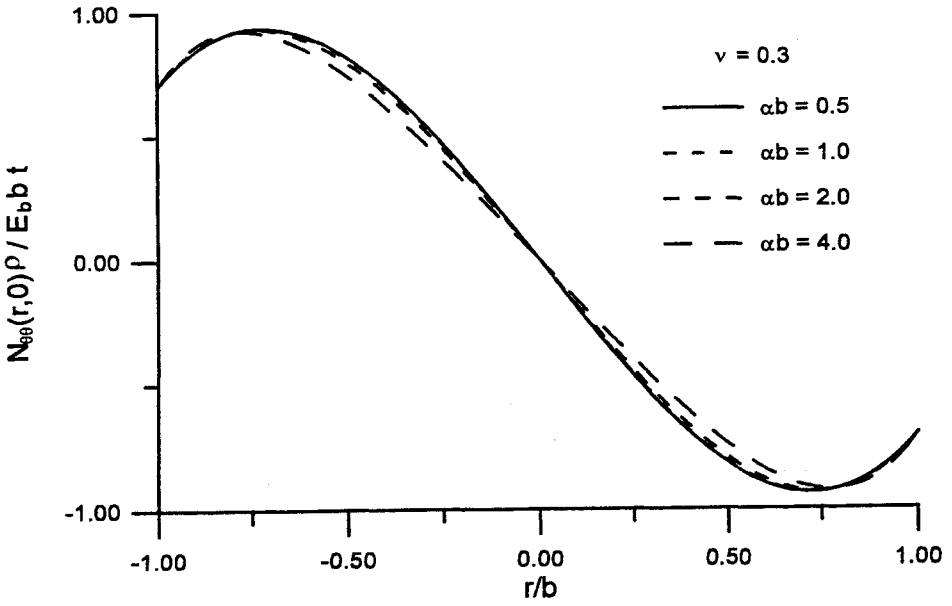

Figure 4.26: Distribution of hoop force in reinforcement of circular pad under pure bending load

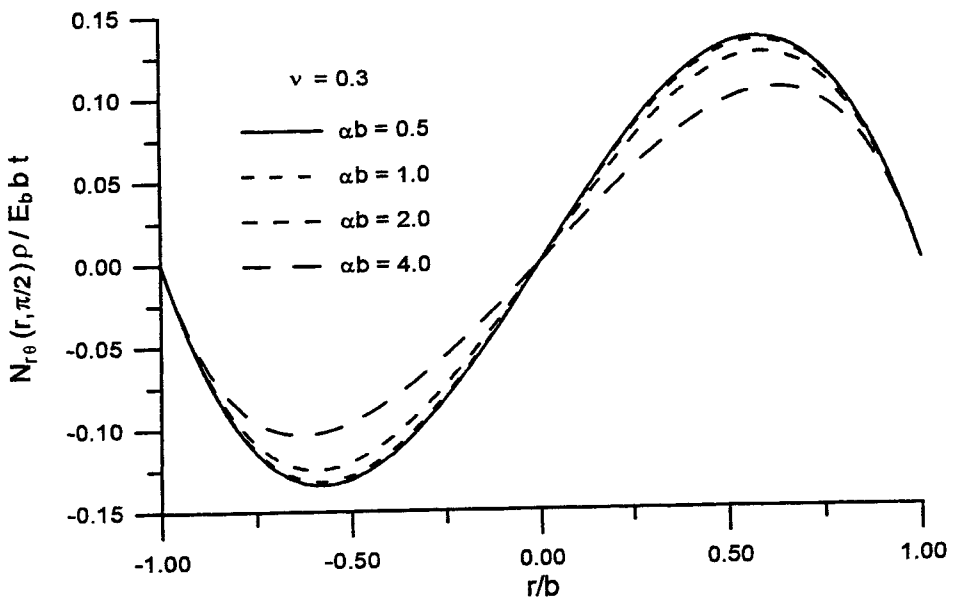

Figure 4.27: Distribution of shear force in reinforcement of circular pad under pure bending load

5 Conclusion

To study the influence of fiber flexibility on the mechanical properties of fiber-reinforced multi-layer elastomeric isolators, theoretical analyses on a single layer of elastomer bonded to flexible reinforcements and subjected to compression loading and pure bending loading are given for infinitely long strip isolators, rectangular isolators and circular isolators. Although it may be derived from the solution of rectangular isolators by setting the aspect ratio to the extreme value, the solution of infinitely long strip isolators directly derived from the plane-strain model provides insight into the approach of the theoretical analyses.

The displacement field of the elastomer is simplified by assuming that horizontal planes remain planar and vertical lines become parabolic after deformation. The displacement field of the reinforcement is idealized in the plane stress state. The assumption of incompressibility on the material of the elastomer produces the first differential equation, a constraint between the displacements of the elastomer and reinforcement. The stress state of the elastomer is assumed to be dominated by the internal pressure, such that the stress equilibrium in the elastomer reduces to the second differential equation relating the pressure with the displacement of the elastomer. The equilibrium in the reinforcing sheet generates the third differential equation in terms of the displacements of the elastomer and the reinforcement. Based on these three differential equations, the governing equations and the boundary conditions for the pressure in the elastomer are established, from which the closed-form solutions of pressure distribution are derived. For the rectangular pads, the boundary conditions of the pressure are established by assuming that the derivatives of the shear forces at

the edges of the reinforcement are negligible. For the circular isolators, the displacements in the reinforcement must be solved before the pressure distributions are derived.

Theoretical solutions show that the compression stiffness and the bending stiffness of the reinforced elastomer, derived from the pressure distribution, are affected by the shape factor of the elastomer and the flexibility of the reinforcement. Similar to the elastomer bonded to rigid reinforcements, the stiffness of the elastomer bonded to flexible reinforcements increases with increasing shape factor, but the flexibility of the reinforcement can decrease the stiffness of the reinforced elastomer. When the reinforced elastomer is subjected to compressive loading, the flexibility of the reinforcement makes the pressure distribution more uniform and decreases the maximum value at the center. When the reinforced elastomer is subjected to pure bending moment, the flexibility of the reinforcement makes the location of the maximum pressure closer to the edge and decreases the maximum value. For the shear stress on the bonding surface between the elastomer and the reinforcement, the flexibility of the reinforcement makes the distribution of the bonding shear stress more concentrating on the edge and increases the maximum value at the edge.

For circular isolators, theoretical solutions show that the stiffness of the reinforced elastomer also varies with the Poisson's ratio of the reinforcement, but this effect becomes minor when the reinforcement becomes more rigid. For rectangular isolators, theoretical solutions of the compression stiffness and the bending stiffness are expressed in series form. Because the approximated boundary conditions are applied, the stiffness solutions of the reinforced elastomer become independent of the Poisson's ratio of the reinforcement. Based on the stiffness formulae of infinitely long strip isolators, simple empirical formulae are derived to provide good approximations for the compression stiffness and the bending stiffness of the rectangular isolators.

References

Gent, A. N. and Lindley, P. B. 1959. The compression of bonded rubber blocks. *Proceeding of the Institution Mechanical Engineers* 173, 111-117.

Gent, A. N. and Meinecke, E. A. 1970. Compression, bending and shear of bonded rubber blocks. *Polymer Engineering and Science* 10, 48-53.

Kelly, J. M. 1997. *Earthquake-Resistant Design with Rubber*, 2nd ed. Springer-Verlag, London.

Kelly, J. M. 1999. Analysis of fiber-reinforced elastomeric isolator. *Journal of Structural and Earthquake Engineering* 2, 19-34.

Koh, C. G. and Kelly, J. M. 1989. Compression stiffness of bonded square layers of nearly incompressible material. *Engineering Structures* 11, 9-15.

Tsai, H.-C. and Lee, C.-C. 1998. Compressive stiffness of elastic layers bonded between rigid plates. *International Journal of Solids and Structures* 35, 3053-3069.

Tsai, H.-C. and Lee, C.-C. 1999. Tilting stiffness of elastic layers bonded between rigid plates. *International Journal of Solids and Structures* 36, 2485-2505.